MAX PLANCK INSTITUTE FOR CHEMISTRY

JOHANNES GUTENBERG UNIVERSITÄT MAINZ

New Particle Formation and Aerosol Dynamics from Polluted Urban to Pristine Rainforest Environments

Dissertation

zur Erlangung des Grades

„Doktor der Naturwissenschaften“

Im Promotionsfach Chemie

am Fachbereich Chemie, Pharmazie, Geographie und Geowissenschaften

der Johannes Gutenberg-Universität Mainz

angefertigt am Max-Planck-Institut für Chemie

Jianqiang Zhu

geb. in Gansu, China

Mainz, 2024

1. Gutachter:

2. Gutachter:

Tag der mündlichen Prüfung: 2025.01.23

Declaration

I hereby declare that I wrote the dissertation submitted without any unauthorized external assistance and used only sources acknowledged in the work. All textual passages which are appropriated verbatim or paraphrased from published and unpublished texts as well as all information obtained from oral sources are duly indicated and listed in accordance with bibliographical rules. In carrying out this research, I complied with the rules of standard scientific practice as formulated in the statutes of Johannes Gutenberg-University Mainz to ensure standard scientific practice.

Jianqiang Zhu

Mainz, 2024.12.12

Abstract

Aerosol particles play a crucial role in cloud formation and the Earth's energy balance, with significant impacts on both climate and human health. This study explores new particle formation (NPF) and aerosol dynamics across three distinct environments: an urban area in Mainz, Germany; a pristine site in the Amazon rainforest (ATTO site, Brazil); and a polluted region in the North China Plain (Gucheng, China). The study employs state-of-the-art instruments to characterize aerosol properties, including particle and cluster number size distribution (PNSD), particle formation rates (J), growth rates (GR), and diurnal variations.

In Mainz, Germany, measurements were conducted between March and July 2022 using the Nano-Scanning Mobility Particle Sizer (Nano-SMPS), Particle Size Magnifier (PSM), and Neutral Cluster and Air Ion Spectrometer (NAIS) to assess NPF events and nucleation mode particle dynamics. The results showed that 11 days (8 %) out of 132 days were identified as NPF event days, which is lower than some megacities such as Beijing and comparable to other European cities such as Leipzig. During event periods, the formation rate ($J \leq 1.5$ nm) ranged from 0.3 to 11.3 cm^{-3} s^{-1}, and the growth rate (particle size range 1.5-20 nm) ranged from 1.9 to 6.6 nm h^{-1}. In addition, the condensation sink (CS) values ranged from (1.8-6.9) × 10^{-3} s^{-1}. It was found that meteorological factors such as low relative humidity, low wind speed and strong solar radiation are favorable for the occurrence of NPF events. Meanwhile, the importance of precise measurement of aerosol PNSD is highlighted. The accurate measurement of particles within the sub-10 nm size range, where technical challenges are present due to low detection efficiency and high diffusion loss, was achieved through the regular calibration of the instrument, the optimization and shortening of sampling lines, and the precise correction of losses.

The Amazon Tall Tower Observatory (ATTO) site in the Amazon rainforest provides a unique opportunity to study aerosol dynamics in a pristine environment. As part of the Chemistry of the Atmosphere: Field Experiment in Brazil (CAFE-Brazil) campaign, particles and cluster ions with diameter smaller than 40 nm were continuously observed in the Amazonian boundary layer in December 2022 and January 2023. The median concentration of sub-3 nm particles during the observation period was 491 cm^{-3}, accounting for 51 % of the total particle concentration, with a median of 969 cm^{-3}. The median concentrations of naturally charged clusters (0.8-2 nm), intermediate (2-7 nm) and large (7-20 nm) ions were 624, 33 and 30 cm^{-3} respectively. Despite the presence of these sub-3 nm particles and ions, typical regional NPF

events were not detected. However sub-3 nm particles showed a clear diurnal variation, with concentrations demonstrating a gradual increase from sunrise until midday, followed by a decline until midnight. Furthermore, on days with minimal pollution influence, daytime concentrations of sub-3 nm were observed to significantly exceed those recorded on polluted days. These daytime maximums are likely related to the photochemical formation of precursor vapors from different sources.

In Gucheng, China, aerosol measurements showed extremely high particle number concentrations (median 20800 cm^{-3}) and mass concentrations (median 121 $\mu g\ m^{-3}$), reflecting the severe pollution in this region. The campaign was conducted during the winter period from November to December 2018. Size-resolved PNSD indicate that Aitken mode particles are less sensitive to relative humidity (RH) than accumulation mode particles. Specifically, the log-normal fitted diameters for Aitken mode particles were 31 nm and 33 nm for high and low RH conditions, respectively, whereas the fitted diameters for accumulation mode particles were 125 nm and 120 nm, respectively. However, the chemical composition of the aerosols clearly varied with RH, with higher RH favoring the formation of secondary inorganic and organic matter (Sun et al., 2020b).

The findings from Mainz contribute to our knowledge of aerosol dynamics, offering insights into NPF processes in urban environments and their potential impact on air quality and climate modeling. The study in the Amazon rainforest provides valuable data on nanoparticle dynamics in pristine environments, and paving the way for future studies of gas-phase precursors to aerosol formation in the Amazon basin and similar regions. The findings in Gucheng highlight the complex interactions between aerosol dynamics, chemical composition and environmental factors in polluted regions. Overall, this study provides valuable insights into aerosol particle dynamics and NPF processes in urban, pristine and polluted environments. The ultimate goal was to improve our understanding of aerosol dynamics and NPF processes in different environments, with a focus on how natural and anthropogenic forcing shape particle size distributions, chemical composition, and diurnal variations. This knowledge will help to improve air quality models, better assess the impact of aerosols on climate change, more precise radiative forcing estimates, and support the development of more effective emission control policies, especially in regions with different levels of human impact.

Zusammenfassung

Aerosolpartikel spielen eine entscheidende Rolle bei der Wolkenbildung und dem Energiehaushalt der Erde und haben erhebliche Auswirkungen auf den Klimawandel und die menschliche Gesundheit. Diese Studie untersucht die Partikelneubildung (NPF) und die Aerosoldynamik in drei verschiedenen Umgebungen: einem Stadtgebiet in Mainz, Deutschland; einem unbelasteten Gebiet im Amazonas-Regenwald (ATTO-Standort, Brasilien); und einer verschmutzten Region in der nordchinesischen Ebene (Gucheng, China). Die Studie verwendet modernste Instrumente zur Charakterisierung der Aerosoleigenschaften, darunter die Partikel- und Cluster- anzahl-Größenverteilung (PNSD), die Partikelbildungsrate (J), die Wachstumsraten (GR) und die tageszeitlichen Schwankungen.

In Mainz, Deutschland, wurden zwischen März und Juli 2022 Messungen mit dem Nano-Scanning Mobility Particle Sizer (Nano-SMPS), dem Particle Size Magnifier (PSM) und dem Neutral Cluster and Air Ion Spectrometer (NAIS) durchgeführt, um NPF-Ereignisse und die Partikeldynamik im Nukleationsmodus zu untersuchen. Die Ergebnisse zeigten, dass 11 Tage (8 %) von 132 Tagen als NPF-Ereignistage identifiziert werden konnten, was weniger ist als in einigen Megastädten wie Peking und vergleichbar mit anderen europäischen Städten wie Leipzig. Während der Ereignisse lag die Bildungsrate ($J \leq 1.5$ nm) zwischen 0.3 und 11.3 cm^{-3} s^{-1}, und die Wachstumsrate (Partikelgrößenbereich 1.5-20 nm) zwischen 1.9 und 6.6 nm h^{-1}. Darüber hinaus lagen die condensation sink (CS)-Werte zwischen $(1.8\text{-}6.9) \times 10^{-3}$ s^{-1}. Es wurde festgestellt, dass meteorologische Faktoren wie eine niedrige relative Luftfeuchtigkeit, eine geringe Windgeschwindigkeit und eine starke Sonneneinstrahlung das Auftreten von NPF-Ereignissen begünstigen. Gleichzeitig wird die Bedeutung einer präzisen Messung der Aerosol-PNSD hervorgehoben. Die genaue Messung von Partikeln im Größenbereich unter 10 nm, bei der aufgrund der geringen Detektionseffizienz und des hohen Diffusionsverlusts technische Herausforderungen bestehen, wurde durch die regelmäßige Kalibrierung des Instruments, die Optimierung und Verkürzung der Probenahmeleitungen und die präzise Korrektur von Verlusten erreicht.

Der Standort des Amazon Tall Tower Observatory (ATTO) im Amazonas-Regenwald bietet eine einzigartige Gelegenheit, die Aerosoldynamik in einer unbelasteten Umgebung zu untersuchen. Im Rahmen der Kampagne „Chemistry of the Atmosphere: Field Experiment in Brazil (CAFE-Brazil) wurden im Dezember 2022 und Januar 2023 kontinuierlich Partikel und Cluster Ionen mit einem Durchmesser kleiner als 40 nm in der Amazonas-Grenzschicht

untersucht. Die mittlere Konzentration von Partikeln mit einer Größe von weniger als 3 nm betrug während des Beobachtungszeitraums 491 cm^{-3}, was 51 % der Gesamtpartikelkonzentration entspricht, mit einem Median von 969 cm^{-3}. Die mittleren Konzentrationen von natürlich geladenen Clustern (0.8-2 nm), intermediären (2-7 nm) und großen (7-20 nm) Ionen betrugen 624, 33 und 30 cm^{-3}. Trotz der Anwesenheit dieser Teilchen und Ionen mit einer Größe von unter 3 nm wurden keine typischen regionalen NPF-Ereignisse festgestellt. Allerdings zeigten Teilchen mit einer Größe von unter 3 nm eine deutliche tageszeitliche Schwankung, wobei die Konzentrationen von Sonnenaufgang bis Mittag einen allmählichen Anstieg zeigten, gefolgt von einem Rückgang bis Mitternacht. Darüber hinaus wurde an Tagen mit minimalem Verschmutzungseinfluss beobachtet, dass die Tageskonzentrationen von Partikeln mit einer Größe von unter 3 nm die an verschmutzten Tagen aufgezeichneten Konzentrationen deutlich überstiegen. Diese Tagesmaxima stehen wahrscheinlich im Zusammenhang mit der photochemischen Bildung Von gasförmigen Vorläuferverbindungen aus verschiedenen Quellen.

In Gucheng, China, zeigten Aerosolmessungen extrem hohe Partikelanzahlkonzentrationen (Median 20800 cm^{-3}) und Massenkonzentrationen (Median 121 µg m^{-3}), was die starke Luftverschmutzung in dieser Region widerspiegelt. Die Kampagne wurde im Winter von November bis Dezember 2018 durchgeführt. Größenaufgelöste PNSD zeigen, dass Aitken-Modus-Partikel weniger empfindlich auf relative Luftfeuchtigkeit (RH) reagieren als Akkumulation-Modus-Partikel. Konkret lagen die logarithmisch-normalverteilten angepassten Durchmesser für Aitken-Modus-Partikel bei 31 nm und 33 nm für Bedingungen mit hoher bzw. niedriger RH, während die angepassten Durchmesser für Akkumulation-Modus-Partikel bei 125 nm bzw. 120 nm lagen. Die chemische Zusammensetzung der Aerosole variierte jedoch deutlich mit der relativen Luftfeuchtigkeit, wobei eine höhere relative Luftfeuchtigkeit die Bildung von sekundären anorganischen und organischen Stoffen begünstigte (Sun et al., 2020b).

Die Ergebnisse aus Mainz tragen zu unserem Wissen über die Aerosoldynamik bei und bieten Einblicke in NPF-Prozesse in städtischen Umgebungen und ihre potenziellen Auswirkungen auf die Luftqualität und die Klimamodellierung. Die Studie im Amazonas-Regenwald liefert wertvolle Daten zur Dynamik von Nanopartikeln in unberührten Umgebungen und ebnet den Weg für zukünftige Studien zu Gasphasenvorläufern der Aerosolbildung im Amazonasbecken und ähnlichen Regionen. Die Ergebnisse in Gucheng verdeutlichen die komplexen Wechselwirkungen zwischen Aerosoldynamik, chemischer Zusammensetzung und

Umweltfaktoren in verschmutzten Regionen. Insgesamt liefert diese Studie wertvolle Erkenntnisse über die Dynamik von Aerosolpartikeln und NPF-Prozesse in städtischen, unbelasteten und verschmutzten Umgebungen. Das letztendliche Ziel bestand darin, unser Verständnis der Aerosoldynamik und der NPF-Prozesse unter verschiedenen Umweltbedingungen zu verbessern, wobei der Schwerpunkt darauf lag, wie natürliche und anthropogene Einflüsse die Partikelgrößenverteilung, die chemische Zusammensetzung und die tageszeitlichen Schwankungen beeinflussen. Dieses Wissen wird dazu beitragen, Luftqualitätsmodelle zu verbessern, die Auswirkungen von Aerosolen auf den Klimawandel besser einzuschätzen, die Abschätzungen des atmosphärischen Strahlungsantriebs zu präziseren und die Entwicklung wirksamerer Emissionskontrollmaßnahmen zu unterstützen, insbesondere in Regionen mit unterschiedlichem Grad an menschlicher Beeinflussung.

Contents

Chapter 1

1. Introduction

1.1 Atmospheric aerosol properties

Atmospheric particles, commonly referred to as aerosols particles, are tiny solid or liquid particles suspended in the air. Aerosols can originate from both natural and anthropogenic sources. Natural sources include phenomena such as dust storms, volcanic eruptions, sea spray, and biological emissions like pollen and spores (Seinfeld and Pandis, 2016). Anthropogenic, or human-made, sources mainly come from industrial emissions, vehicle emissions, fossil fuel combustion, and agricultural activities (Seinfeld and Pandis, 2016). These particles have a significant impact on climate, air quality, and human health.

Aerosol particles in the atmosphere can interact with solar radiation and therefore play a crucial role in climate regulation (Myhre, 2009). They affect the Earth's energy balance by scattering or absorbing sunlight in a process known as aerosol-radiation interaction (Ipcc, 2022; Charlson et al., 1992). In addition, aerosol particles can serve as cloud condensation nuclei (CCN), influencing cloud formation, brightness, and lifetime (Su et al., 2020; Gunthe et al., 2011; Merikanto et al., 2009; Reutter et al., 2009; Rosenfeld et al., 2008). This impact on clouds can either enhance or reduce their net cooling effects, depending on the type and concentration of aerosols (Bellouin et al., 2020; Williamson et al., 2019). Aerosol particles are therefore an important but complex player in the global climate system, with the potential to both slow and accelerate climate change, depending on their properties.

Aerosol particles can also have a significant impact on air quality, particularly in urban and industrial regions (Li et al., 2017; Reche et al., 2011). Fine particulate matter, especially particles smaller than 2.5 micrometers ($PM_{2.5}$), can remain suspended in the atmosphere for long periods of time. High concentrations of $PM_{2.5}$ from human activities such as vehicle emissions, industrial processes, and biomass burning can lead to poor air quality, often seen in the form of smog and haze (Shang et al., 2020; Guo et al., 2014; Fu et al., 2014). These particles can react with other pollutants to form secondary particles, further degrading air quality (Cheng et al., 2016; Zheng et al., 2015). Regions with high levels of aerosol pollution often experience reduced visibility, which can affect traffic safety and lead to the general decline in environmental quality.

In addition to their impact on climate and air quality, aerosol particles pose a serious threat to human health (Schraufnagel, 2020; Pöschl, 2005). When inhaled, fine particles can penetrate

deep into the lungs and into the bloodstream, causing inflammation and exacerbating pre-existing conditions such as asthma, bronchitis, and heart disease (Manisalidis et al., 2020; Burnett et al., 2018). Long-term exposure to high concentrations of aerosol particles has been linked to chronic respiratory diseases, cardiovascular diseases, and lung cancer (Ni et al., 2024; Lelieveld et al., 2019; Lelieveld et al., 2015). In addition, aerosol particles may carry toxic substances, including heavy metals and organic compounds, which further increase health risks (Pöschl and Shiraiwa, 2015). Given their widespread presence and diverse impacts, aerosol particles represent an important intersection of environmental and public health concerns that require careful monitoring and regulation.

The size of particles varies from a few nanometers to several micrometers. When classifying aerosol particle by size, the particle number size distribution (PNSD) is commonly divided into four main modes (Seinfeld and Pandis, 2016): the coarse mode (particle with diameter larger than 1000 nm), the accumulation mode (diameter from ~100 to ~1000 nm), the Aitken mode (diameter from ~25 to ~100 nm), and the nucleation mode (particles with diameter smaller than ~25 nm). Particle with diameter of less than 2.5 μm are referred to as fine particles, while fine particles with diameter of less than 100 nm are often referred to as ultrafine particles (Hussein, 2005). The typical PNSD is shown in **Figure 1.1**.

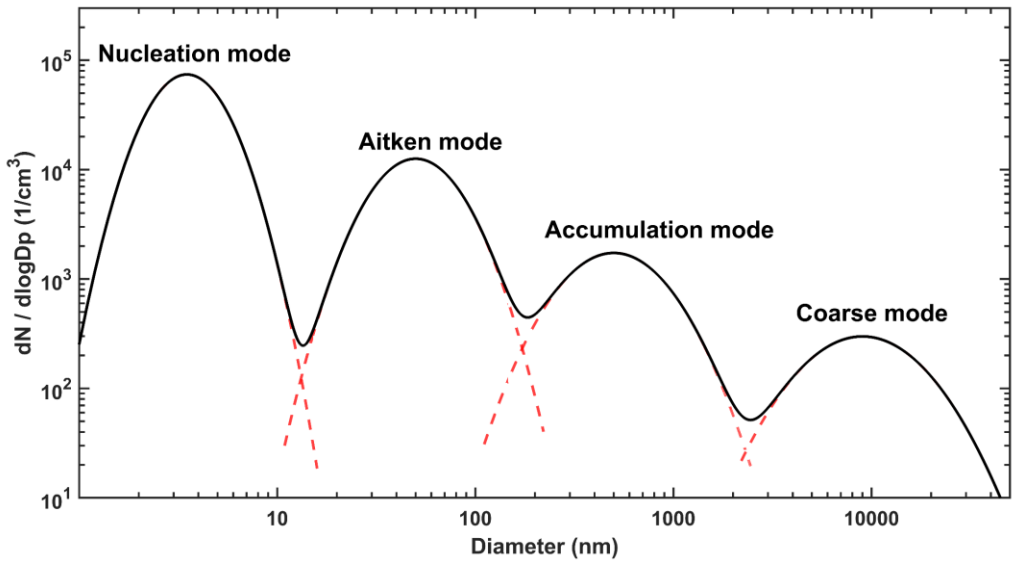

Figure 1.1: Typical number size distributions of atmospheric particles with the different modes. The figure was plotted based on the Seinfeld and Pandis (2016) and Hussein (2005).

1.2 Aerosols in polluted urban environments

Urban PNSD measurements are critical to understanding the size-dependent processes that

influence the transport, transformation, and fate of particles in the urban atmosphere. Furthermore, by assessing the deposition and inhalation toxicity of particles in the respiratory system, PNSD can enhance our understanding of the health effects of air pollution (Burnett et al., 2018). In urban areas, the PNSD typically exhibits a unique pattern influenced by local sources, meteorology, and urban activities. The typical PNSDs in Europe are shown in **Figure 1.2**, and the total number concentration of particle larger than 10 nm in EU cities ranges from 5000 to 20000 cm^{-3} (Wu and Boor, 2021).

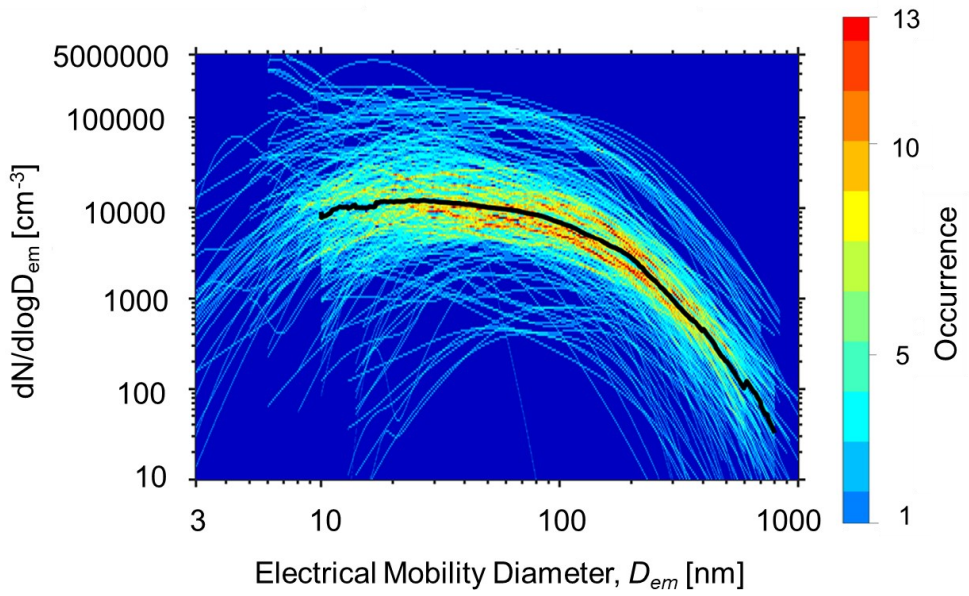

Figure 1.2: Urban aerosol PNSDs in European cities. The colors indicate the frequency of occurrence of the PNSD for a given particle size at a certain concentration. The black line indicates the median PNSD. This figure is taken from Wu and Boor (2021).

In urban environments, nucleation and Aitken mode particles are generally dominant in the PNSD (Ghassoun et al., 2015; Tuch et al., 2003). The nucleation mode is strongly influenced by vehicle emissions and new particle formation events (Ridolfo et al., 2024; Vu et al., 2015). The Aitken mode is common in urban areas and is mainly associated with vehicle emissions and local combustion sources (Costabile et al., 2009; Wehner and Wiedensohler, 2003). These particles account for a large proportion of the total number concentration of particles. The accumulation mode is not dominant in terms of number concentration but plays a critical role in terms of mass concentration, and is caused by regional transport, aged particles, and secondary aerosol formation (Costabile et al., 2009; Voigtländer et al., 2006).

The particle number concentrations in cities usually peaks in the morning and evening due to traffic emissions during rush-hour (Von Bismarck-Osten et al., 2013; Voigtländer et al., 2006;

Tuch et al., 2003). This pattern is associated with high numbers of nucleation and Aitken mode particles. Accumulation mode particles tend to show less pronounced diurnal variation, as they usually originate from regional or aged particles, and are more consistently distributed throughout the day (Wehner and Wiedensohler, 2003). Temperature, wind speed, and atmospheric stability have a significant effect on PNSD. The stable atmospheric conditions with low wind speeds lead to a concentration of particles near the source, while strong winds tend to disperse them (Voigtländer et al., 2006). Seasonal variations are also pronounced, with higher particle numbers in winter due to increased heating activities and stagnant atmospheric conditions (Wehner and Wiedensohler, 2003; Tuch et al., 2003).

Nucleation mode particles are formed by the condensation of gas-phase molecules (usually from gases such as sulfuric acid, ammonia or organic compounds) to form new particles (Lee et al., 2019; Zhang et al., 2012). After nucleation, these particles can grow to larger sizes through condensation from vapor and coagulation with other particles (Zhang et al., 2012). This process is often referred to as regional new particle formation (NPF) in the atmosphere (Kulmala et al., 2022; Kulmala et al., 2012), and will be referred to later as “regional NPF”. Nucleation mode particles are usually the first stage in the life cycle of aerosols, and their growth and evolution are crucial for understanding particle dynamics of particles in the atmosphere. There are numerous measurements of PNSD and NPF worldwide, in environments ranging from cities to forests, coasts and even the Arctic (Nieminen et al., 2018; Kerminen et al., 2018).

A summary of the NPF measurement for urban areas is presented in **Table 1.1**. NPF events are relatively common in European cities, particularly during the spring and summer months (Crumeyrolle et al., 2023; Bousiotis et al., 2021b). The requisite conditions for NPF formation are provided by the presence of precursors, including sulfuric acid (derived from sulfur dioxide in emissions), ammonia (e.g., from vehicle exhaust), and volatile organic compounds (resulting from traffic and industrial activities) in urban areas (Yan et al., 2021; Smith et al., 2021; Cai et al., 2021; Brean et al., 2020). In urban areas, NPF typically exhibits a diurnal cycle, with particle nucleation occurring in the late morning or early afternoon. This is driven by photochemical that are most active when sunlight and temperature are at their peak. The newly formed particles typically persist into the night, and as they grow in mass through condensation and coagulation, the particles transition from the nucleation mode to the larger Aitken mode particles (Zhang et al., 2012).

The NPF frequency is typically observed on approximately 5-50 % of days in urban environments (Stolzenburg et al., 2023; Nieminen et al., 2018). In some cities in Germany, the frequency of NPF is around 5-30 % (Bousiotis et al., 2021b; Größ et al., 2018). Cities with higher pollution levels may experience a reduction in the frequency of NPF events due to the higher concentrations of pre-existing particles, which have the potential to scavenge the nucleating vapors and inhibit particle formation (Stolzenburg et al., 2023; Größ et al., 2018). However, in certain megacities, including Beijing and New Delhi, the observed frequency of NPF events exceeded 50 % (Chu et al., 2019; Mönkkönen et al., 2005). Despite the presence of a high condensation sink (CS), the prevalence of nucleation precursors continues to favor the occurrence of NPF events (Hong et al., 2023).

The growth rate (GR) is defined as the rate at which newly formed particles increase in diameter over time. The particle GF is typically observed to be between 1 and 10 nm h^{-1} (Stolzenburg et al., 2023). In the German city of Leipzig, the measured GF ranged from 3 to 7.5 nm and from 7.5 to 22 nm, with respective values of 4.0 and 5.2 nm h^{-1} (Rowell et al., 2024). In Lille (France), the measured GFs were within the range of 0.8 to 15.7 nm h^{-1} (Crumeyrolle et al., 2023). The GF is dependent upon the environmental conditions and the specific region. In environments with high concentrations of sulfuric acid, organic vapors, low condensation sink, and favorable meteorological conditions (e.g., high humidity, lower temperatures), the GF can be significantly higher (Lee et al., 2019; Yao et al., 2018).

The formation rate (J) is defined as the rate at which new particles are formed from vapor-phase precursors. It typically ranges from clusters of a few molecules to a particle size that can be detected (Kulmala et al., 2012). Also, the nucleation rate during NPF events is found to be significantly dependent on local conditions and the types of precursors present. The value of J can span up to 4 orders of magnitude, from less than 1 cm^{-3} s^{-1} to more than 100 cm^{-3} s^{-1} (Brean et al., 2020; Kerminen et al., 2018; Yao et al., 2018). A higher nucleation rate is typically observed in environments characterized by a high concentration of sulfuric acid and organic vapors, as evidenced by studies conducted in urban areas, such as Eastern China, India and parts of Europe and the United States (Zhao et al., 2024; Chu et al., 2019; Nieminen et al., 2018).

Table 1.1 Summary of New Particle Formation (NPF) measurements in European and Chinese cities

Location	Measurement period	Instrument	Size range (nm)	Frequency (%)	Growth rate (nm h^{-1})	Formation rate (cm^{-3} s^{-1})	References
Europe							
Leipzig, Germany	Jul-Aug 2022	NAIS	0.8-42 (Ion)	30	4.0 (3-7.5 nm) 5.2 (7.5-22 nm)	0.33 (>3 nm)	(Rowell et al., 2024)
Lille, France	Jul 2017-Dec 2020	SMPS	15.7-800	11	0.8 – 15.7 (15.7-30 nm)	-	(Crumeyrolle et al., 2023)
Copenhagen, Denmark	2008-2017	DMPS	6-700	5.8	3.2 (6-30 nm)	0.03 (>10 nm)	(Bousiotis et al., 2021a)
Leipzig, Germany	2008-2011	TDMPS	3-800	9	4.2 (3-30 nm)	0.1 (>10 nm)	
Helsinki, Finland	2008-2011 2015-2018	TDMPS	3-1000	5	2.9 (3-30 nm)	0.01 (>10 nm)	
Barcelona, Spain	2012-2015	SMPS	10-478	13.1	3.4 (10-30 nm)	0.02 (>10 nm)	
Athens, Greece	2015-2018	SMPS	10-550	8.5	3.7 (10-30 nm)	0.005 (>10 nm)	
Barcelona, Spain	Jun-Jul 2018	SMPS PSM	4.5-478 1.4-2.4	-	4.4 (1.9-4.5 nm) 4.7 (4.5-20 nm)	178 (>1.9 nm)	(Brean et al., 2020)
Budapest, Hungary	2014-2016	SMPS	6-1000	21	-	-	(Németh et al., 2018)
Vienna, Austria	2014-2016	SMPS	10-926	12	-	-	
Prague, Czech	2014-2016	SMPS	7-540	30	-	-	

Table continued on the next page…

Table continued from the previous page

Location	Measurement period	Instrument	Size range (nm)	Frequency (%)	Growth rate (nm h^{-1})	Formation rate (cm^{-3} s^{-1})	References
China							
Xiamen, China	Dec 2019	SMPS	7-300	41	0.94 (>10 nm)	2.0 (7-25 nm)	(Wang et al., 2022)
Beijing, China	2018-2019 (summer)	DMPS Nano-SMPS	6-856 3-55	48	7.8 (7-15 nm)	5.4 (>7 nm)	(Zhou et al., 2021)
Beijing, China	Jan-Mar 2020	SMPS	3-698	36	1.1-9.7 (3-25 nm)	9.5 (>3 nm)	(Tang et al., 2021)
Beijing, China	2018-2019	SMPS PSD [a]	1-7.5 3-10000	31	0.9 (1-3 nm) 1.7 (3-7 nm) 2.9 (7-25 nm)	79 (>1.5 nm)	(Deng et al., 2020)
Shanghai, China	2014-2016	SMPS NAIS PSM	3-736 0.8-42 1.2-3	15.6	1.5 (<3 nm) 6.5 (3-7 nm) 9.9 (7-25 nm)	106 (>1.7 nm)	(Yao et al., 2018)
Beijing, China	2015-2016	SMPS NAIS	14-673 2-42	-	3.5 (2-10 nm)	26 (>2 nm)	(Jayaratne et al., 2017)
Nanjing, China	2014-2015	SMPS PSM	3-750 1.4-3	10	7.6 (3-10 nm)	26 (>2 nm)	(Yu et al., 2016)
Shanghai, China	2014-2015	SMPS PSM	3-615 1.34-3	21	2.0 (1.3-2.4 nm) 10.9 (2.4-7 nm) 11.4 (7-20 nm)	188 (>1.34 nm)	(Xiao et al., 2015)
Nanjing, China	Nov 2011-Mar 2012	DMPS AIS [b]	6-800 0.8-42	20	6.3 (3-7 nm)	1.1 (>6 nm)	(Herrmann et al., 2014)

- No data available

[a] PSD, particle size distribution system (TSI aerodynamic particle sizer and two parallel SMPSs)

[b] AIS, air ion spectrometer

In urban areas, NPF is commonly driven by the interaction of sulfuric acid, ammonia, and organic compounds, which together contribute significantly to the growth of nucleated particles (Zhao et al., 2024; Wang et al., 2020). Sulfuric acid, typically formed through the oxidation of sulfur dioxide, is a key precursor in NPF, initiating the formation of stable particle nuclei (Almeida et al., 2013; Kulmala et al., 2013; Sipilä et al., 2010). Ammonia and amine play an important role in neutralizing acidic compounds, promoting particle growth by forming ammonium salts with inorganic acids (Wang et al., 2020; Kirkby et al., 2011). Organic compounds, both anthropogenic and biogenic, can contribute to NPF (Kirkby et al., 2023; Kirkby et al., 2016). It also can further enhance NPF by contributing to particle mass and influencing their physical and chemical properties through condensation and coagulation processes (Bianchi et al., 2016; Ehn et al., 2014). The potential mechanisms behind NPF include gas-phase nucleation, particle condensation, and growth processes, which are modulated by environmental factors such as temperature, humidity, and the availability of precursor gases (Zhang et al., 2012).

In regions like China, particularly under heavily polluted environments, the chemical composition of new particles is influenced by a wider range of precursors and atmospheric conditions. The high concentrations of pollutants, such as sulfates, nitrates and organic aerosols, also contribute to both the nucleation and growth of particles (Chu et al., 2019; Yao et al., 2018; Wang et al., 2017; Guo et al., 2014; Huang et al., 2014). However, in such polluted environments, the multiphase chemistry (gas-to-particle conversion and aqueous-phase reactions) becomes increasingly important, especially under different RH conditions (Su et al., 2020; Cheng et al., 2016). At high RH, aerosol particles may undergo multiphase reactions in aerosol water, leading to enhanced particle growth, particularly in the presence of ammonium sulfate or organic acids (Sun et al., 2020b). On the other hand, at lower RH, evaporation of water may alter particle size and composition, impacting the stability of nucleated particles and their ability to grow further (Riemer et al., 2019). These multiphase processes are complex and highly sensitive to the interplay between gas-phase precursors, aerosol composition, and atmospheric humidity, making NPF in highly polluted regions like China a critical area of study for understanding air quality and climate dynamics.

In conclusion, although the number of PNSD measurements have been carried out across diverse urban regions in recent years, notable limitation and discrepancies remain in the evaluation of nucleation mode particles and NPF-related parameters. Many NPF-related studies reported the results using instruments with the detection limit higher than 10 nm (Sun

et al., 2024; Crumeyrolle et al., 2023; Bousiotis et al., 2021b; Bousiotis et al., 2019; Chu et al., 2019). These discrepancies include differences between the measured values of the PNSD obtained with various instruments, particularly for sub-10 nm particles. These differences are frequently several times, and at low number concentrations, may exceed an order of magnitude (Kangasluoma et al., 2020). NPF parameters also exhibit considerable variation across different regions. For instance, formation rates vary by more than four to five orders of magnitude (Stolzenburg et al., 2023). These nanoparticles represent the earliest stage of atmospheric NPF, and their growth processes affects the concentration and characteristics of aerosol particles. Research on these particles is crucial to understanding the mechanisms of particle formation, the dynamics of aerosol behavior, and their broader impacts on air quality and climate. Precise measurement of sub-10 nm particles will improve our knowledge of atmospheric chemistry and the role these particles play in urban environments.

1.3 Aerosols in pristine rainforest environments

The Amazon rainforest is frequently referred to as the 'lungs of the Earth', reflecting its essential function within the Earth's atmospheric system. The Amazon rainforest is the largest tropical rainforest on Earth, covering an area of over 4.7 million square kilometers (Ahlm et al., 2009). It plays an important role in regulating the global climate, atmospheric chemistry and water cycles. The Amazon rainforest's vast ecosystem supports complex interactions between the biosphere and the atmosphere, with significant implications for global air quality, cloud formation, and precipitation patterns (Artaxo et al., 2022). One of the Amazon's most significant contributions to atmospheric science is its capacity to sequester carbon dioxide through photosynthesis, thereby functioning as a major carbon sink (Hubau et al., 2020). Furthermore, the Amazon River Basin releases significant amounts of water vapor into the atmosphere through transpiration, which affects not only the local weather patterns but also the regional and even global climate system.

In addition to its role in the carbon and water cycles, the Amazon is a pivotal location for the investigation of aerosols and trace gas emissions (Artaxo et al., 2022). It has been demonstrated that the biogenic volatile organic compounds (BVOCs) from forests will induce the formation of new particles and secondary organic aerosols (SOAs) (Bianchi et al., 2019; Ehn et al., 2014). These particles have a significant impact on CCN and cloud microphysics, which are critical for cloud formation, albedo and precipitation. The pristine environment of the Amazon, largely isolated from anthropogenic pollution particularly during the wet season (Artaxo et al., 2022; Rizzo et al., 2018), provides a unique opportunity to study natural atmospheric processes as a

benchmark for understanding the impact of human activities on air quality and climate. As the Amazon rainforest faces increasing threats from human activities, it is becoming clearer that it plays a critical role in regulating global climate and influencing atmospheric processes (Hubau et al., 2020; Hansen et al., 2020). This highlights the urgent need for continued research and conservation efforts.

Atmospheric aerosol measurements in the Amazon Basin have been carried out since the 1990s (Martin et al., 2010a; Martin et al., 2010b; Andreae et al., 2002). The first comprehensive campaign was the Cooperative LBA Airborne Regional Experiment (CLAIRE) in 1998 (Zhou et al., 2002). Since then, several ground and aircraft measurements have been carried out over the past two decades (Pöhlker et al., 2016; Martin et al., 2010a; Rissler et al., 2004; Guyon et al., 2003). The Amazon Tall Tower Observatory (ATTO) is located in a pristine rain forest region in the central Amazon Basin, approximately 150 km northeast of the city of Manaus. Two 80-metre towers have been operational at the site since 2012, while a 325-meter tower has been in operation since 2017 (Andreae et al., 2015). The towers are fully instrumented to continuously measure vertical profiles of aerosol properties, trace gases, and meteorological parameters.

In this study, our focus is on particle size measurements, particularly in the nucleation, Atkin, and accumulation modes. The first earlier PNSD measurement in Amazon showed that two aerosol particle modes (Aitken and accumulation mode) were always present, with the mean number concentration of 239 and 177 cm^{-3} and geometric mean diameters of 68 and 151 nm, respectively (Zhou et al., 2002). Subsequently, an increasing number of studies were conducted on PNSD measurements in the Amazon, as detailed in **Table 1.2.** The PNSD demonstrates a strong seasonal variability in the Amazon region. As shown in **Figure 1.3**. during the wet season, the Aitken mode and accumulation mode contribute similarly to the particle size spectra by number concentration at forest sites in Central Amazonia (Rizzo et al., 2018). However, during the dry season, the accumulation mode particles were the dominant in term of number concentration (Rizzo et al., 2018). The particle number concentrations were observed in the range of 300-400 cm^{-3} for particles in the 10-600 nm size range (Artaxo et al., 2022; Rizzo et al., 2018; Andreae et al., 2015). The total particle number concentrations typically increased three times from the wet to the dry season, with mean values in the range 1000-1400 cm^{-3} for particles between 10 nm and 600 nm at forest sites in Central Amazonia (Artaxo et al., 2022; Rizzo et al., 2018).

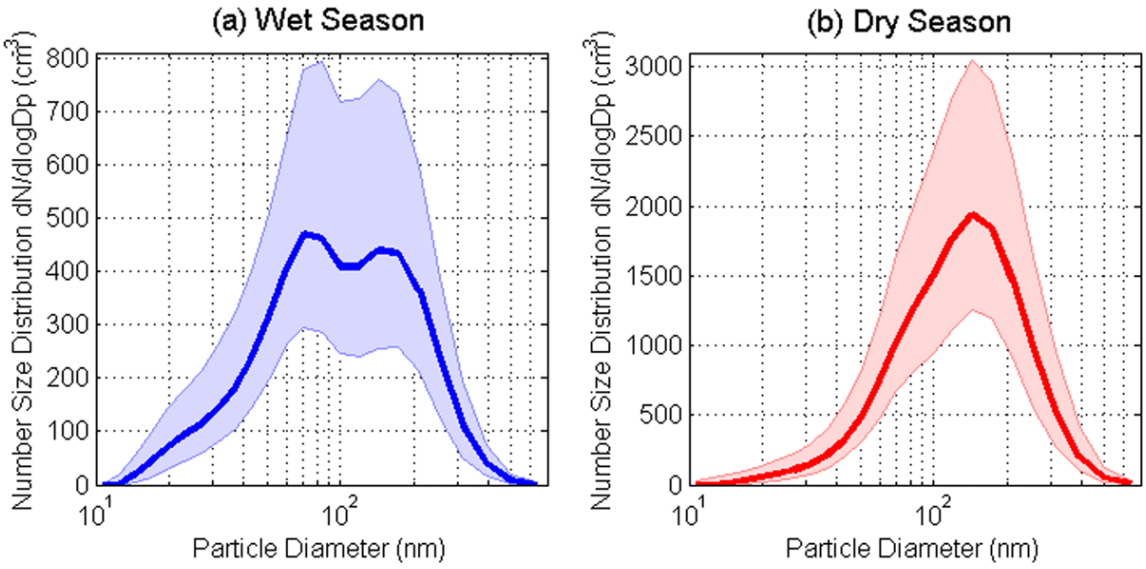

Figure 1.3: Median particle number size distributions for the (a) wet and (b) dry season. Shadows represent the 25-75th percentile range. This figure and caption are taken from Rizzo et al. (2018).

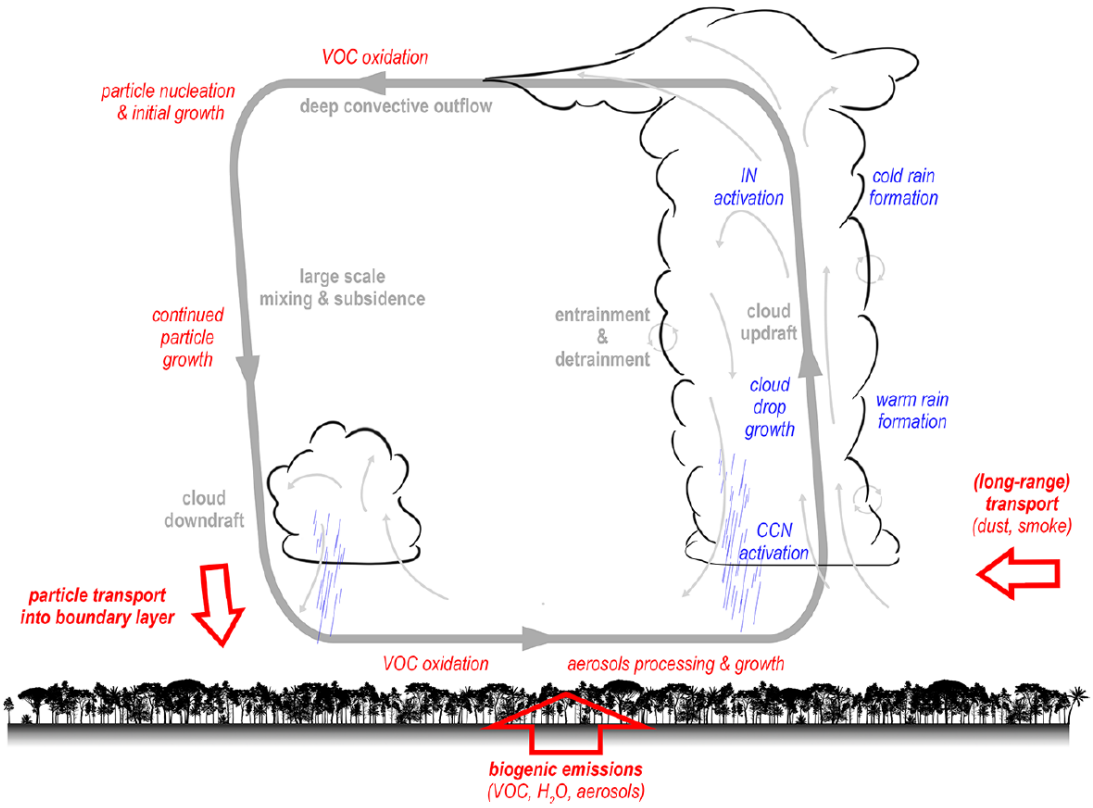

Figure 1.4: The conceptual scheme of sources, processing, and removal of aerosol particles and CCN over the Amazon. This figure is taken from Franco et al. (2022).

Table 1.2 Summary of the particle number size distribution (PNSD) measurements in the Amazon region

Location	Type	Period	Campaign	Instrument	Size range	Reference
Surinam	Aircraft	Mar 1998	LBA-CLAIR	CPC OPC	6-18 nm 0.12-3.5 μm	(Krejci et al., 2003) (Krejci et al., 2005)
Balbina	Ground	Mar-Apr 1998	CLAIRE-98	DMPS	3-850 nm	(Zhou et al., 2002)
Rondônia	Tower	Apr-May 1999 Sep-Oct 1999	LBA-EUSTACH	CPC PCASP	0.01-3 μm 0.1-3 μm	(Guyon et al., 2003)
Balbina	Ground	July 2001	CLAIRE-01	DMPS	3-850 nm	(Rissler et al., 2004)
Rondônia	Aircraft	Sep-Oct 2002	LBA-SMOCC	SMPS	15-414 nm	(Guyon et al., 2005)
Rondônia	Ground	Sep-Nov 2002	LBA-SMOCC	DMPS	3-850 nm	(Rissler et al., 2006b)
TT34 (02°35.657 S, 60°12.557 W)	Tower	Feb-Mar 2008	AMAZE-08	SMPS CPC OPC	10-500 nm >10 nm 0.2-10 μm	(Martin et al., 2010b)
ATTO	Tower	Jan 2014- Dec 2015	GoAmazon2014/5	SMPS UHSAS OPS	10-430 nm 60-1000 nm 0.3-10 μm	(Martin et al., 2016)
ATTO	Ground	Sep 2011- Jan 2014	GoAmazon2014/5	NAIS PSM DMPS	2-40 nm >1.5 nm 6-800 nm	(Wimmer et al., 2018)
Amazon Basin	Aircraft	Sep-Oct 2014	ACRIDICON-CHUVA	CPC DMPS OPC	5 nm - 1 μm 5-350 nm 250 nm - 3 μm	(Wendisch et al., 2016) (Andreae et al., 2018)
ATTO	Tower	Feb 2008- Oct 2014	Long-term	Lund SMPS TSI SMPS DMPS	10-600 nm 10-500 nm 6-800 nm	(Rizzo et al., 2018)
ATTO	Tower	Feb 2014- Sep 2020	Long-term	CPC SMPS	>4 nm 10-400 nm	(Franco et al., 2022)

PCASP: passive cavity aerosol spectrometer probe
OPC: optical particle counter
UHSAS: Ultra-High Sensitivity Aerosol Spectrometer

Figure 1.4 illustrates the three main sources of aerosol particles in the Amazon. One of the main sources of aerosol particles are biogenic particles, which directly emitted by the rain forest. This includes the primary biological aerosol particles (such as, pollen, spores and fragments) and biogenic volatile organic compounds (VOCs) which may further undergo atmospheric oxidation and contribute to SOA formation (Pöhlker et al., 2012). During the wet season, when the pristine atmospheric conditions prevail, biogenic emissions are the primary source of aerosol particles in the Amazon (Artaxo et al., 2022). Secondly, the regional biomass burning smoke, and long-range transported aerosols (the Saharan dust, African biomass burning, and sea salt) also contribute to aerosol particle in the amazon region (Holanda et al., 2020; Pöhlker et al., 2018). During the dry season, fine particle mode is the primary mode, and is strongly influenced by regional biomass burning emissions (Artaxo et al., 2022). Thirdly, driven by deep convective clouds, biogenic VOCs can be transported into the upper troposphere, where VOC oxidation, nucleation, and initial particle growth occur. Then the freshly formed particles are transported downward into the planetary boundary layer (PBL), where they continue to grow (Wang et al., 2016). Machado et al. (2024) recently analyzed aerosol and trace gas changes during downdrafts and attributed the characteristic particle bursts to boundary layer NPF, driven by a sudden increase in ozone and decrease in the condensation sink due to rain events.

The regional NPF has been observed worldwide in a variety of environmental conditions, including urban environments, rural and remote continental areas, the Arctic and Antarctic, marine areas, mountain sites, and boreal and other forested regions (Kerminen et al., 2018). However, the classical regional NPF has yet to be observed in the Amazon. Despite the existence of reports concerning NPF, the evidence is inconclusive. On the one hand, the measured particle size was often only above 10 nm, as is typical with a standard SMPS system (Rizzo et al., 2018), while on the other hand it may be contributed to the anthropogenic emission, rather than representing the real pristine condition (Wimmer et al., 2018). In other continental locations, 3-nm particles are regularly observed at near-surface measurement sites and are also observed to grow into the Aitken mode above 30 nm (Kontkanen et al., 2017). In contrast to the prevailing assumption that particle growth commences at a few nanometers, the long-term report frequently indicated that the particle growth process initiates at 20-40 nm (Franco et al., 2022).

Occasional occurrence of nucleation mode particles within the boundary layer has been reported, and their contribution to particle number concentrations to be insignificant (Artaxo

et al., 2022). Zhou et al. (2002) reported that the nucleation mode particles exhibited a number concentration and a mean diameter of 92 cm^{-3} and 24 nm, respectively, and occurred only at 18 % of the time. The reasons for absence of nucleation mode particles and NPF in Amazon is still unclear, and several hypotheses have been proposed to explain this phenomenon. The following factors have been identified as potential causes for the absence of NPF in the Amazon:

1) the scavenging of OH radicals by isoprene, which reduces the rate of monoterpene oxidation (Heinritzi et al., 2020; Mcfiggans et al., 2019). As the most abundant VOC in the Amazon atmosphere, isoprene competes with monoterpenes for OH radicals, potentially limiting the formation of highly oxidized molecules (HOMs) from monoterpenes (Bianchi et al., 2019; Andreae et al., 2018). Monoterpenes are generally more impactful on NPF than isoprene, as their oxidation produces low-volatility HOMs essential for particle nucleation and growth (Stolzenburg et al., 2023).

2) the very low concentrations of SO_2, which limits the formation of nucleating sulfuric acid, an essential precursor for particle nucleation (Kulmala et al., 2013; Sipilä et al., 2010). Additionally, the low concentrations of basic compounds, such as ammonia and amines, further reduce the likelihood of nucleation events, as these bases play a key role in stabilizing newly formed clusters (Yao et al., 2018; Kirkby et al., 2011). For instance, the mixing ratios of NH_3 were found to be below 1 ppb in the Amazon Basin during the wet season (Trebs et al., 2004). However, the ammonia from traffic, industrial emissions and agriculture can reach 8 ppb in urban conditions (Wang et al., 2020).

3) high levels of RH, which are associated with a reduced occurrence of NPF. Elevated RH can hinder nucleation by favoring the growth of existing particles through condensation rather than promoting the formation of new particles, thus decreasing the likelihood of NPF events (Franco et al., 2022; Hamed et al., 2011).

Despite the extensive research conducted in the Amazon in recent years, significant gaps remain in our understanding, particularly concerning nucleation mode particles, especially those smaller than 10 nm. The occurrence of NPF in this region regarding the specific conditions and mechanisms that may either promote or inhibit NPF is not yet fully understood. The lack of clarity on particle dynamics and the processes behind potential NPF in the Amazon underscores the necessity for comprehensive studies to unravel how unique environmental factors in the region influence particle formation and growth.

1.4 Research objectives and thesis outline

The objective of this thesis is to enhance our understanding of aerosol behavior, inform atmospheric models, and support the development of effective policies for air quality management and climate change mitigation. To achieve these goals, the main research objectives are as follows:

- **Instrument comparison for the measurement of sub-10 nm particles**: An intercomparison and characterization of advanced aerosol instruments, including a TSI Nano-SMPS, an Airmodus PSM, and an Ariel NAIS, was conduct to evaluate their performance and identify discrepancies in measuring sub-10 nm particles. This objective aims to demonstrate and quantify the potential discrepancies in particle number concentrations and size distributions recorded by different instruments, thereby highlighting the challenges in obtaining consistent measurements in NPF studies and underscoring the need for further standardization and refinement in sub-10 nm particle measurement techniques.
- **Study of NPF in the different environments**: NPF in different environments was measured to investigate its occurrence and characteristics. Key parameters, including the frequency of NPF events, particle formation rate (J) and growth rate (GR), were analyzed to characterize the dynamics of particle formation and growth. The study also investigated how these processes are influenced by meteorological factors such as temperature, relative humidity, and solar radiation. By integrating these observations, the study provides a detailed understanding of the variations in NPF processes at different locations and highlights the critical factors driving these variations.
- **Analysis of aerosol dynamics**: The study includes PNSD and diurnal variation. The aim is to describe changes in aerosol properties and behavior under different environmental conditions, such as changes in particle growth and distribution patterns over the course of the day. In addition, the relationship between particle size and chemical composition under different relative humidity conditions was studied to gain an in-depth understanding of the impact of relative humidity on the size distribution of aerosols, especially in polluted environments.

These objectives were achieved through direct on-site measurements conducted during three different campaigns in different environmental conditions, details of each campaign are shown in **Figure 1.5**. Each location offered unique insights: Gucheng (China) represented a heavily polluted region with high aerosol concentrations and strong anthropogenic influence; Mainz

(Germany) typified an urban environment characterized by a mix of local and regional emissions; and ATTO (Brazil) provided a pristine setting within the Amazon rainforest, offering a rare perspective on natural aerosol processes. The state-of-the-art instruments with a focus on nucleation mode particles were employed to investigate NPF processes and aerosol dynamics across these diverse settings.

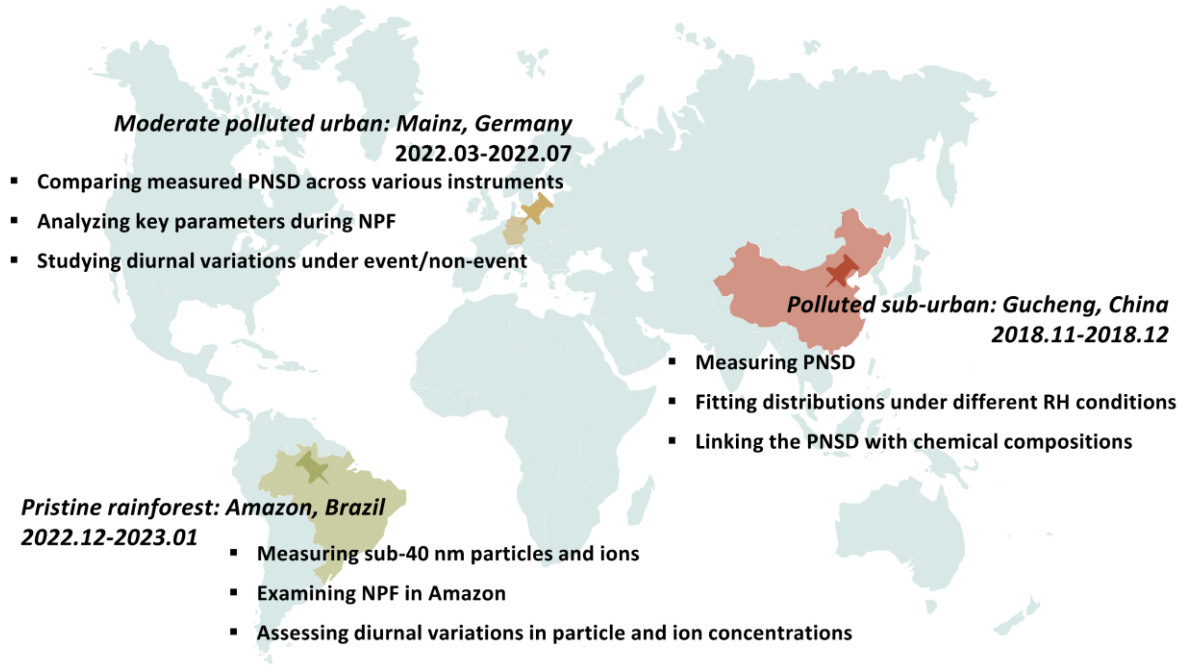

Figure 1.5: Structure of this thesis. The location, measurement periods and main objectives of each study are listed.

Chapter 1 provides an overview of the current knowledge base on aerosol particles, outlines the current research status of PNSD and NPF in urban and Amazonian environments, and underscores the limitations of existing knowledge.

Chapter 2 provides a detailed overview of the principles behind each instrument employed in the study and includes a brief introduction to each field campaign.

Chapter 3 presents the detailed NPF results for the Mainz measurement. A comprehensive sub-40 nm PNSD is reported across different instruments. The NPF frequency, the particle formation rate, and growth rate are calculated. Furthermore, the diurnal variation of the particle and the relationship between particle number concentration and meteorological parameters (such as, RH, temperature, solar radiation, and condensation sink) are discussed.

Chapter 4 presents the measurement results conducted at the ATTO site during the CAFE-Brazil campaign. As one of the few observational data sets, we report the PNSD down to 1 nm in the Amazon rainforest and the total number concentration of the full spectrum. Furthermore, the daily variation of sub-3 nm particles and naturally charged ions is presented.

Chapter 5 investigates the aerosol properties within a highly polluted environment in China, focusing on PNSD under varying relative humidity conditions. Furthermore, the sensitivity of particle size modes to high and low humidity levels was also explored.

In Chapter 6, the results of the dissertation are summarized and their implications are discussed in a broader perspective. The limitations of this study and suggestions for further research are also briefly discussed.

Chapter 2

2. Methods

2.1 Instruments for nanoparticle measurement

Over the years, considerable progress has been made in the development and improvement of instruments specifically designed to measure particle and cluster number concentrations below 10 nm, which are essential for studying NPF processes. **Figure 2.1** provides an overview of the various instruments that can detect the particles and clusters in the sub-50 nm nanosize ranges, including the Particle Size Magnifier (PSM), the Condensation Particle Counter (CPCb), the Scanning Mobility Particle Sizer (SMPS), and the Neutral cluster and Air Ion Spectrometer (NAIS). These instruments are critical for capturing the dynamic processes of particle formation and growth. Each instrument covers a specific size range, and together they provide a comprehensive view of NPF events. The Chemical Ionization Mass Spectrometer (CIMS) is also included, though it focuses primarily on resolving the chemical composition of clusters and gas precursors rather than directly measuring particle size. Notably, there is no uniform correlation between atomic mass and particle diameter, as molecular shape and structure play an important role in determining particle dimensions.

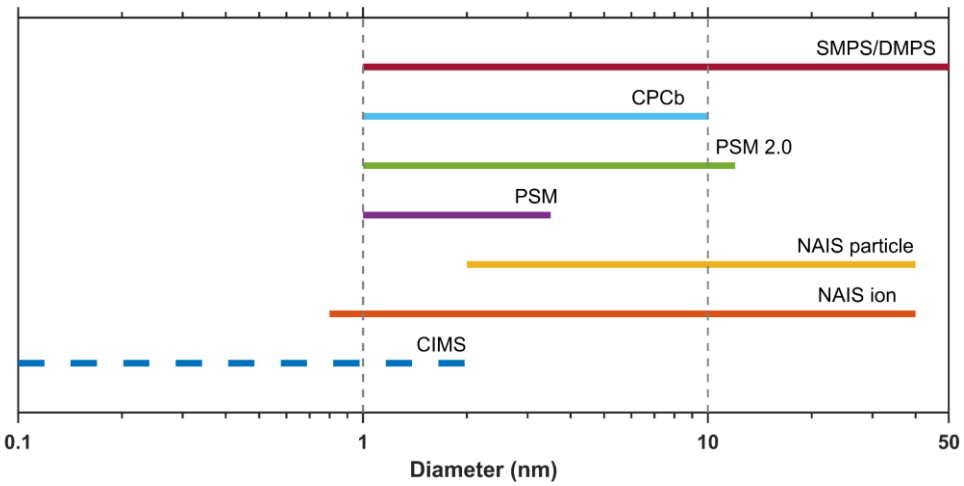

Figure 2.1: Overview of the diameter ranges for instruments commonly used in NPF research. The solid lines indicate instruments that measure physical particle size, while the dotted line represents instrument that infer size based on chemical composition. The figure was plotted based on the Sulo et al. (2024), Kangasluoma et al. (2020) and Ehn et al. (2011).

Currently, two primary types of instruments are commonly employed for the measurement of particle size distribution below 10 nm. These include condensation-based measurement systems and mobility-based measurement systems. Kelvin-based instruments detect particles

based on their ability to overcome the Kelvin barrier, which mainly depends on the particle size in the sub-10 nm range. In contrast, mobility-based instruments classify particles based on their electrical mobility, which is directly related to mobility size. This allows for high-resolution measurements of particles down to the nanometer scale. Together, these instruments provide a comprehensive analysis of nucleation and growth patterns, which is critical for understanding NPF dynamics under different atmospheric conditions.

2.1.1 Condensation-based methods

The condensation particle counter (CPC) is one of widely used detector for sub-10 nm particle number concentration counting, due to its extremely low background noise levels (Kangasluoma et al., 2020). The CPC was developed and continuously optimized since 1970s (Stolzenburg and Mcmurry, 1991; Okuyama et al., 1984; Agarwal and Sem, 1980; Sinclair and Hoopes, 1975). The CPC is capable of detecting and counting aerosol particles. This is achieved by first growing the particles using a supersaturated selected vapor (such as butanol and water), which condenses onto the particles. Those enlarge particles are then counted by an optical detector. The most fundamental model for predicting the required supersaturation is the Kelvin effect (Kangasluoma and Attoui, 2019), which implies that the vapor pressure over a curved surface is higher than over a flat surface of the same substance (Seinfeld and Pandis, 2016). The Kelvin equation can be expressed as (Seinfeld and Pandis, 2016):

$$p_A = p_A^o \exp\left(\frac{4\sigma M}{RT\rho_l D_p}\right)$$

where p_A indicates the actual equilibrium partial pressure over the liquid particle and $p_A°$ refers to the vapor pressure of pure A over a flat surface. σ is the surface tension of A and M is the molecular weight of the substance A. R is the ideal-gas constant and ρ_l is the liquid-phase density. Dp is the drop diameter. The measured diameter is called Kelvin equivalent diameter based on the threshold vapor supersaturation (Kangasluoma and Attoui, 2019).

The supersaturated vapor can be operated either by stepwise or scanning condition or by operating a battery of CPCs in a parallel (Kangasluoma et al., 2020). The CPC battery (CPCb) are typical laminar flow CPC and data are provided for smaller sizes depending on the number of supersaturation channels employed. The supersaturations are typically achieved by varying the condenser temperature. The assumption is that two CPCs with different particle size response functions can be described by the particle size with 50 % counting efficiency (cutoff size, D50). And it is assumed that all particles larger than that size are counted, while smaller

particles are not detected. The measured size range of CPCb is often dependent on the number of CPCs employed (each CPC has a different cutoff size), with a lowest particle size detection limit of ~1 nm (Kangasluoma and Attoui, 2019; Kulmala et al., 2007). In practice, the challenges of CPCb measurements include the counting efficiency over a wide size range, the counting efficiency also related composition, and the complex data inversion procedure (Kangasluoma et al., 2020). However, the obvious advantages of the CPCb are its fast response speed and low sensitivity (Kangasluoma and Attoui, 2019).

The PSM is a representative for the mixing-scanning CPC, where supersaturation is achieved by adjusting a specific working flow (Kangasluoma et al., 2016; Vanhanen et al., 2011). The size range for PSM is often between 1 nm and 4 nm depending on the temperature settings (Lehtipalo et al., 2022). In the latest version, the size range can extend from 1 to 12 nm (Sulo et al., 2024). The Airmodus nano condensation nuclei counter (nCNC, model A11) operates as a two-stage CPC, comprising a mixing-type particle size magnifier and a separate CPC (Vanhanen et al., 2011). The instrument is commonly referred to as the PSM. The instrument and schematic diagrams are shown in **Figure 2.2**. In the instrument, an inlet flow rate of 2.5 L min^{-1} (lpm) is mixed with a 0.1-1.3 lpm flow saturated with diethylene glycol (DEG) in a T-shaped chamber. The mixed flow is directed to a condenser, where supersaturation peak occurs, activating particles and growing them to a diameter of approximately 100 nm. The particles grown by DEG in this first stage are transported to a CPC downstream of the condenser, and then further enlarged to detectable sizes using butanol as the working fluid. Adjusting the DEG-saturated flow rate modifies the peak supersaturation in the condenser, thereby altering the cut-off diameter. Size-resolved particle concentrations can be determined using various inversion methods, with cut-off values typically ranging from 1 to 3 nm (Kangasluoma and Attoui, 2019). The disadvantages of PSM include composition-dependent courting efficiency and sensitivity to air mass fluctuations (Lehtipalo et al., 2022).

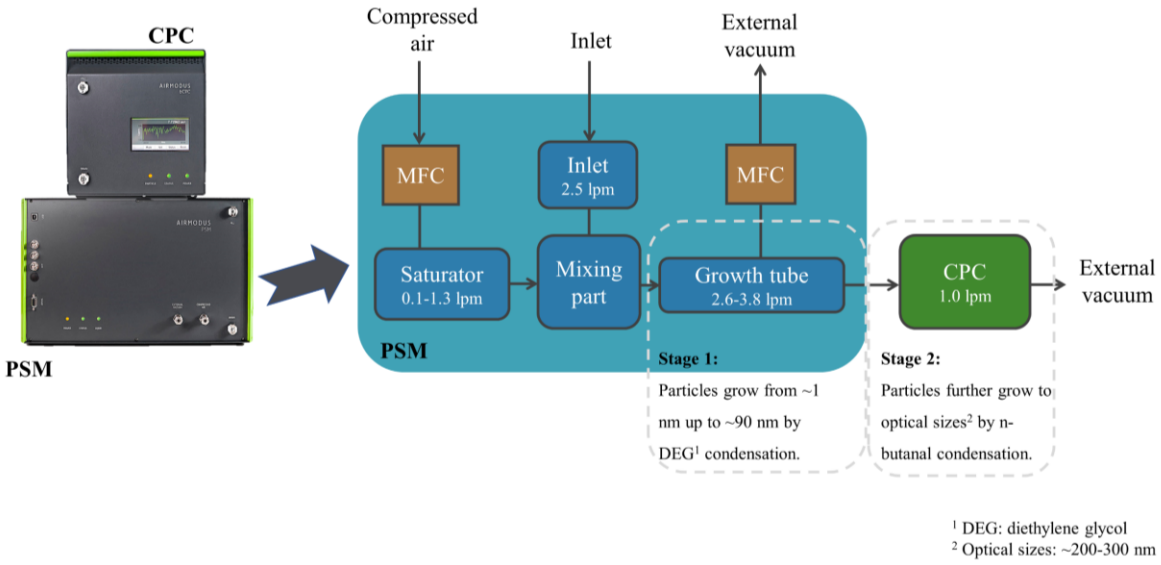

Figure 2.2 Appearance and schematics of the Airmodus nano condensation nuclei counter (nCNC, model A11). The figure integrates concepts based on the user manual.

2.1.2 Mobility-based methods

The mobility-based methods refer to the particle electrical mobility theory. Electrical mobility is a parameter that measures the ability of a particle to move in an electric field. In an electric field E, an aerosol particle carrying n charges is subject to an electric field force, which causes it to move in the suspended gas. The resistance generated on the particle is given by Stokes law, and the particle's electrical mobility can be determined by equating it to the electric field force. The definition of electrical mobility Zp is:

$$Z_p = \frac{neC_c}{3\pi\eta D_{p\_e}}$$

where n is the number of elementary charges on the particles. The e is the elementary charge (1.6022×10^{-19} A·s). C_c is Cunningham slip correction factor, η is the dynamic gas viscosity and D_{p_e} is the particle electrical mobility diameter.

In the mid-1970s, the differential mobility analyzer (DMA) started to be commercialized and hence widely introduced for measuring atmospheric particles (Liu et al., 1978; Tang et al., 1977). The DMA classifies particles based on their electrical mobility, selecting particles of a specific mobility by controlling the electric field within the device, which can then be correlated to particle size. The DMA was later combined with a CPC to form the differential mobility particle sizer (DMPS), significantly improving the size resolution of atmospheric particle size distribution measurements (Knutson and Whitby, 1975). Building on this, Wang

and Flagan (1990) reduced the time resolution to a few minutes in the scanning electrical mobility spectrometer (SEMS; commercialized as the scanning mobility particle sizer, SMPS) by continuously scanning the DMA voltage and counting the particles into size bins.

With the development of CPC and DMA, SMPS systems have been capable of measuring size distributions down to approximately 1 nm over the past two decades (Jiang et al., 2011b; Iida et al., 2009). In order to measure such small particle, the DEG was also employed to initially active the particle, which were then couple with a butanol-based CPC to count the particles. The DEG CPC was later commercialized by TSI as the 3077 nano Enhancer, and when coupled to their soft x-ray charger and 3086 DMA, it become the Nano-SMPS, as shown in **Figure 2.3**. The SMPS provides high size resolution, which depends the sheath-to-aerosol flow rate ratio (Knutson and Whitby, 1975). However, the performance of the SMPS systems is limited by the low charging efficiency in the neutralizer of particles size smaller than 10 nm and by high particle losses (Kangasluoma et al., 2020; Wiedensohler et al., 1986; Fuchs, 1963).

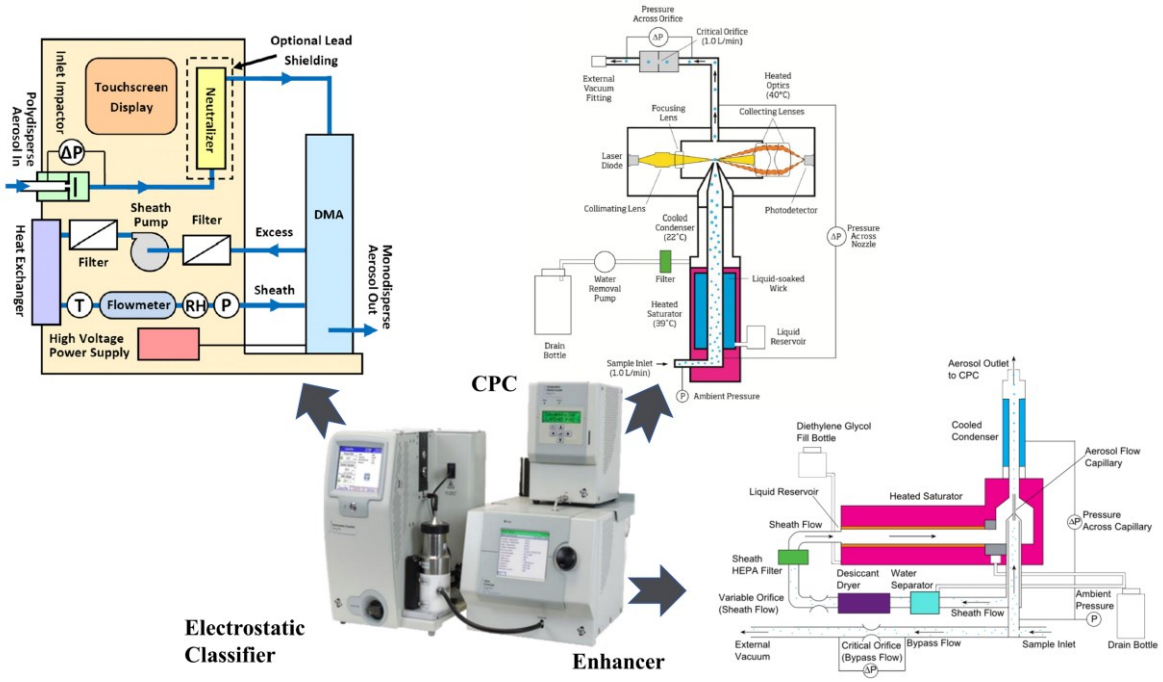

Figure 2.3 Appearance and schematics of the TSI Nano-SMPS system (Electrostatic classifier with DMA, Enhancer and CPC). The figure integrates concepts based on the user manuals.

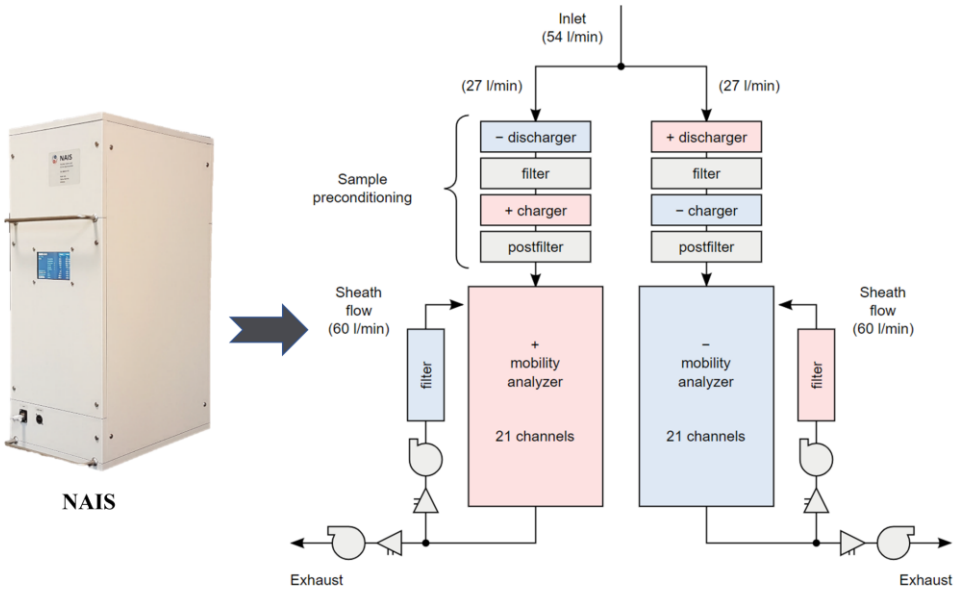

Figure 2.4 Appearance and schematics of the Ariel NAIS. The figure integrates concepts based on the user manual.

In addition to SMPS, various other types of electrical mobility spectrometers (EMS) are also widely used. One representative EMS instrument is the neutral cluster and air ion spectrometer (NAIS), developed by Mirme et al. (2007). As shown in **Figure 2.4**, NAIS employs two multi-channel differential mobility spectrometers to measure the size distribution of both naturally positively and negatively charged ions, as well as particles. Each channel operates at a high flow rate of 27 lpm, giving a total sample flow rate of 54 lpm. The aerosol sample first passes through a charger-filter unit, which allows the instrument to either apply unipolar charging for detecting total particles or leave the sample untouched to detect naturally charged particles (ions). The sample is then classified by mobility in a parallel DMA, where particles are deposited on 21 collecting electrodes. The signals are measured in parallel by 21 highly sensitive electrometers and are processed using a mathematical deconvolution procedure to produce a complete particle size or mobility distribution. The NAIS measurement size range for particles is 2-40 nm, while the size range for ions extends from 0.8 to 40 nm. A limitation of the NAIS at smaller sizes arises from corona charging. Despite filtering excess ions before sizing, some ions can still reach the DMA, making it difficult to differentiate them from charged aerosols smaller than 2 nm (Manninen et al., 2016). However, with the high aerosol flow rate and high sensitivity of electrometers, the concentration detection limits of the NAIS can be lower than of the most advanced SMPS/DMPS systems.

Other methods, such as diffusion battery and inertial separations, are little use beyond initial demonstration (Dubtsov et al., 2017; Arffman et al., 2014). Mass spectrometers, while essential for online cluster measurements and understanding the chemistry processes that lead to atmospheric cluster formation below 2 nm, currently lack sufficient detection methods in the 2-10 nm size range in atmospheric science (Jen et al., 2015; Jokinen et al., 2012; Ehn et al., 2011). The CIMS instrument was employed during the Amazon measurements; however, the data generated by this instrument will not be included in this study until the analysis is complete.

2.2 Field measurement campaign

2.2.1 ATTO campaign

The Amazon Tall Tower Observatory (ATTO) is a 325-meter-tall tower located in the Amazon rainforest (2.1459° S, 59.0056° W, 130 meters above sea level) in Brazil. The nearest city, Manaus, is situated approximately 150 km southwest of the tower, emphasizing the observatory's pristine environment with minimal influence from human activities. Operational since its completion in 2015, ATTO is equipped with comprehensive scientific instruments to measure micrometeorological and atmospheric chemical variables, and their range has continued to broaden over the last few years (Andreae et al., 2015). ATTO is designed to observe and collect data on various atmospheric processes, including greenhouse gases, aerosols, clouds, and meteorological conditions. The site serves as a critical platform for studying the interactions between the Amazon rainforest and the atmosphere. This research is essential for understanding the Amazon's role in global climate processes. Further details on the ATTO site can be found in Andreae et al. (2015).

The Field Experiment in Brazil (CAFE-Brazil) campaign is part of the CAFE series (short for Cloud, Aerosol, and Precipitation Experiment) and represents a major atmospheric research initiative conducted in Brazil (Halo-Research, 2022). The campaign focuses on exploring the interactions between aerosols, clouds, and precipitation in the tropical environment of the Amazon region. This field campaign aims to understand how aerosols and other atmospheric particles influence cloud formation, precipitation processes, and the broader climate system. As part of the tower-based measurements, the campaign primarily targeted aerosol concentrations and properties, with a particular focus on NPF and nucleation mode particles. The field campaign took place from 29 November to 18 December 2022 and from 2 to 26 January 2023, with a total of 20 days in November and December and 25 days in January. The measurements were conducted at the 54-meter platform above the canopy, as shown in **Figure**

2.5. Three instruments were employed for the measurement of ions and neutral aerosol particles with diameters ranging from 1 nm to 40 nm, including a PSM (model A11, Airmodus), a NAIS (Airel), and a SMPS (model 3938, TSI).

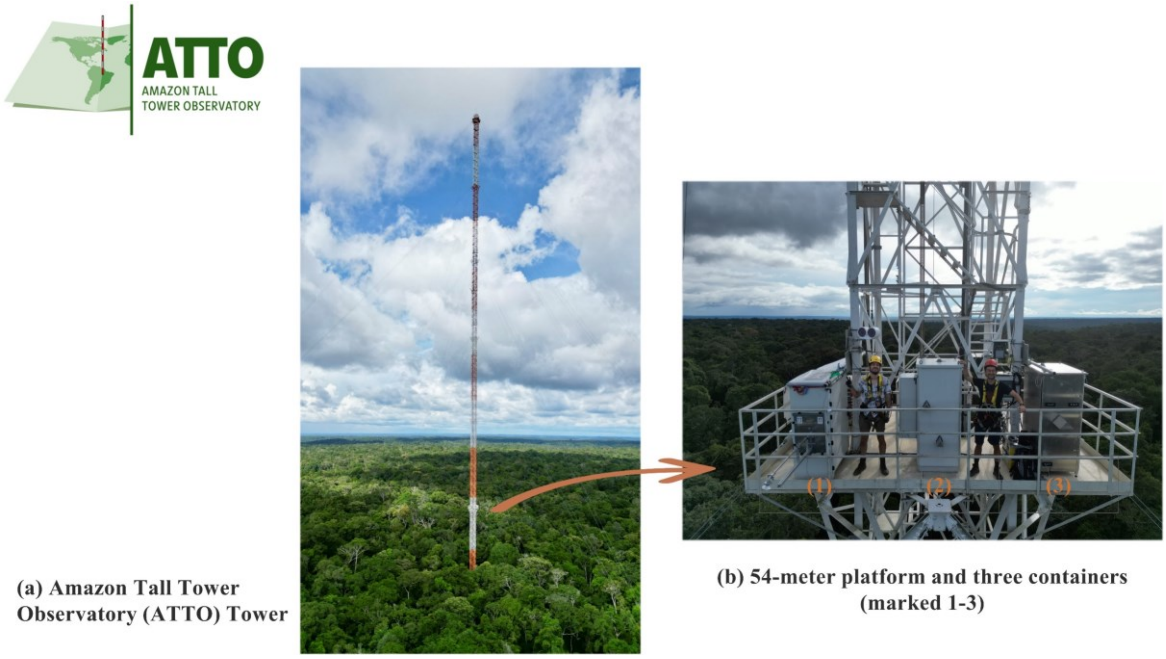

Figure 2.5: An overview of the ATTO measurement site. (a) The full view of the ATTO tower. (b) The 54-meter platform and three containers, from left to right, are equipped with the following instruments: (1) CIMS; (2) Nano-SMPS & PMS; (3) NAIS.

2.2.2 Mainz campaign

The measurements were conducted in the rooftop laboratory of the Max Planck Institute for Chemistry (MPIC) in Mainz, Germany (49°59' N, 8°13' E), as shown in **Figure 2.6**. This observation site at the border of the city is close to residential areas, the city center and roads, representing a typical urban environment. Located less than 200 meters from two busy roads, the site is also affected by traffic emissions. The measurements were recorded continuously between 1 March and 10 July 2022. In this study, three advanced aerosol instruments were employed for the measurement of particle size distributions and concentrations. These included a Nano-SMPS (Model 3938E77, TSI), a PSM (Model A11, Airmodus), and a NAIS (Airel). Additionally, a second SMPS (Model SMPS+C, Grimm) was employed for the measurement of larger particles. A smart weather sensor (Model WS800-UMB, Lufft) was equipped for the monitoring of meteorological data.

Figure 2.6: (a) The rooftop laboratory at the MPIC building and its surroundings. Photos of the instruments in operation in the laboratory (b) Nano-SMPS and PSM. (c) NAIS.

2.2.3 McFAN campaign

The Multiphase Chemistry Experiment on Fog and Aerosols in the North China Plain (McFAN) is a major atmospheric research initiative designed to study the interactions between aerosols, fog, and the multiphase chemical processes occurring in the atmosphere in the North China Plain (NCP), one of the most heavily polluted and industrialized regions in China. The experimental site was located at the Ecological and Agricultural Meteorological Experimental Station of Gucheng, Hebei Province (39°09′ N, 115°44′ E), situated 110 km southeast of Beijing and 35 km northeast of the nearest city, Baoding (as shown in **Figure 2.7**). The station is surrounded by cultivated land, but there were no agricultural activities in the vicinity of the station during the observation period. This station is minimally affected by urban pollution and can therefore represent background pollution conditions for the NCP regime. The campaign was conducted in winter from 12 November to 24 December 2018. During the campaign, a SMPS was employed to measure the PNSD. The SMPS consists of an electrostatic classifier (Model 3082, TSI), an X-ray neutralizer, a differential mobility analyzer (DMA, Model 3081, TSI), and a condensation particle counter (CPC, Model 3772, TSI) capable of measuring mobility-equivalent diameters from 15 to 750 nm. A detailed description of the instruments and an overview of this campaign can be found in Li et al. (2021).

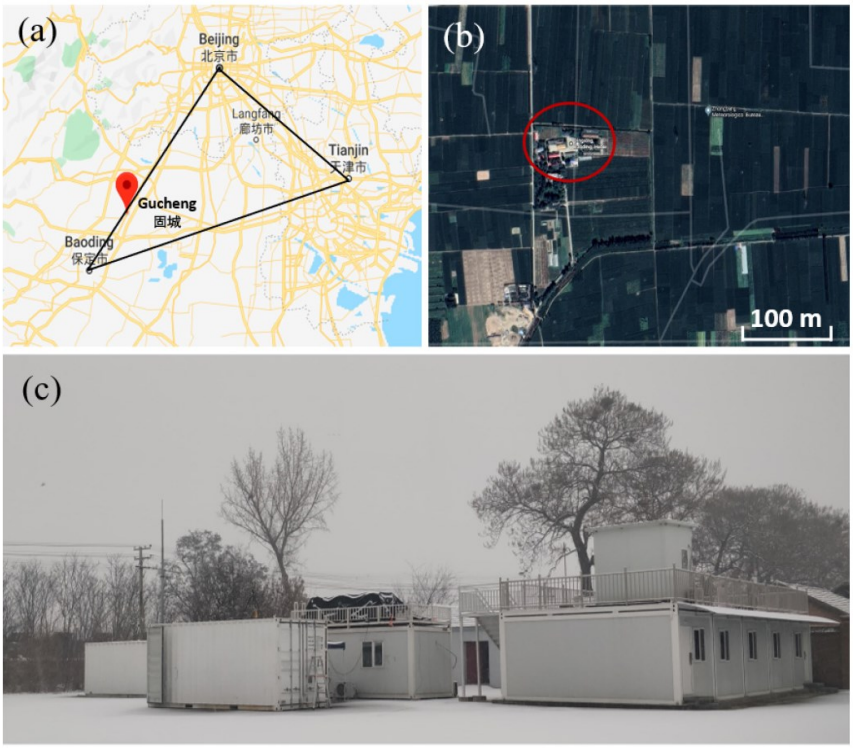

Figure 2.7: (a, b) The geographical location of the site (red dot and circled; © Google Maps) where our field measurements were carried out. (c) The measurement containers in which the sampling instruments were set up. This figure and caption are taken from Hong et al. (2023).

2.3 Instrument calibration

As the standard procedure recommended by Lehtipalo et al. (2022), the calibration of the TSI system (Nano-enhancer 3777 + CPC 3772) and the Airmodus system (A10 PSM + A20 CPC) was conducted prior to each measurement. Additionally, a comparison was conducted to assess the counting efficiency of the CPC between two systems. The schematics of the calibration setup is shown in **Figure 2.8**. During the experiment, tungsten oxide nanoparticles were employed, generated by a WOx generator (model 7860, GRIMM) using tungsten wire. Subsequently, the particles were selected by DMA via fixed voltage, and the number concentrations of these certain size particles were measured by two systems and also a Faraday Cup Electrometer (FCE, model 5705, GRIMM). The selected particle size range is between 1.2 nm and 4 nm. The detection efficiency is calculated by dividing the concentration measured by the TSI or Airmodus systems with the concentration measured by the electrometer. However, in order to achieve a high DMA transfer function (10:1) and to be limited by the DMA sheath flow rate, the number concentration was barely above 1000 (cm^{-3}) during our measurement.

Meanwhile, a DMA with high resolving power (20:1) was recommended in order to achieve a sufficiently monodisperse aerosol population downstream of the DMA (Lehtipalo et al., 2022).

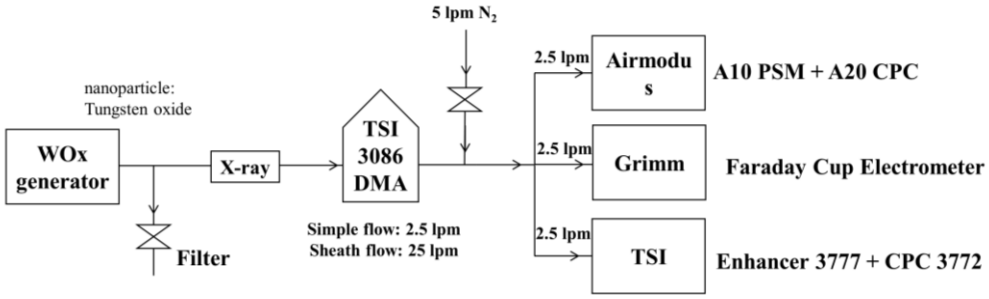

Figure 2.8: Schematic diagram of the calibration setup for the TSI system (Nano-enhancer 3777 + CPC 3772) and the Airmodus system (A10 PSM + A20 CPC).

Chapter 3

3. Atmospheric New Particle Formation in the city of Mainz, Germany

This work is to be submitted as Zhu et al. (2025):

I am the first-author of this work and my contributions include conducting intercomparison experiments, setting up and operating instruments during the measurement periods, performing data analysis, generating all the figures and tables, interpreting and discussing the findings with co-authors, and drafting the manuscript.

The following text, figures, and tables quoted (within"") from page 33 to page 60 are exactly the same as the manuscript which is cited on page 32.

"**Abstract**: New particle formation (NPF) represents a pivotal atmospheric process that exerts a profound influence on aerosol number concentrations and properties, particularly in urban environments where it significantly affects air quality and human health. This study presents measurements of NPF in Mainz, Germany, taken from 1 March to 10 July 2022. The measurements were conducted using advanced aerosol setups that allows the particle number size distributions to be measured down to 1.5 nm. Over the 132-day period, 11 days (8 %) were identified as NPF event days. The key parameters such as formation rates, growth rates (GFs) and condensation sink (CS) were calculated. Observed formation rates ($J \leq 1.5$ nm) during the event days exhibited a range of 0.3 to 11.3 cm^{-3} s^{-1}, with the growth rates (size range 1.5-20 nm) of 1.9 to 6.6 nm h^{-1}. Additionally, the CS values displayed a range of (1.8-6.9) × 10^{-3} s^{-1}. The discrepancies were observed in the sub-10 nm size range, which underscores the importance of comprehensive techniques to accurately capture the dynamics of particles nucleation. Meteorological conditions such as low relative humidity, low wind speed and high solar radiation were conducive to the occurrence of NPF. These findings improve our understanding of NPF in urban environments and highlight the importance of standardized measurements to reduce uncertainties.

Introduction

Atmospheric particles, or aerosols, are defined as tiny solid or liquid particles suspended in the air. They originate from both natural sources, including dust, sea spray, and volcanic eruptions, as well as from human activities such as industrial emissions and vehicle exhaust (Seinfeld and Pandis, 2016). These aerosols play a critical role in the Earth's climate system by influencing both the radiation budget and cloud formation. Aerosols have the capacity to directly scatter or absorb sunlight, thereby exerting an influence on radiative forcing and altering the Earth's overall energy balance (Kanakidou et al., 2005). For instance, aerosols that reflect sunlight assist in cooling the planet by reducing the amount of solar energy reaching the Earth's surface, whereas those that absorb solar radiation contribute to warming by trapping heat in the atmosphere, thereby influencing the overall climate balance (Ipcc, 2022; Myhre, 2009; Charlson et al., 1992) . Additionally, aerosols may also serve as cloud condensation nuclei (CCN), which are essential for the formation of cloud droplets (Bellouin et al., 2020; Merikanto et al., 2009) . The presence and concentration of aerosols can have a significant impact on the microphysical properties of clouds, including their lifetime and reflectivity (Rosenfeld et al.,

2008). This, in turn, can influence regional and global climate patterns. In addition to their environmental impacts, atmospheric particles also pose significant health risks. Fine particulate matter (PM) has been linked to an increased risk of respiratory and cardiovascular diseases, contributing to a major global public health burden (Lelieveld et al., 2019; Pöschl and Shiraiwa, 2015; Lelieveld et al., 2015; Pöschl, 2005).

New particle formation (NPF) in the atmosphere has been the subject of considerable research over the past few decades (Kerminen et al., 2018; Nieminen et al., 2018; Kulmala et al., 2013). NPF refers to the process by which gaseous molecules nucleate into molecular clusters, which then grow through condensation of vapors and coagulation with larger particles (Kulmala et al., 2012). As particles increase in size, they can eventually reach a size sufficient to act as CCN, thereby influencing cloud properties and atmospheric radiative forcing. It is estimated that nucleation is responsible for generating more than half of the global CCN (Zhao et al., 2024; Merikanto et al., 2009). A considerable number of laboratory experiments and field measurements have been conducted with the objective of gaining insight into the fundamental mechanisms of nucleation, the impact of precursor gases and the influence of environmental conditions on the process. Classical nucleation theory identified sulfuric acid as a critical component in this process due to its low vapor pressure and high reactivity (Sipilä et al., 2010). Additionally, ammonia and amines can enhance the stability of sulfuric acid clusters, thereby facilitating their growth through condensation (Yao et al., 2018; Kirkby et al., 2011; Almeida et al., 2013). Furthermore, organic vapors, particularly those derived from biogenic emissions, have been identified as a significant contributor to particle formation and growth (Bianchi et al., 2016; Jimenez et al., 2009; Zhang et al., 2004). The dominant precursor gases and conditions that drive nucleation in different atmospheric environments, such as coastal regions, forests, or urban areas, vary significantly. This leads to diverse particle formation and growth mechanisms. It is therefore essential to gain an understanding of NPF in order to assess its implications for air quality, climate change and human health.

NPF measurements were conducted in a range of European environments, including urban areas, rural forests, coastal regions, and mountain ranges (Kerminen et al., 2018; Kulmala et al., 2013; Manninen et al., 2010; Kulmala et al., 2004). NPF events are more prevalent in rural and remote regions (Nieminen et al., 2018). For instance, in the boreal forests of Finland, where the highest frequency was observed in spring with 47 % of days classified as NPF days (Dada et al., 2018). At the high-altitude site of Jungfraujoch in the Swiss Alps, NPF events were observed on 5 % to 30 % of days (Boulon et al., 2010). In urban areas, the frequency of NPF

is typically lower due to the scavenging of high concentrations of pre-existing particles, acting as a coagulation sink, thereby reducing the likelihood of nucleation (Hong et al., 2023). The occurrence of NPF in urban areas is still relatively common, with studies indicating that it takes place on approximately 5 % to 20 % of days in cities such as Helsinki, Lille, and Copenhagen (Crumeyrolle et al., 2023; Bousiotis et al., 2021b; Nieminen et al., 2018). A high fraction of NPF events has been reported in German background sites, with more than 17 % of days, compared to a lower frequency of approximately 9 % in roadside locations (Bousiotis et al., 2021b). This variability in frequency across different regions underscores the influence of local environmental conditions, precursor gas concentrations, and atmospheric dynamics on the occurrence of NPF events.

In addition to the frequency of NPF, other key parameters for understanding the nucleation process are the formation rate (J) and the growth rate (GF). The nucleation rate, typically expressed in cm^{-3} s^{-1}, describes the rate at which new aerosol particles are produced. The growth rate, expressed in nm h^{-1}, indicates the rate at which these particles grow to larger sizes (Kulmala et al., 2012). Atmospheric measurements show considerable variability in these rates. This variability can be attributed to differences in nucleation mechanisms and precursor vapor concentrations (Almeida et al., 2013; Kirkby et al., 2011; Sipilä et al., 2010), with an increasing number of nucleation mechanisms being proposed based on both laboratory and field measurements. Conversely, the observed nucleation rates are significantly influenced by the employed measurement techniques and there are still considerable uncertainties within the sub-10 nm measurements (Kangasluoma et al., 2020).

A variety of cutting-edge instruments have been developed with the objective of capturing the lowest particle size. Among these instruments, the Nano-SMPS (Nanoparticle Scanning Mobility Particle Sizer), NAIS (Neutral Cluster and Air Ion Spectrometer), and PSM (Particle Size Magnifier) are particularly valuable for the nanoparticle measurement. The Nano-SMPS is capable of measuring the size distribution of particles in the sub-10 nm range (Kuang et al., 2012; Jiang et al., 2011a). while the NAIS provides insights into the size range and charge state of nanoparticles (Manninen et al., 2016; Manninen et al., 2010; Mirme et al., 2007). The PSM enhances the measurement capabilities by enabling the accurate sizing of particles down to ~1 nanometers (Lehtipalo et al., 2022; Vanhanen et al., 2011). However, it is crucial to take into account the potential sources of uncertainty associated with these measurements. These uncertainties have their origins in a number of factors, including instrument calibration, particle losses, and sizing algorithms (Kangasluoma and Kontkanen, 2017; Kangasluoma et al., 2020).

It is of paramount importance to gain an understanding of these sources of uncertainty and to address them in order to ensure the accuracy of nanoparticle measurements and subsequent analysis.

This paper presents the findings of an atmospheric NPF measurement campaign conducted in Mainz between 1 March 2022 and 10 July 2022. A comprehensive suite of instruments, including Nano-SMPS, PSM, and NAIS, was employed to measure particles at sizes as small as 1.5 nm. Over the course of 132 days, the frequency of NPF events was determined, nucleation and growth rates were calculated, and the correlations between NPF and meteorological conditions were investigated. This study offers valuable observational data to understand the underlying mechanisms of NPF in the urban environment and provides a detailed characterization of particle formation in the region.

Methods

2.1 Measurement site description

The measurements were conducted in the rooftop laboratory of the Max Planck Institute for Chemistry (MPIC) building in Mainz (49º59’ N, 8º13’ E, 130 m above sea level), as illustrated in **Figure 1**. The site is situated within a mixed-use area, with the University campus located to the east and farmland to the west, which provides a distinctive contrast between urban and semi-rural influences. Two principal roadways are situated within 200 meters of the measurement location, and the emissions from these vehicles are likely to have exerted a considerable influence on the observation. Additionally, the site's proximity to residential areas and the city center, both within a 3 km radius, classifies it as a representative urban location. Measurements were conducted continuously from 1 March to 10 July, 2022, with only brief interruptions for instrument maintenance and troubleshooting.

2.2 Instrumentation

In this study, three advanced aerosol instruments were employed for the measurement of particle size distributions and concentrations. These included a 1 nm Scanning Mobility Particle Sizer (Nano-SMPS, Model 3938E77, TSI), a Nano Condensation Nucleus Counter (nCNC, Model A11, Airmodus), and a Neutral Cluster and Air Ion Spectrometer (NAIS, Airel).

The 1 nm SMPS system is composed of several components, including an electrostatic classifier (Model 3082, TSI), a 1 nm differential mobility analyzer (DMA, Model 3086, TSI), a Nano Enhancer (Model 3777, TSI), and a condensation particle counter (CPC, Model 3772,

TSI). This configuration permits precise measurement of aerosol particles with diameters down to 1.5 nm. The instrument operates with a sample flow rate of 2.5 liters per minute (lpm) and a sheath flow of 15 lpm, enabling the measurement of particle sizes ranging from 1.5 to 38.5 nm.

The Airmodus A11 nCNC system, which consists of a particle size magnifier (PSM, Model A11, Airmodus) and a CPC (Model A20, Airmodus), has been developed to enable the measurement of the size distribution of particles within the critical size range of 1.5 to 3 nm, as well as the total concentration of sub-micron aerosol particles. The Airmodus A11 employs a Kelvin-effect-based particle activation process, whereby particles are subjected to a high saturation ratio through the mixing of cooled sample air, with heated diethylene glycol (DEG)-saturated clean air. This process causes nanoparticles to grow through condensation to approximately 90 nm in diameter, thus enabling their detection by the CPC. This system is particularly useful to capture the earliest stages of particle formation that occur during NPF events.

The Neutral Cluster and Air Ion Spectrometer (NAIS) is equipped with the capability to detect both the mobility distribution of ions and the size distribution of neutral aerosol particles. The NAIS comprises two unipolar corona needle chargers and two DMA columns, within which a series of electrometers have been positioned at the inner surface. The design is based on a large inlet flow rate, which serves to overcome the electrical noise present in the electrometers. The instrument measures ion mobility distributions within a range from 3.2 to 0.0014 $cm^2/V/s$, corresponding to particles of a size between 0.8 and 40 nm. With regard to neutral aerosols, the NAIS provides size distribution measurements between 2 and 40 nm.

Additionally, a second SMPS (Model SMPS+C, Grimm) was utilized for measurements of larger particles. The system comprised a SMPS (Model 5420, Grimm) coupled with a CPC (Model 5416, Grimm). The sample and sheath flow rates were set to 0.3 L min^{-1} and 3.0 L min^{-1}, respectively. The measured particle size range was between 5 and 350 nm, using both upward and downward scanning modes.

A smart weather sensor (Model WS800-UMB, Lufft) was equipped to monitor the meteorological data, including air temperature, relative humidity, precipitation intensity, solar radiation, air pressure, wind direction and wind speed.

2.3 Inlet details and losses correction

All instruments (with the exception of the Grimm SMPS) were positioned in close proximity to the laboratory outer walls, with the aerosol inlet situated at a height of 2.5 meters above the floor at the window, in order to facilitate the optimal sampling of ambient air. To minimize particle losses due to deposition of inlet tube and ensure the comparable nano-particle size measurements, the Nano-SMPS and Airmodus A11 nCNC systems shared the same inlet. To further minimize particle losses within the inlets, the total length of the inlet tube was kept short at 1 meter, and the sample flow rate was maintained at 5 lpm. The NAIS employed the original inlet tube, with a total sample flow rate of 54 lpm. The inlets for all three instruments, including the NAIS, were positioned in parallel, enabling simultaneous, high-quality measurements of particle number size distributions.

The Grimm SMPS, utilized for larger particles, sampled air from a nearby analytical system, where a 4-meter-long inlet tube was equipped with a 48 cm corrugated stainless-steel shell Nafion dryer to reduce the sample relative humidity to below 20 %. Subsequently, the sample was conveyed through a 4-metre inlet tube prior to distribution via a 1-to-4 splitter to the designated instruments, with a total inlet flow rate of 4.7 L min^{-1}.

To account for potential losses during sampling, a particle loss calculation software tool was employed that calculates size-dependent transmission efficiencies. This software takes into consideration aerosol diffusion and deposition, as well as turbulent inertial deposition and deposition at bends or constrictions in the inlet tube (Von Der Weiden et al., 2009). The size-dependent transmission efficiency curve, as shown in **Figure S1**, was used to correct all particle number concentration data obtained by the Nano-SMPS, PSM and Grimm-SMPS. This correction ensures that the reported concentrations better reflect the actual particle numbers in the ambient air.

2.4 Instrument intercomparison

Both the TSI system (Nano-enhancer 3777 + CPC 3772) and the Airmodus system (A10 PSM + A20 CPC) first employed the DEG supersaturated vapor to grow the particles, followed by the addition of butanol to enlarge the particles to a size sufficient for counting by the optical detector. The cutoff size determined by DEG supersaturated vapor was an essential factor for both systems. To assess the preference of the two systems, a laboratory intercomparison was conducted before and after ambient measurements. The procedure was similar to that used by Kangasluoma et al. (2015), in which a WOx generator (model 7860, GRIMM) was employed to generate the tungsten particles. Then the particles with certain size were selected by DMA,

and the number concentration of the selected particles was measured simultaneously using both systems. The tungsten particle size range during our experiment was between 1.5 nm and 4 nm. **Figure S2** shows the intercomparison results between two systems. The measured number concentration between two systems matched well, with R^2 value is 0.9972. However, due to the different chemical compositions of particles, the performance of the instrument may be different under the ambient condition (Lehtipalo et al., 2022).

2.5 NPF event classification

The categorization of days as either NPF events, non-events, or undefined days can be achieved through the analysis of particle size distributions as a function of time. In accordance with the criteria set forth by Kulmala et al. (2012) , three characteristics must be taken into account to categorize a day as an NPF event day. 1) A discernible increase in particle concentration within the nucleation mode, particularly for particles below 25 nm in diameter; 2) The emergence of distinctive nucleation patterns, typically manifested as distinct, sustained patterns that persist for several hours, suggesting that nucleation is a continuous process; 3) The observable growth of these nucleated particles over several hours, as they transition to larger sizes through the condensation of vapors.

In the absence of any of the aforementioned features, the day is classified as a non-event day. In days that only some of the aforementioned features are observed, or if the evidence is ambiguous, the day in consideration is classified as undefined. If all the requisite features are observed on a given day, it is identified as an event day. The occurrence of undefined days may be attributed to atmospheric conditions that are not conducive to sustained particle growth, or to partial interference from local sources, which impedes the ability to distinguish regional NPF processes. The detection of regional new particle formation is contingent upon the presence of stable air masses that remain constant throughout the growth phase of nucleated particles. The disruption of these processes may occur as a result of changes in wind direction or atmospheric mixing. Furthermore, local sources, such as traffic emissions, industrial activity, or biomass burning, have the potential to obscure or overlap with regional NPF signatures, thereby complicating the classification.

2.6 Growth rate (GR)

The observed particle growth rate (GR) is determined by calculating the rate of change in diameter of the growing particle population, based on the following formula:

$$GR = \frac{d_{p2} - d_{p1}}{t_1 - t_1}$$

where dp1 and dp2 are the representative particle diameter at times t1 and t2, respectively. Two commonly employed methods for determining representative particle diameters are the maximum-concentration method and the log-normal distribution function method. The growth rate can be calculated for the entire duration of the particle formation event, or for specific time or size windows. Particle size windows are commonly used to categorize particles according to their diameter. These include windows with diameters less than 3 nm, between 3 and 7 nm, between 7 and 20 nm, and greater than 20 nm (Kulmala et al., 2012).

2.7 Formation or nucleation rate (J)

The formation rates of particles were calculated from particle number size distribution data using the method presented by Kulmala et al. (2012):

$$J_{dp} = \frac{dN_{dp}}{dt} + CoagS_{dp} * N_{dp} + \frac{GR}{\Delta d_p} * N_{dp} + S_{losses}$$

where N_{dp} indicates the particle number concentration in the size range [dp, dp+Δdp]; GR is corresponding growth rate; S_{losses} includes additional losses; $CoagS_{dp}$ represents the size distribution-dependent particle loss parameter and particle with diameter dp can be calculated from the measured size distribution:

$$CoagS_{dp} = \sum_{d'_p = d_p}^{d'_p = max} K(d_p, d'_p)\, N_{d'_p}$$

Where K (dp,dp') represents the coagulation coefficient of particle sizes dp and dp'. Here dp accounts the smallest particle size detected by particle size spectrometer and the values are 3 and 1.5 nm for Nano-SMPS/NAIS and PSM measurement, respectively. The upper size limits depend instruments, which is 7 nm for Nano-SMPS/NAIS and 3 nm for PSM.

The coagulation coefficient K (dp,dp') can be derived from kinetic theory, and it's influenced by Brownian motion, but can also be approximated by the following equation:

$$K(d_p, d'_p) = \frac{2k_B T}{3\mu}\left(\frac{d_p + d'_p}{d_p d'_p}\right)$$

Where k_B is Boltzmann's constant (1.380649×10^{-23} m^2 kg s^{-2} K^{-1}); T represents the absolute temperature in Kelvin; μ accounts the dynamic viscosity of the surrounding medium, here we

used the reference value taken from Kim et al. (2005) which is 1.83245 × 10-5 kg s^{-2} K^{-1} for air.

2.8 Condensation sink

The condensation sink describes the condensing vapor sink caused by the particle population and was calculated from particle size distribution data using the method described by Kulmala et al. (2012):

$$CS = 2\pi D \sum_{d_p'} \beta'_{m,dp}\, d_p' N_{d_p'}$$

Where D is the diffusion coefficient of condensing vapor, normally assumed sulfuric acid which also used in the case here; N_{dp} is the particle number concentration with diameter dp;

βm represents the transitional correction factor:

$$\beta_m = \frac{1 + K_n}{1 + 0.337K_n + \frac{4}{3}\alpha^{-1}K_n + \frac{4}{3}\alpha^{-1}K_n^2}$$

$$\beta_m = \frac{1 + K_n}{1 + 1.677K_n + 1.333K_n^2}$$

Where Kn denotes Kundsen number defined as a function of the gas mean free path λ and particle diameter dp (Kn = 2 λ/dp). α stands for the accommodation coefficient. When calculating the value of CS, there is an assumption that the accommodation coefficients for mass and heat transfer are unity.

The diffusion coefficient D (m^2 s^{-1}) can be estimated using the Stokes-Einstein equation:

$$D = \frac{k_B T}{3\pi\mu D_p}$$

Results and discussion

Figure 2 shows the time series of meteorological parameters and aerosol properties observed during this observation. **Figure 2a** shows the wind speed and direction; **Figure 2b** shows temperature and relative humidity (RH); **Figure 2c** shows solar radiation intensity; **Figure 2d** shows the PNSD in the size range of 1.5-350 nm, where 1.5-3 nm is from the measurement of PSM, 3-38.5 nm is from the measurement of Nano-SMPS, and 38.5-350 nm is from the measurement of Grimm-SMPS; **Figure 2e** shows total particle number concentration from the PSM and calculated condensation sink (CS). The wind speeds in this study were typically

below 5 m s^{-1}, with a median value of 1.9 m s^{-1}. Low wind speeds usually indicate stagnant meteorological conditions with limited dilution of air pollutants at the current location. The southeast winds prevailed, with strong winds mostly from the northwest. The temperature and RH showed opposing daily variations over the observation period. The lowest temperature was 0 °C while the highest temperature was 34.9 °C. The median values of temperature and relative humidity were 15.0 °C and 58.6 %, respectively. The mean value of solar radiation was 255.8 W m^{-2} during the day.

3.1 Particle number size distribution

The particle number concentrations measured across different instruments and in different size ranges are listed in **Table 1**. During the entire measurement period, the median total particle number concentration in Mainz based on PSM measurement was 12279 cm^{-3}. On event days, the total number concentration was 50 % higher than on non-event days. The Nano-SMPS with the particle size range of 1.3-38.5 nm recorded the number concentration of 4936 cm^{-3} over the entire period, and the Grimm-SMPS with the particle size range of 5-350 nm measured the particle number concentration of 5099 cm^{-3}. The median particle number concentrations recorded by the NAIS was 7896 cm^{-3} in the negative mode, and 9062 cm^{-3} in the positive mode. According to Manninen et al. (2016), total number concentration for negative and positive results should typically agree within a range of 10-20 %. Our measurements show a good agreement between the two NAIS channels.

Compared to some other cities in Germany like Dresden and Leipzig, the median number concentrations of 20 to 800 nm particles were 8400 to 9000 cm^{-3}, respectively (Birmili et al., 2016). In some other Europe cities, such as Helsinki and London, the measured number concentrations of 8 to 700 nm particles were often around 7000 cm^{-3} (Von Bismarck-Osten et al., 2013). However, in some highly polluted cities, such as Beijing and Delhi, these values can be as high as 20000 to 40000 cm^{-3} (Gani et al., 2020; Wang et al., 2013). Particle number concentrations in cities can be highly variable due to a number of factors such as traffic density, industrial activities, weather conditions, and local geography.

The particle number concentration measured by the Nano-SMPS was significantly lower at 4,936 cm^{-3}, which difference of up to 45 % compared to the NAIS values. NAIS has been reported to detect particle number concentrations several times higher than those measured by SMPS, particularly for particles smaller than 10 nm. In some cases, the difference can be a factor of 10 or more (Kangasluoma et al., 2020). The main reason for this difference is the

sensitivity of in the instruments to different size ranges, particularly for particles smaller than 10 nm. The higher particle number concentrations reported by NAIS can be attributed to its better sensitivity in the sub-10 nm range, where nucleation mode particles dominate during NPF events (Manninen et al., 2016). In our data, the main difference between the results of the two instruments was indeed concentrated within this size range.

Figure 3 shows the median particle size distribution for the different instruments over the entire measurement period. The results showed that for particle sizes above 10 nm, the NAIS and SMPS measurements were in agreement, with differences of 10-40 %. However, for particle sizes smaller than 10 nm, the uncertainty increased significantly, up to a factor of 2 or more. The previous studies on ambient measurement showed that the NAIS detected a size distribution function in the sub-10 nm size range that was a factor of 2-8 higher than that measured by two DMPS systems (Kangasluoma et al., 2020). There were also significant differences between NAIS negative and positive results for the sub-3 nm range, especially at 2.3 nm. This may be due to the corona-generated ions, as the lowest detection limit of NAIS varies depending on the environmental conditions (Manninen et al., 2016). Between 2-3 nm, there are some overlaps between PSM and NAIS, with PSM data showing the highest concentration. Possible reasons could be that the particle composition (Lehtipalo et al., 2022), or that PSM can also measure neutral particles in this range. Below 2 nm, PSM shows reasonable values, since other instruments cannot obtain the size distribution in this range. Overall, we have shown that the particle size distributions between the different instruments are in good agreement with a reasonable discrepancy.

3.2 New particle formation

The monthly frequency distribution of NPF events in Mainz is presented in **Figure 4**, with a detailed daily classification shown in **Table S1**. During the measurement period, 11 days (8 %) were classified as NPF event days, 40 days (30 %) as non-event days and 81 days (61 %) as undefined days. The frequency of NPF events ranged from 3 % to 10 % over the five months, while non-event and undefined days accounted for 19 % to 42 % and 48 % to 71 % of the days, respectively. In our study, more than 50 % of the days were classified as undefined. This is largely due to the fact that on these days, the nucleation mode was detected but did not show sustained growth or only grew briefly. **Figure S2** illustrates the PNSD on typical undefined days. In general, no burst of sub-3 nm clusters or clear particle growth was observed during the undefined days, indicating that these particles are unlikely to have originated from gas phase nucleation (Hong et al., 2023). Undefined days often signal particle formation processes driven

by local or point sources, such as traffic exhaust, rather than regional NPF events (Kulmala et al., 2012).

The frequency of NPF occurrences varies among locations and at different times of the year. In urban areas, NPF events can occur several times a week, especially in areas with high air pollution and high concentrations of precursor gases such as sulfur dioxide (SO_2) and volatile organic compounds (VOCs). For instance, annual averages of NPF frequency range from 11 % in Helsinki to over 60 % in heavily polluted areas like Beijing and Marikana (Nieminen et al., 2018). In the vicinity of Lille, a study reported an 11 % frequency of NPF events between 2017 and 2022 (Crumeyrolle et al., 2023). Similarly, urban background locations like Leipzig had an NPF frequency of 17 %, while roadside measurements in the same city were only 9 % (Bousiotis et al., 2021b). In remote regions, the frequency of NPF is lower but still noteworthy, usually occurring a few times per month. For example, the high-latitude site at Alert, Canada, reported NPF frequencies of only 5.1 % (Brean et al., 2023), and no NPFs were observed in the Amazon rainforest (Artaxo et al., 2022). This highlights the variability of NPF occurrence, which is influenced by local conditions, pollution levels, and the availability of precursor gases.

Figure 5 illustrates a typical NPF event observed on 25 March. The event started around 10:00 am (UTC) and was marked by a significant increase in particle number concentrations. The total particle number concentration larger than 1.5 nm peaked at 11:30 am and was approximately 4.1×10^4 cm^{-3}. At the same time, the particle number concentration of the two SMPS systems coupled (covering the 3-350 nm size range) also peaked at around 3.1×10^4 cm^{-3}. During this period, a significant burst of sub-3 nm cluster concentrations was also observed, with concentrations rising to nearly 1.5×10^4 cm^{-3}, signaling the beginning of an active nucleation event. The sharp rise in sub-3 nm clusters concentrations is strong evidence for the rapid nucleation of gaseous precursors, which is also a feature of the NPF.

At the same time, the CS value, which quantifies the rate of condensation of vapor on pre-existing particles, exhibited a rapid decrease during the NPF event. This decrease in the CS value reflects the predominance of newly formed particles with smaller surface areas, which are less efficient at scavenging condensable vapors compared to larger pre-existing particles. These newly nucleated particles were numerous, so more vapor was available for condensation and further growth of the particles. The average CS value for this NPF event day was 0.0055 s^{-1}. As the event progressed, particles larger than 3 nm in diameter began to grow through condensation and coagulation, forming the characteristic "banana shape" in the PNSD, as shown in **Figure 5a**. This shape is a well-known feature of NPF events and represent the growth

process of newly nucleated particles as they accumulate condensable vapors and increase in size.

For all the identified NPF events, the calculated formation rate at 1.5 nm ($J_{1.5}$) and growth rate (GR) are summarized in **Table 2**. Growth rates for the 1.5-3 nm, 3-7 nm, and 7-20 nm size intervals were evaluated to investigate potential size-dependent trends and to facilitate comparisons with other studies (Stolzenburg et al., 2023). The GR for the 1.5-3 nm, 3-7 nm, and 7-20 nm size ranges were 7.3, 6.5, and 2.4 nm h^{-1}, respectively, as of 25 March 2022. The overall GR for particles in the 1.5-20 nm range was calculated as 3.0 nm h^{-1}. In contrast, at two other locations in Germany, Melpitz and Hohenpeissenberg, the GR measured in the 1-3 nm range was 2.6 and 4.8 nm h^{-1}, respectively (Manninen et al., 2010). Globally, nanoparticle growth rates are generally reported within the range of 1-10 nm h^{-1} (Nieminen et al., 2018; Kerminen et al., 2018). These GR values are not only highly variable between locations, but also within the same location across different seasons. This variability is driven by multiple factors, including the type and concentration of local precursor vapors, the intensity of photochemical activity, and the levels of condensation and coagulation sinks, all of which influence particle growth behavior (Stolzenburg et al., 2023).

The calculated CS values during NPF events in Mainz ranged between 1.8×10^{-3} and 6.9×10^{-3} s^{-1}, while the formation rate at 1.5 nm (J1.5) varied from 0.27 to 11.17 cm^{-3} s^{-1}. In comparison, reported CS values at other sites in Germany, such as Melpitz and Hohenpeissenberg, were 8.4×10^{-3} s^{-1} and 4.1×10^{-3} s^{-1}, respectively, with corresponding J2 values of 22.4 and 3.0 cm^{-3} s^{-1} (Manninen et al., 2010). These values suggest that the NPF at Mainz occurred under relatively moderate CS conditions. In rural areas, CS can be considerably lower due to fewer pre-existing particles. For example, in the Jungfraujoch, a remote high-altitude site, the CS has been reported as low as 5.9×10^{-4} s^{-1} (Manninen et al., 2010). In such environments, the reduced CS allows for a higher availability of nucleating vapors, resulting in enhanced conditions for NPF. However, even with low CS values, nucleation rates can remain relatively low, as indicated by the J3.2 nm values of 0.2 to 1.5 cm^{-3} s^{-1} at Jungfraujoch (Bianchi et al., 2016). Similarly, at the Hyytiala site in Finland, the measured CS was 1.5×10^{-3} s^{-1}, with a corresponding J2 of 5.9 cm^{-3} s^{-1} (Kulmala et al., 2013).

In general, the particle formation rate is inversely proportional to the CS value, as the higher CS values result in faster scavenging of nucleation precursors or small clusters, thereby limiting the available vapors for nucleation. Under these conditions, the rate of nanoparticle formation slows down, resulting in a lower nucleation rate. However, in highly polluted megacities such

as Beijing, Nanjing, and Shanghai, CS values are typically one or two orders of magnitude higher (on the order of 10^{-2} s^{-1}) than in less polluted regions, where CS values are typically around 10^{-3} to 10^{-4} s^{-1} (Hong et al., 2023; Zhou et al., 2021; Kerminen et al., 2018; Herrmann et al., 2014). Despite these elevated CS values, which would normally suppress NPF, particle formation rates in these urban environments can still exceed 100 cm^{-3} s^{-1} (Dai et al., 2017; Xiao et al., 2015). The paradox of high particle formation rates occurring alongside elevated CS can be explained by the abundance of nucleating precursors in these highly polluted atmospheres (Yan et al., 2021; Xiao et al., 2015). Studies measuring or calculating sulfuric acid concentrations in these regions have shown the availability of sulfuric acid and other precursors is sufficient to maintain NPF even under high CS conditions (Zhou et al., 2021; Cai et al., 2021). This suggests that the high precursor concentrations essentially "overwhelm" the scavenging effects of the condensation sink, allowing for efficient nucleation despite the presence of large number of pre-existing particles. These comparisons between different sites highlight the complex interplay between CS and nucleation rates, which vary significantly depending on the local atmospheric conditions.

3.3 Diurnal variation patterns of particles

The diurnal patterns of meteorological parameters (temperature, relative humidity, wind speed, and solar radiation), particle number concentration across different size ranges, and the calculated CS for event, non-event, and undefined days are presented in **Figure 6**. On event days, temperatures were generally higher compared to on non-event days, exhibiting the typical diurnal upward trend with a peak around 14:00-15:00 (UTC time, same as below). Lower temperatures generally favor NPF because lower temperatures enhance condensation, stabilize nucleating clusters, and reduce the loss of nucleation vapors to pre-existing particles (Xiao et al., 2021). However, the temperature difference between event and non-event days in this study was relatively modest, amounting to approximately 4 °C. Meanwhile, studies conducted in Lille and Beijing have observed temperatures that are even higher during NPF event days, suggesting that temperature itself may not be a straightforward indicator of NPF activity (Crumeyrolle et al., 2023; Zhou et al., 2021). During our measurement period, NPF was observed over a wide range of temperatures from 6 °C to 30 °C. This suggests that, while lower temperatures may enhance nucleation, NPF is not strictly limited to cooler conditions.

The relationship between RH and temperature is inversely proportional, with the lowest humidity levels occurring at approximately 14:00. The lowest recorded RH values were 35 % and 49 % on days with and without events, respectively. By the time the RH reached its peak

at 04:00, the RH values on event and non-event days were comparable, with both exhibiting a value of approximately 76 %. It is commonly accepted that elevated RH levels facilitate NPF by stabilizing nucleation clusters, promoting condensation and aiding particle growth through water uptake (Stolzenburg et al., 2023). However, the findings of this study indicate that RH was lower on NPF event days compared to non-event days. This observation is consistent with the results of several other studies, where lower RH levels during NPF events have been reported (Hong et al., 2023; Crumeyrolle et al., 2023; Zhou et al., 2021; Größ et al., 2018). One potential explanation for this discrepancy is that, the lower RH may coincide with higher solar radiation, which drives photochemical reactions necessary for nucleation, thereby compensating for the lower humidity. Additionally, lower RH tends to occurs under stable atmospheric conditions, which may further promote NPF.

The wind speed exhibited a general increase during the morning, reaching a peak around noon. Although the maximum wind speed observed on both event and non-event days was comparable, reaching approximately 3 m s^{-1}, wind speeds during the remainder of the day were consistently approximately half as high on event days compared to non-event days. This reduction in wind speed is a key factor in maintaining NPF, as a lower wind speed helps to maintain a stable air mass and minimizes dilution (Kulmala et al., 2012). Previous studies have consistently demonstrated that low wind speeds are a characteristic of NPF events, providing support for the assertion that calm meteorological conditions are conducive to particle formation (Crumeyrolle et al., 2023; Hong et al., 2023)

Following sunrise, solar radiation increased until reaching a peak at noon. On event days, the maximum value of 720 W m^{-2} were recorded, while on non-event days, the maximum value of 564 W m^{-2} were observed. Solar radiation remained consistently higher on event days than on non-event days throughout the remainder of the day. The elevated solar radiation levels during event days are likely to a critical role on the enhancement of NPF by driving photochemical reactions that generate nucleating vapors, such as sulfuric acid, and by increasing the atmospheric oxidation capacity (Wang et al., 2023). This direct link between solar radiation and NPF is consistent with the findings of previous studies, which identified a positive relationship between increased solar radiation and the frequency of NPF events (Hong et al., 2023; Bousiotis et al., 2021a; Zhou et al., 2021)

The number concentration of particle with a diameter between 5 and 350 nm exhibited a gradual increase throughout the day on event days, reaching a peak around 20:00. This pattern is typical of NPF events, whereby nucleated particles emerge around noon and undergo further

growth during the afternoon and evening, ultimately becoming the larger-sized particles. In contrast, during non-event days, the particle number concentration was typically higher during the night and decreased in the morning, remaining relatively stable throughout the day due to the absence of the NPF. The absence of fresh particle formation on non-event days results in concentrations being influenced to a greater extent by local sources and existing background aerosols, as opposed to the burst of new particles that are typically observed during NPF. The particle number concentration on event days was 2-3 times higher than on non-event days.

The number concentration of sub-3 nm cluster showed a pronounced increase from around 10:00 on the event days, peaking shapely at approximately 13:00 before declining rapidly by 18:00. This temporal pattern is characteristic of NPF events, where nucleation occurs in the late morning, driven by all meteorological factors and precursors, leading to a burst of new particles. In contrast, on non-event days, there was only a slight increase in sub-3 nm particle concentrations, indicating that nucleation processes were absent and it could contribute by the vehicles emission (Stolzenburg et al., 2023). The peak concentration observed during NPF events was over four times higher than that recorded on non-event days. The pronounced increase in sub-3 nm particles is a key indicator of NPF, as these ultrafine particles represent the initial stages of new particle formation. The rapid growth and subsequent decline of these clusters during the day suggest that the nucleation phase is highly dynamic, with particles either growing rapidly to larger sizes or being scavenged by pre-existing aerosols.

The calculated CS exhibited a comparable trend to that of the particle number concentration between 5 and 350 nm, showing a slight increase during the daytime and reaching a peak in the early night. It is noteworthy that CS values were higher on days on which events occurred, in comparison to days on which no events took place. Generally, a lower CS is associated with conditions that favor cluster formation and NPF, as fewer pre-existing particles are available to scavenge the nucleating vapors. However, as has been observed in previous studies (Hong et al., 2023; Yan et al., 2021), high CS values can sometimes coexist with NPF events. This indicates that particle growth and nucleation can still occur in environments with elevated aerosol loads, although this may depend on other factors such as vapor production rates and meteorological conditions.

Overall, the meteorological variables - such as low RH, low wind speed, and high solar radiation - frequently act in conjunction to create favorable conditions for NPF. High solar radiation level drives photochemical reactions that produce nucleating vapors, while low RH and wind speed limit dilution and provide a stable environment for particle growth. The

combination of these factors highlights the importance of considering both aerosol and meteorological dynamics in order to gain an understanding of NPF processes, especially in the context of varying environmental conditions.

Conclusions

In this study, Mainz was selected as a representative urban city in Germany and three advanced aerosol measurement instruments were employed, including the TSI Nano-SMPS, Airmodus PSM, and Ariel NAIS, which can measure the particle number size distributions from 40 nm down to 1 nm. The measurement period spanned from 1 March to 10 July 2022, a total of 132 days. Based on the NPF event days, several parameters were calculated, including formation rates (J≤1.5 nm), growth rates (GFs), and condensation sink (CS). Additionally, meteorological differences between event and non-event days were also analyzed.

Throughout the measurement period, 11 days (8 %) were classified as NPF event days, 40 days (30 %) as non-event days, and 81 days (61 %) as undefined days. The total sub-3 nm particle number concentrations were 2564 cm^{-3} and 1343 cm^{-3} for event and non-event days, respectively. The sub-40 nm particle concentrations measured by the NAIS were 10405 cm^{-3} and 6384 cm^{-3} for event and non-event days, respectively, while the Nano-SMPS reported 7749 cm^{-3} and 3722 cm^{-3}. A comparison of the overall PNSDs of the two instruments showed that the main differences were observed in the sub-10 nm range.

During event days, the formation rates (J1.5 nm) exhibited a range of 0.27 to 11.17 cm^{-3} s^{-1}. These values were found to be significantly lower than those observed in certain megacities, but exhibited a slight increase when compared to remote areas. The GFs between 1.5 and 20 nm ranged from 1.9 nm h^{-1} to 6.6 nm h^{-1}, and the size intervals of GFs (1.5-3 nm, 3-7 nm, and 7-20 nm) for each event day were also obtained. The calculated CS values ranged between 1.8 and 6.9 × 10^{-3} s^{-1}. Furthermore, favorable conditions for NPF were found to be associated with specific meteorological variables, including low relative humidity, low wind speed, and high solar radiation. Significant differences in these parameters were observed between event and non-event days.

Our findings provide valuable insights into the behavior of ultrafine particle dynamics in urban environments and contribute to a better understanding of the factors influencing NPF in European cities. These findings underscore the necessity of employing a comprehensive array of instrumentation to mitigate uncertainties in sub-10 nm aerosol measurements, thereby facilitating a more consistent characterization of NPF processes.

Table and Figure

Tables

Table 1. Summary of measured particle number concentration by each instrument across different size ranges. The numbers present median values and the 25th -75th percentiles are in brackets.

Instrument	Size range (nm)	Concentration (cm^{-3})			
		All period	Event days	Non-event days	Undefined days
PSM	1.5-1000	12279 (8511-18237)	15556 (10765-21893)	10161 (7524-14213)	13126 (8998-19513)
	1.5-3	1619 (705-3380)	2564 (1107-5642)	1343 (591-2715)	1695 (733-3511)
	3-1000	9710 (6856-13948)	13133 (8971-17478)	8145 (6062-10920)	10442 (7183-14868)
NAIS	2-42 (negative)	7896 (5348-12055)	10405 (7146-15950)	6384 (4572-8987)	8553 (5729-13191)
	2-42 (positive)	9062 (5967-14080)	12472 (8440-18895)	7206 (5055-10390)	9802 (6418-15407)
Nano-SMPS	1.3-38.5	4936 (3026-8187)	7749 (4458-12259)	3722 (2367-5668)	5500 (3362-8964)
Grimm-SMPS	5-350	5099 (3493-7347)	7810 (5018-10935)	4382 (3187-6302)	5446 (3600-7926)

Table 2. Summaries of the formation rate of 1.5 nm particles ($J_{1.5}$), particle growth rates ($GR_{1.5\text{-}20}$, $GR_{1.5\text{-}3}$, $GR_{3\text{-}7}$, and $GR_{7\text{-}20}$), condensation sink (CS) of NPF event during this and other measurement.

Location	Date	Instrument [a]	CS * 10^{-3} (s^{-1})	$GR_{1.5\text{-}20}$ (nm h^{-1})	$GR_{1.5\text{-}3}$ (nm h^{-1})	$GR_{3\text{-}7}$ (nm h^{-1})	$GR_{7\text{-}20}$ (nm h^{-1})	$J_{1.5}$ (cm^{-3} s^{-1})	Type	Ref.
Mainz, Germany	14 Mar 2022	SMPS+NAIS +PSM	1.8	4.4	2.5	4.6	4.9	0.9	Urban	This study
	24 Mar 2022		6.9	4.0	3.6	9.1	3.5	5.6		
	25 Mar 2022		6.0	3.0	7.3	6.5	2.4	11.2		
	18 Apr 2022		5.1	5.2	3.2	10.5	4.7	2.1		
	14 May 2022		4.7	2.8	1.7	8.2	2.4	1.5		
	17 May 2022		6.6	3.7	1.4	6.9	3.8	0.5		
	29 May 2022		1.8	1.9	1.7	2.0	1.9	0.3		
	17 Jun 2022		-[b]	6.6	4.1	5.3	7.8	2.9		
	21 Jun 2022		6.5	4.6	2.9	4.8	4.9	1.6		
	28 Jun 2022		4.9	5.4	10.0	6.2	4.9	7.2		
	04 Jul 2022		-[b]	4.5	4.6	3.9	4.8	2.4		
	Mar-Jul 2022		4.9	4.2	3.9	6.2	4.2	3.3		
Melpitz, Germany	Apr 2008-Apr 2009	DMPS+NAIS	8.4		2.6	5.7	7	23.1 (J_2)	Rural	(Manninen et al., 2010)
Hohenpeissenberg, Germany	Mar 2008-Apr 2009	SMPS+NAIS	4.1		4.8	4.2	4.6	3.0 (J_2)	Rural	
Cabauw, Netherlands	Apr 2008-Mar 2009	SMPS+NAIS +AIS	2.9		3.8	5.5	6.7	32.4 (J_2)	Rural	
Jungfraujoch, Switzerland	Apr 2008-Apr 2009	AIS+SMPS	0.59		3.7	7.2	8.2	0.9 (J_2)	Remote	
Mace Head, Ireland	Jun 2008-Apr 2009	SMPS+NAIS	0.64		5.5	2.7	5.4	11.8 (J_2)	Remote	
Pallas, Finland	Apr 2008-Apr 2009	DMPS+NAIS	0.63		3.8	5.6	3.8	1.2 (J_2)	Remote	
Hyytiälä, Finland	Mar 2011	DMPS+NAIS +PSM	1.5		1.9	2.8	3.8	5.9	Remote	(Kulmala et al., 2013)
Po Valley, Italy	Jun-Jul 2012	DMPS+NAIS	45		4.3	6.2	7.2	6	Rural	(Kontkanen et al., 2016)

Agia Marina, Cyprus	Jan 2018-Jan 2019	SMPS+NAIS+PSM	7.9		9.2	11.7	15 (J_2)	Rural	(Baalbaki et al., 2021)
Gucheng, China	Nov-Dec 2018		21	0.5 ($GR_{1.3-2.4}$)			22.0 ($J_{1.3}$)	Rural	(Hong et al., 2023)
Barcelona, Spain	Jun-Jul 2018	SMPS+PSM	16	4.4 ($GR_{1.9-4.5}$)			178	Urban	(Brean et al., 2020)
Shanghai, China	Feb 2014-Feb 2016	SMPS+NAIS+PSM	21	1.5	6.5	9.9	106	Urban	(Yao et al., 2018)
Shanghai, China	Nov 2014-Jan 2015	SMPS+PSM	60	2.0 ($GR_{1.3-2.4}$)	10.9 ($GR_{2.4-7}$)	11.4	188 ($J_{1.3}$)	Urban	(Xiao et al., 2015)
Beijing, China	Jan 2018-Aug 2019	DEG-SMPS+PSD	19	0.9	1.7	2.8 (GR_{7-15})	79	Urban	(Deng et al., 2020)
Beijing, China	Oct 2015-Jan 2016	SMPS+NAIS	4.2			3.5 (GR_{2-10})	26 (J_2)	Urban	(Jayaratne et al., 2017)
Nanjing, China	May 2014-Mar 2015	SMPS+PSM	23	4.7		7.6 (GR_{3-10})	659 ($J_{1.4}$)	Urban	(Yu et al., 2016)

[a] DMPS: Differential Mobility Particle Sizer; AIS: air ion spectrometer; DEG-SMPS: diethylene glycol scanning mobility particle spectrometer; PSD: particle size distribution system.
[b] Lack of Grimm-SMPS data, no results.

Figure 1. The geographical location of the measurement site on the map (map by © Google Earth).

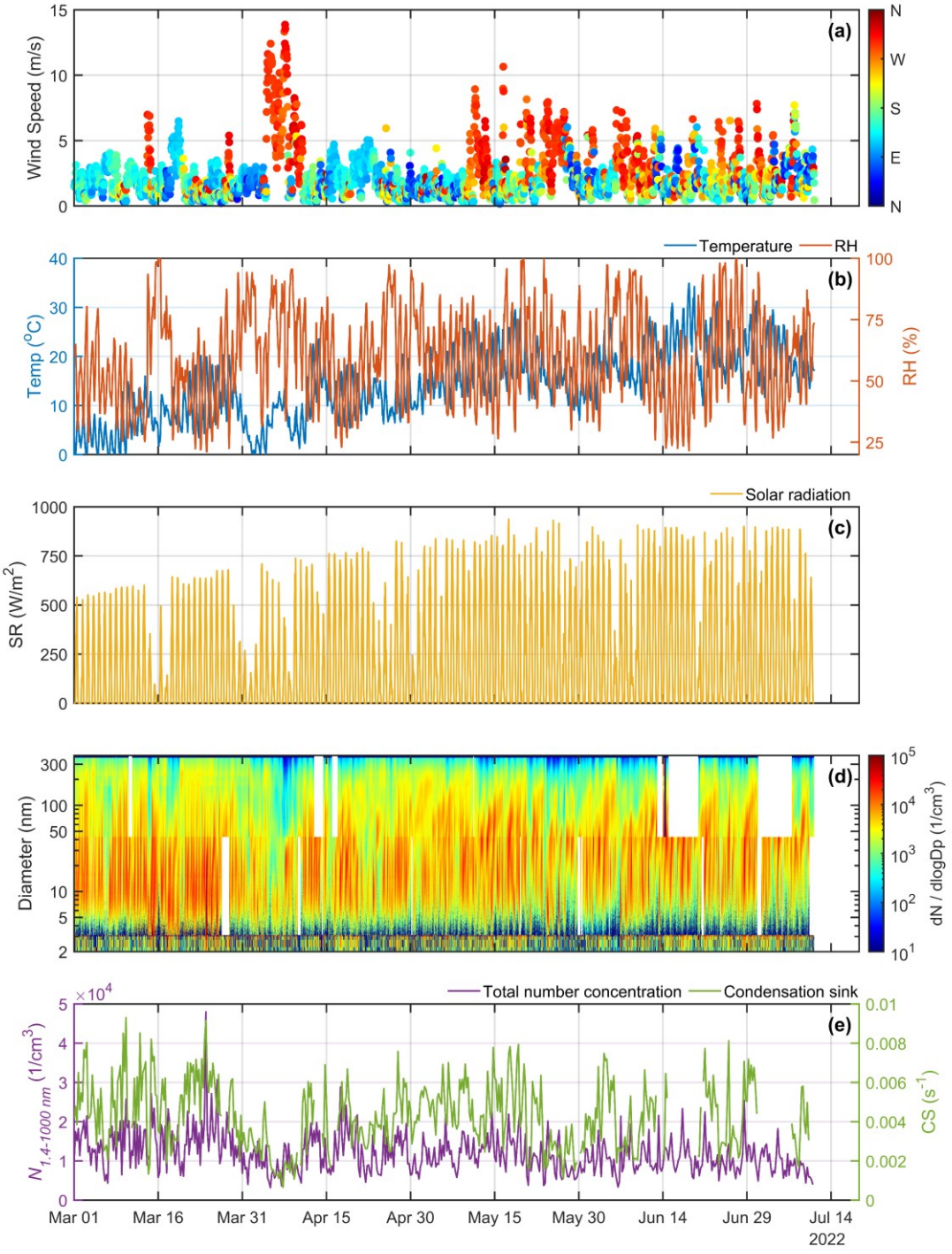

Figure 2. Time series of the following parameters throughout the measurement period (1 March - 10 July, 2022): (a) wind speed and direction; (b) temperature (Temp.) and relative humidity (RH); (c) solar radiation (SR); (d) particle number size distribution (PNSD) within the size range of 1.5-350 nm; (e) total particle number concentration between 1.4 and 1000 nm, along with the calculated condensation sink (CS). The PNSD is derived from the particle size measurements using the PSM (1.4-3 nm), Nano-SMPS (3-38.5 nm), and Grimm-SMPS (38.5-350 nm). The white sections in the PNSD time series indicate data gaps due to instrument maintenance or technical issues with the SMPS systems.

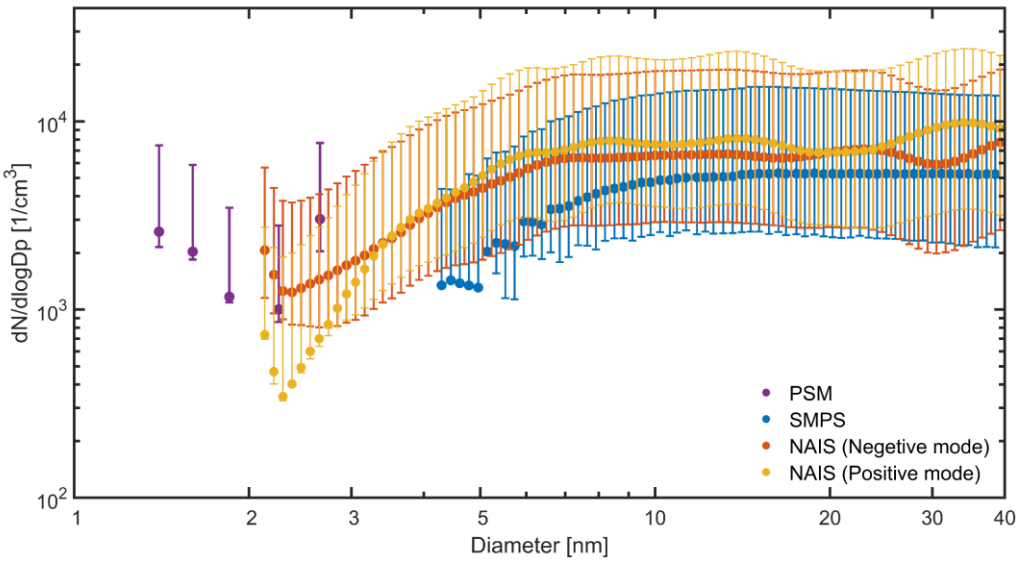

Figure 3. The particle number size distribution of three instruments (PSM, Nano-SMPS, and NAIS) over the entire measurement period.

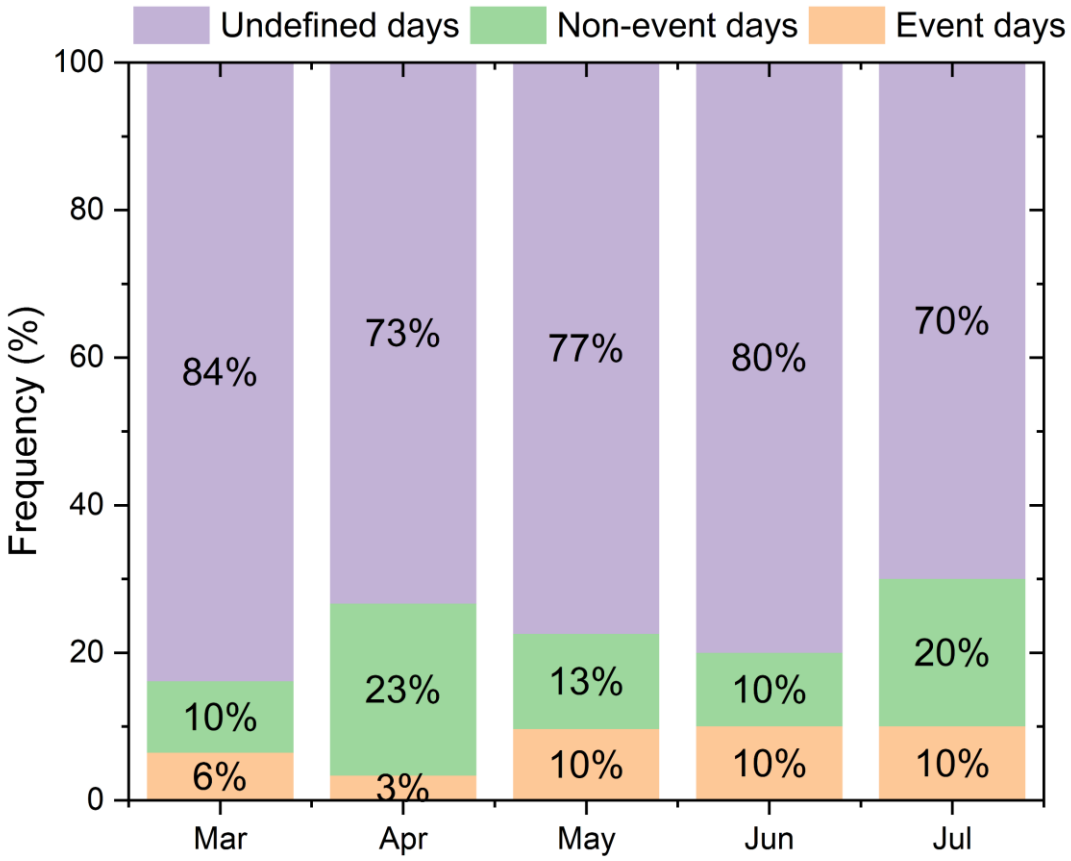

Figure 4. Monthly frequency of event days (orange), non-event days (green), and undefined days (purple) in Mainz during 1 March - 10 July 2020.

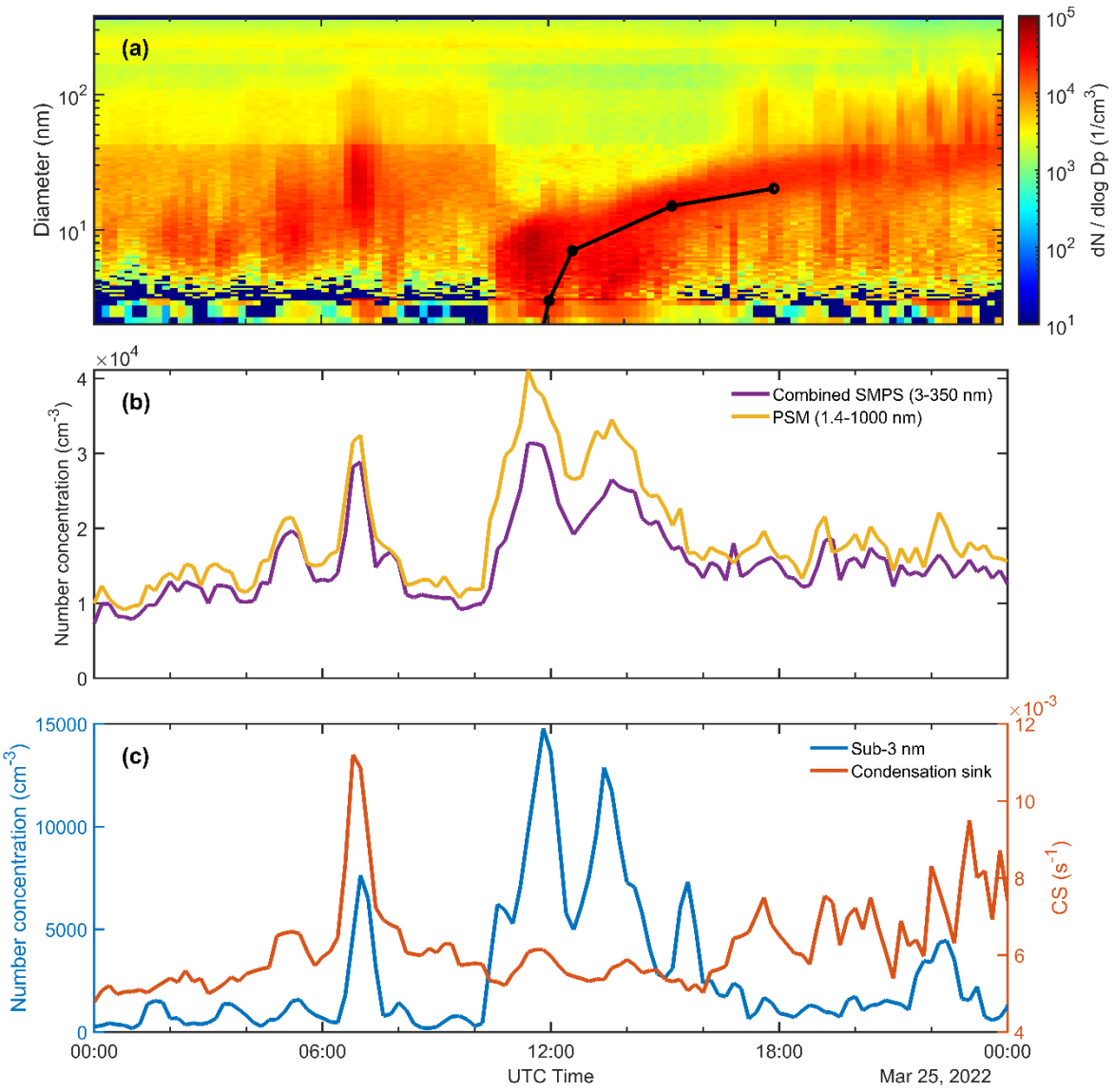

Figure 5. A case of a new particle formation (NPF) event observed on March 25 during the measurement period. The time series are presented as follows: (a) the particle number size distribution (PNSD) in the size range of 1.4-350 nm, with particles below 3 nm measured by the PSM, particles between 3 nm and 38.5 nm by the Nano-SMPS, and the remaining size range by the Grimm-SMPS. Black dots indicate peak times determined by the maximum-concentration log-normal distribution method, while the black line shows a polynomial fit of the peak times. (b) The particle number concentration from the SMPS instruments (3-350 nm, purple line) and the PSM (1.4-1000 nm, yellow line). (c) The particle number concentration of sub-3 nm clusters (blue line) and the calculated condensation sink (CS, orange line).

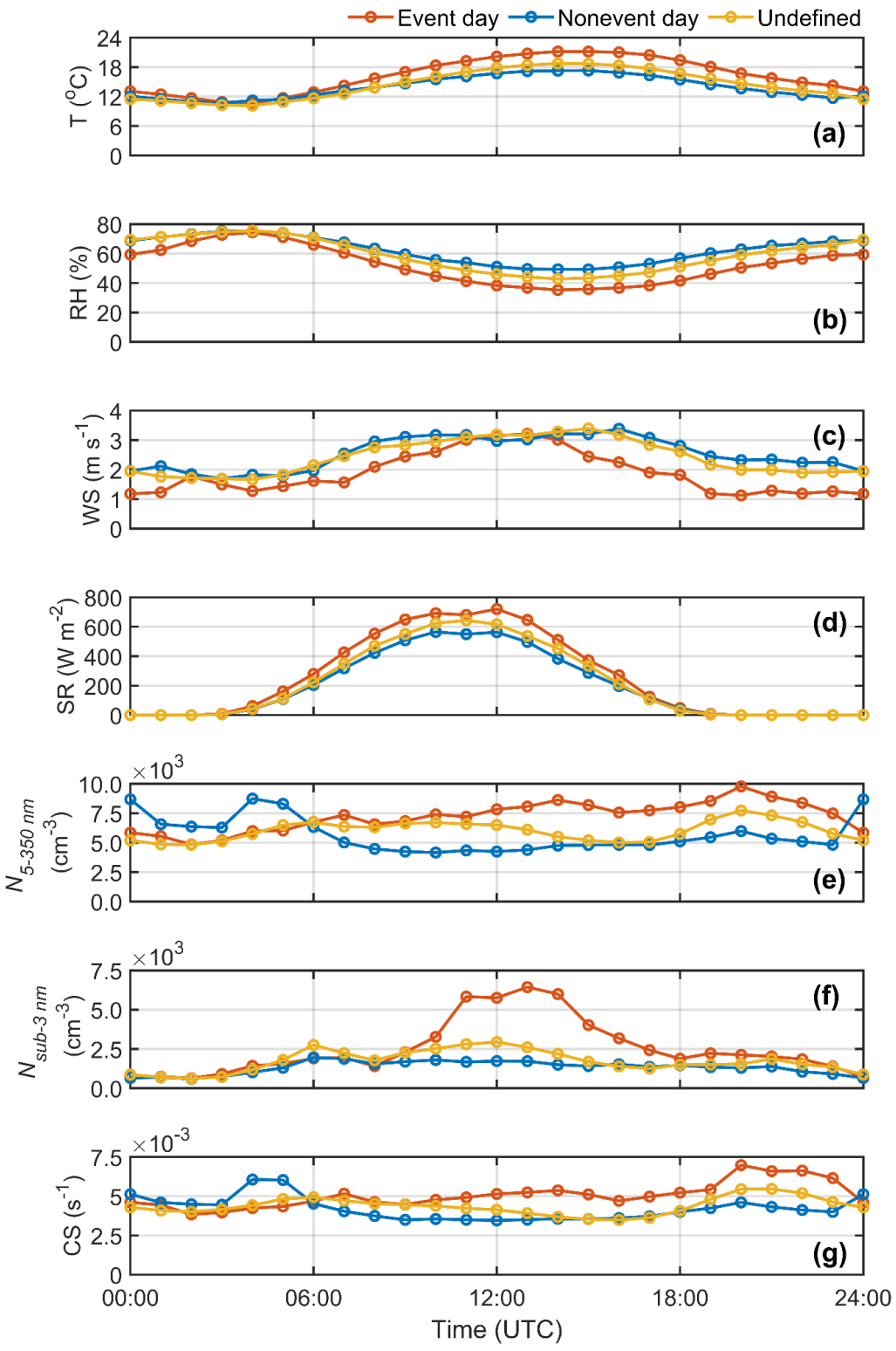

Figure 6. Diurnal variation of (a) temperature (T), (b) relative humidity (RH), (c) wind speed (WS), (d) solar radiation (SR), (e) particle number concentration (5-350 nm) measured by Grimm-SMPS, (f) sub-3 nm particle number concentration, and (g) calculated condensation sink (CS) during NPF events, non-events, and undefined days. Mean values are derived from 11 NPF days, 40 non-event days, and 81 undefined days over the entire measurement period.

Supplementary Material

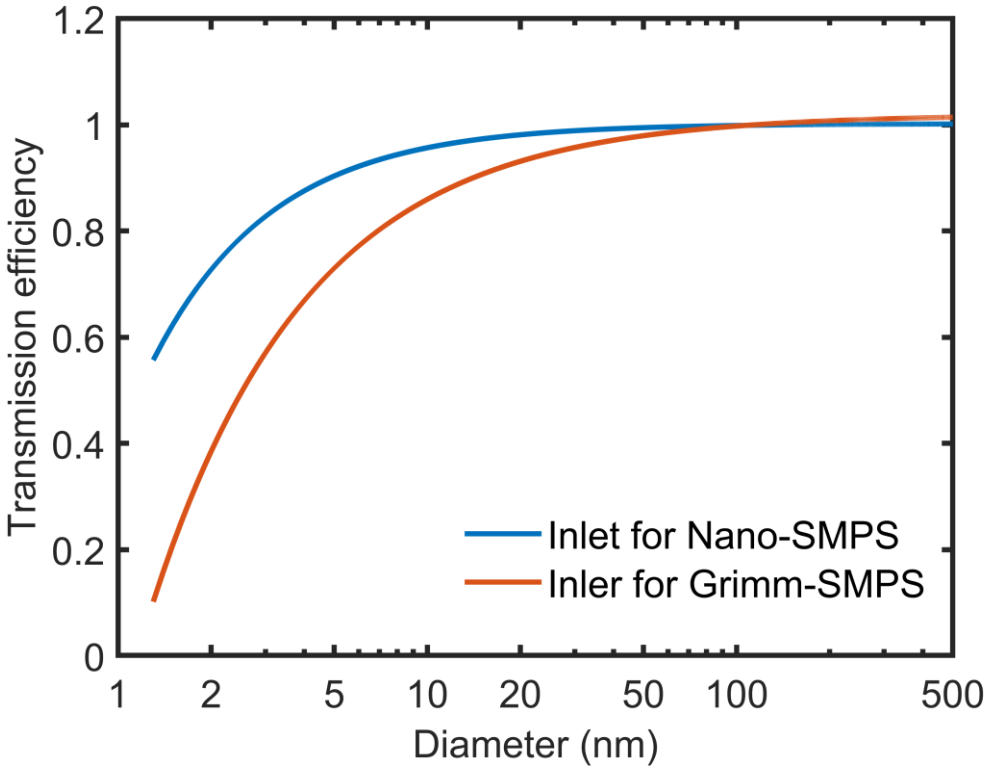

Figure S1. Calculated particle transmission efficiency for Nano-SMPS (blue line) and Grimm-SMPS (orange line) inlet.

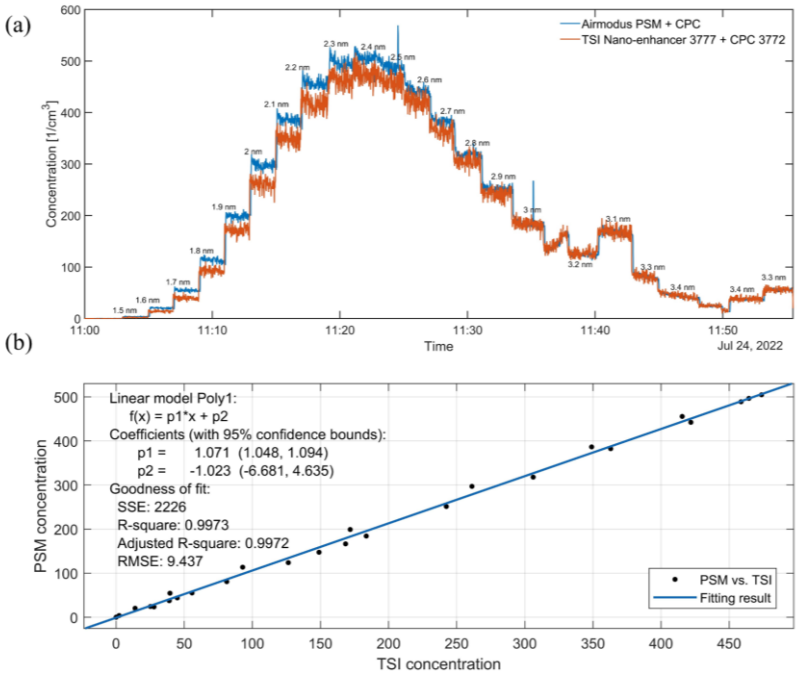

Figure S2. (a) Time series plot of the measured number concentration between Airmodus (A10 PSM + A20 CPC, orange line) and TSI system (Nano-enhancer 3777 + CPC 3772, blue line). (b) The result of the linear fit between the Airmodus and TSI systems. The black dots indicate the mean number concentration value for each selected size, and blue line represents result of the linear fit (R^2 = 0.9972).

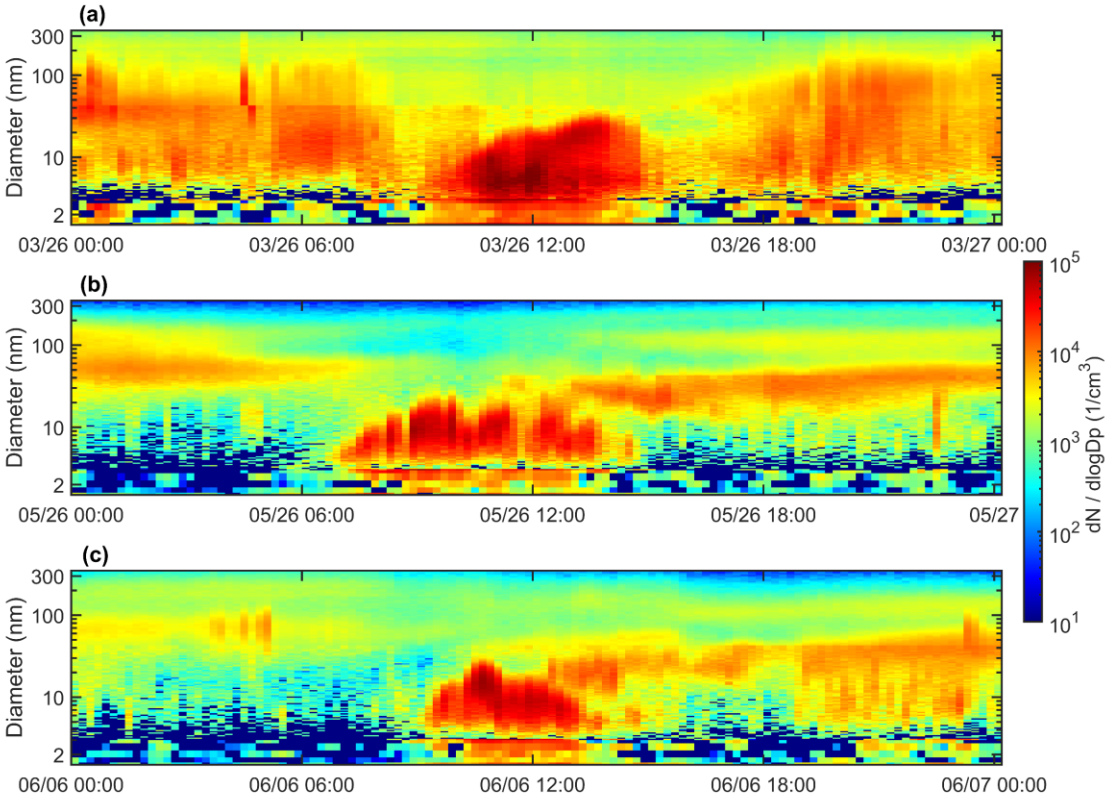

Figure S3. The PNSD for three typical undefined days (26 March (a), 26 May (b), and 6 June (c) 2022). The PNSD is derived from the particle size measurements using the PSM (1.4-3 nm), Nano-SMPS (3-38.5 nm), and Grimm-SMPS (38.5-350 nm).”

Chapter 4

4. Number Size Distribution of Sub-40 nm Particles in the Amazon Rainforest

This work is to be submitted as Zhu et al. (2025):

I am the first-author of this work and my contributions include conducting intercomparison experiments, setting up and operating instruments during the measurement periods, performing data analysis, generating all the figures and tables, interpreting and discussing the findings with co-authors, and drafting the manuscript.

The following text, figures, and tables quoted (within"") from page 65 to page 95 are exactly the same as the manuscript which is cited on page 64.

"**Abstract:**

The Amazon rainforest is a unique environment to investigate aerosol properties with limited impact from human activities, further providing a new perspective to look at the aerosol characteristics in regions heavily affected by anthropogenic emissions. Obtaining the size distributions of nucleation mode particles in the atmosphere is key to understanding aerosol formation, evolution and their impacts. Although routine and long-term aerosol measurements have been conducted in the Amazon region, information regarding sub-10 nm particles is still limited. In this study, we performed aerosol measurements from December 2022 to January 2023 on a 54-meter-high platform of the Amazon Tall Tower Observatory (ATTO). Three advanced instruments namely the Nano Condensation Nuclei Counter (nCNC), the Neutral Cluster and Air Ion Spectrometer (NAIS), and the Nano-Scanning Mobility Particle Sizer (SMPS), were employed to measure the number size distributions of aerosol particles and naturally charged ions smaller than 40 nm. The results reveal that the median total number concentration of the measured particles with diameters ranging from 1.5 nm to 1000 nm was 969 cm^{-3}. We found a large number of particles smaller than 3.5 nm, which accounted for up to 59 % of the measured total number concentration. There was a significant increase in the number concentration of sub-3 nm particles in January 2023 (median, 573 cm^{-3}) compared to December 2022 (371 cm^{-3}). The median number concentration of particles above 3.5 nm in December and January were 481 and 335 cm^{-3}, respectively. No typical regional new particle formation events were observed throughout the measurement period. However, clear diurnal variations were observed for the sub-3nm particles under pristine conditions, with the maximum concentration around noontime. Similar diurnal patterns were also observed for natural cluster ions (0.8-2 nm), with their concentration in January slightly higher than in December. Quantifying the properties of the aerosol particles in the Amazon rainforest helps to understand the processes governing the aerosol budget in the pristine atmosphere, and is essential for determining the impact of anthropogenic aerosols on climate.

Introduction

Atmospheric aerosol particles significantly impact atmospheric chemistry and the Earth's climate directly and indirectly (Ipcc, 2022; Seinfeld and Pandis, 2016). Aerosols affect the atmospheric chemistry by directly serving as reactive surfaces/matrixes to facilitate and alter

chemical reactions in the atmosphere (Pöschl and Shiraiwa, 2015; Farmer et al., 2015). Heterogenous and multiphase reactions occurring on aerosols can be an important source/sink for many critical gas species (Su et al., 2020; Ravishankara, 1997). Meanwhile, aerosols can influence the Earth's radiation balance by absorbing and scattering sunlight, which modulates the amount of energy reaching the ground surface (Myhre, 2009; Charlson et al., 1992). In addition, by acting as cloud condensation nuclei (CCN), aerosols impact cloud formation and precipitation patterns, in a way affecting the Earth's climate indirectly (Williamson et al., 2019; Merikanto et al., 2009; Rosenfeld et al., 2008).

Probing the basic properties of aerosols, such as their size distribution, is key to understanding their impacts. The size distribution of atmospheric aerosol particles is typically characterized by several different modes: nucleation mode (particles with diameter smaller than ~25 nm), Aitken mode (from ~25 to ~100 nm), the accumulation mode (from ~100 to ~1000 nm), and coarse mode (particle with diameter larger than 1000 nm) (Seinfeld and Pandis, 2016; Whitby, 1978). With the development of instrumentation and the growing interest in the formation of new particles, more and more measurements were used to investigate the properties of nucleation mode particles in the last decade (Kulmala et al., 2013). However, global observations of particles below 10 nm and particularly sub-3 nm aerosols are still challenging, because these small particles are bearing high diffusive loss, low charging efficiency, and unknown chemical compositions (Stolzenburg et al., 2023; Kangasluoma et al., 2020; Kangasluoma and Attoui, 2019). With the rapid development of aerosol measurement techniques, some advanced instrumentation such as the diethylene glycol-based electrical mobility spectrometer (DEG-SMPS), the particle size magnifier (PSM), and the neutral cluster and air ion spectrometer (NAIS) have made the characterization for the sub-3 nm aerosols possible (Mirme and Mirme, 2013; Jiang et al., 2011a; Vanhanen et al., 2011). These instruments have been widely used in several field measurements in recent years (Huang et al., 2024; Hong et al., 2023; Gonzalez Carracedo et al., 2022; Olin et al., 2022; He et al., 2021; Kangasluoma et al., 2020; Baccarini et al., 2020).

The Amazon rainforest is a globally important ecosystem and plays a major role in the climate system (Andreae et al., 2015). Measurements of particle number size distribution (PNSD) in the Amazon have been conducted during several field campaigns over the past several decades (Artaxo et al., 2022; Martin et al., 2016; Andreae et al., 2015; Martin et al., 2010a; Rissler et al., 2006a; Guyon et al., 2005; Rissler et al., 2004; Krejci et al., 2003; Zhou et al., 2002; Andreae et al., 2002). Seasonal variations of emissions and meteorology significantly alter the

size distribution of submicron particles in the Amazon are significant (Artaxo et al., 2022). During the wet season, Aitken and accumulation modes contribute almost equally to the particle size spectrum, with particle number concentrations ranging from 300-400 cm^{-3} in the Central Amazon (Rizzo et al., 2018; Martin et al., 2010a; Zhou et al., 2002). Biogenic sources and processes are dominant in the wet season, and the composition of the Amazon atmosphere approximates pre-industrial conditions during certain periods (Pöhlker et al., 2018). During the dry season, the particle number concentration is around 1000-1400 cm^{-3}, and their size distribution is mainly dominated by the accumulation mode (Artaxo et al., 2022; Rizzo et al., 2018). This is mainly influenced by local biomass burning emissions and long-term transport (Holanda et al., 2023; Artaxo et al., 2022; Andreae et al., 2018).

Nucleation mode particles were infrequently observed in the planetary boundary layer (PBL) of the Amazon, suggesting that new particle formation (NPF) events rarely occurred (Artaxo et al., 2022; Rizzo et al., 2018; Andreae et al., 2015). This is different from other forest regions, such as the boreal forest of Hyytiälä (Finland), where typical NPF days account for 10 to 40 % of all measurement days (Kulmala et al., 2022; Kerminen et al., 2018). Based on multi-year measurements on a site (2.594 °S, 60.209 °W) located 60 km northwest of Manaus, NPF and apparent growth event days accounted for only 3 % of the total measurement periods (Rizzo et al., 2018). However, no NPF events were observed at ground level inside the rainforest site (2.609°S,60.209°W) (Wimmer et al., 2018). The same study conducted on an open pasture site in the Amazon region observed the NPF events, and authors linked the NPF event to the pollution plume from Manaus (Wimmer et al., 2018). Previous observations in the Amazon were technically restricted to measure particles larger than 10 nm only, and occasionally observed particle growth starting from about 20 to 40 nm commonly related to downdrafts (Franco et al., 2022; Rizzo et al., 2018). The source of these particles, however, remains unclear. One of the possible sources is vertical transport during precipitation events, where ultrafine particles formed in the upper troposphere and were subsequently injected into the PBL by convective downdrafts (Machado et al., 2021; Andreae et al., 2018; Wang et al., 2016). Despite that, Machado et al. (2024) recently analyzed aerosol and trace gas changes during downdrafts and attributed the characteristic particle bursts to boundary layer NPF, driven by a sudden increase in ozone and decrease in the condensation sink.

In order to fill the gap in measurements of particles and ions smaller than 10 nm in the Amazon region, we performed comprehensive measurements on the Amazon Tall Tower Observatory (ATTO) tower from 29 November 2022 to 26 January 2023. This measurement has been part

of the Chemistry of the Atmosphere: Field Experiment in Brazil (CAFE-Brazil) campaign, designed to study tropospheric oxidant photochemistry in combination with particle formation and growth mechanisms under clean, pristine conditions over the Amazon rainforest (Halo-Research, 2022). This study presents the results of the fundamental properties of particles and ions obtained from a suite of advanced aerosol instruments. The main objectives of the present study are: (1) to characterize the number size distribution of particles, especially in the sub-10 nm size range; (2) to elucidate the life cycle dynamics of aerosol particles by investigating their diurnal variability in different size ranges; (3) to assess the potential occurrence of NPF events in the Amazon rainforest by examining the formation and growth properties of nucleation mode particles.

Methods

2.1 Field Measurement

2.1.1 ATTO site

The measurements were conducted at the 54-meter platform of the Amazon Tall Tower Observatory (ATTO), situated at the center of the Amazon Basin (2.1459° S, 59.0056° W, 130 meters above sea level). The Amazon Basin features minimal large-scale relief, but a dense drainage network has resulted in the formation of a landscape comprising plateaus and valleys on a smaller scale (Andreae et al., 2015). The region comprises a varies of forested ecosystems, with non-flooded upland forests predominantly found on the plateaus (Artaxo et al., 2022). As a key research site, ATTO is of great significance for the comprehensive study of atmospheric processes and their complex interactions with climate and ecosystems (Pöhlker et al., 2019; Andreae et al., 2015). The height of the platform enables the measurement of aerosols above the canopy level. The nearest city, Manaus, is located approximately 150 km southwest of the tower, highlighting the pristine feature of the observatory with limited impact from human activities. Further details regarding the ATTO site can be found in Andreae et al. (2015).

2.1.2 Measurement periods

The field campaign took place from 29 November to 18 December 2022 and 2 January to 26 January 2023, with a total of 20 days in November and December, and 25 days in January. According to the definition on Amazonian seasons, the dry season lasts from August to November and the wet season from February to May (Pöhlker et al., 2016; Andreae et al., 2015). Therefore, the measurements carried out in December and January can be considered as representative of the end of the dry season and the beginning of the wet season, respectively.

2.2 Instrumentation overview

The measurement setup consisted of an ensemble of complementary instruments designed for quantification of ions and neutral aerosol particles with diameters ranging from 1 nm to 40 nm. This ensemble included a Nano Condensation Nucleus Counter (nCNC, model A11, Airmodus, Finland), a Neutral cluster and Air Ion Spectrometer (NAIS, Airel, Estonia), and a Nano-Scanning Mobility Particle Sizer Spectrometer (SMPS, model 3938, TSI, USA). The status of each instrument was regularly monitored on a daily basis throughout the entire campaign. The NAIS was housed in a temperature-controlled enclosure, while the nCNC and SMPS were housed in an air-conditioned container. All the inlet lines, except for NAIS, were positioned horizontally without bends. In addition, a rain cover was designed for each inlet to prevent potential pipe flooding caused by heavy raining events.

2.2.1 A11 Nano Condensation Nucleus Counter (nCNC)

The nCNC includes a particle size magnifier (PSM, model A10, Airmodus) and a condensation particle counter (CPC, model A20, Airmodus). The PSM acts as a pre-conditioner for the CPC, utilizing diethylene glycol (DEG) as a working fluid to activate and grow nano-sized particles, enabling their detection by the CPC (Vanhanen et al., 2011). Throughout the entire measurement period, the PSM was operated in scanning mode, providing size-resolved information on particles in an approximate size range of 1 to 4 nm with a time resolution of 4 minutes. The cut-off diameter of the detected particles is dependent upon the mixing ratio of DEG vapors, which in turn is controlled by varying the flow rate of saturated DEG vapors. Therefore, the size distribution can be determined by measuring total particle concentration above a certain cut-off diameter as a function of the flow rate through the saturator (Chan et al., 2020). For this study, we strictly followed the previously established standard operating procedure to ensure accurate instrument configuration, calibration, and measurement performance (Lehtipalo et al., 2022). A straight 20 cm long inlet was used to minimize particle losses within the sampling line. Due to a technical issue in the first phase of our measurement, a design of core sampling (for inlet) was only used during the second phase to further reduce diffusion losses of particles and ensure laminar flow conditions in the sampling line. To better judge the effect of the core sampling, size-dependent transmission efficiency was calculated based on the work of Von Der Weiden et al. (2009). **Figure S1** shows the transmission curves for the scenarios with and without core sampling. The transmission curves were further used to correct for the data obtained via the nCNC. Daily routine check was performed to assess the background level of particles potentially caused by DEG homogeneous nucleation. The median

background value corresponding to the highest DEG flow rate was 4.7 cm^{-3}, which was subtracted from the raw counts for the subsequent data analysis.

2.2.2 Neutral cluster and Air Ion Spectrometer (NAIS)

The NAIS instrument is a multi-channel aerosol instrument designed to measure the mobility distribution of airborne ions and the size distribution of aerosol particles. It operates over a mobility range of 3.2 to 0.0014 $cm^2/V/s$, corresponding to a mobility diameter range of 0.8 to 40 nm. By simultaneously collecting signals from multiple electrometers, NAIS can detect both ions and particles. The choice of measuring ions or particles is associated with the operating mode of the preconditioner, which includes ion mode, particle mode and offset mode. Through switching on and off the preconditioning unit, NAIS can achieve measurement switch between ion mode and particle mode. Moreover, the offset mode is utilized for the periodic verification of the instrument's operation, including the evaluation of noise levels and the measurement of parasitic currents (Manninen et al., 2016). During our field measurements, NAIS was operated between these three modes with each lasting for 60 seconds, therefore an entire measurement cycle took 3 minutes. The NAIS inlet originally provided with the instrument was a 50 cm long metal tube (inner diameter: 35 mm) with a 90-degree downward bend to prevent rain from entering the instrument. A metal mesh (1 mm mesh size) was placed at the very front of the inlet tube to keep big insects out. The sample flow rates in the NAIS system was 54 L min^{-1}, resulting in a shorter residence time, which further reduced diffusion losses and electrical losses for charged clusters and nanoparticles (Manninen et al., 2016). It should be noted that the measurement results below 2 nm are strongly biased by the corona self-charging cluster when the instrument is running in particle mode (Manninen et al., 2016). Thus, the results for particles below 2 nm were not used for subsequent data analysis.

2.2.3 Nano-Scanning Mobility Particle Sizer Spectrometer (SMPS)

The SMPS system consists of an Electrostatic Classifier (model 3082, TSI), a Differential Mobility Analyzer (DMA, model 3086, TSI), a Nano-enhancer (model 3777, TSI) and a Condensation Particle Counter (CPC, model 3772, TSI). Operating at an aerosol flow rate of 2.5 L min^{-1} and a sheath flow rate of 10 L min^{-1}, SMPS can achieve number size distribution measurements in the mobility diameter range of 1.3-38.5 nm. During our field measurements, the system was operated without the Nano-enhancer because of its non-functionality. Using an aerosol flow of 1 L min^{-1}, the measured size range was adjusted to 10-38.5 nm due to the fact that the minimum particle size detected by the CPC was 10 nm. The following discussions also

include data from another long-term SMPS measurement (particle size range: 40-414 nm), which was carried out at the INSTANT tower located 600 m east of the ATTO tower. The sampling inlet was positioned at a height of 60 m, which was only slightly higher than that of the SMPS on the ATTO tower. More detailed information regarding this long-term SMPS setup can be found in Franco et al. (2022) and Pöhlker et al. (2016).

2.2.4 Instrument intercomparison

Prior to the ambient measurements, a laboratory intercomparison was carried out between two systems: PSM A10 + CPC A20 (Airmodus) and the Nano-enhancer 3777 + CPC 3772 (TSI). A similar procedure was also carried out in previous studies (Lehtipalo et al., 2022; Kangasluoma et al., 2018; Vanhanen et al., 2011). The details of the intercomparison experiment setup are illustrated in **Fig. S2**. Tungsten oxide particles with a diameter of 1.4 to 3.8 nm were used, and the desired particle size was achieved through the optimization of wire current and carrier gas flow rate. Subsequently, particles of varying sizes were selected using a DMA, with specific diameter particles simultaneously measured by both systems. For particles below 1.8 nm, the measurement was conducted without the charger, as the WOx generator (model 7860, GRIMM) produced sufficient self-charged clusters through hot-wire generation (Kangasluoma et al., 2015).

Figure 1(a) shows the linear correlation between the concentrations measured by the two systems (Airmodus and TSI) during a laboratory instrument intercomparison prior to the field campaign. The linear fit line with the R^2 value of 1.0 indicates a high degree of agreement between the two systems. **Figure 1(b)** illustrates the size-dependent ratio of the measured particle concentrations under different sizes. The discrepancy in concentration between the Airmodus instruments and the TSI setup remained below 20 % for particle diameters above 1.8 nm, indicating a decent agreement between the measured concentrations by the two systems. It is important to note that the effect of charging efficiency may increase the uncertainty of the ambient measurement results due to the different chemical compositions of the measured particles (Kangasluoma et al., 2020). In addition to chemical composition, several other factors including different charge states and relative humidity, may also contribute to the overall uncertainty (Lehtipalo et al., 2022).

Results and discussion

3.1 Number size distribution of particles

Here we present the particle number size distributions across multiple measurement ranges made by the different instruments introduced in the Methods section. The number concentration of sub-3 nm particles was quantified by PSM. The distribution of particles in the size range of 2-40 nm was characterized by NAIS, and those for a larger size range of 40-414 nm were provided by SMPS. Additionally, the ion number size distribution in the 0.8-40 nm range was obtained from NAIS.

Figure 2 illustrates the temporal evolution of meteorological parameters and aerosol properties for our ambient measurements. The wind speed was typically low, with an average of 1.8 m s^{-1} over the entire measurement period which is well within the typical range of 0-4 m s^{-1} (Andreae et al., 2015). The mean temperature was 25.8 ± 3.0 ℃ and the mean RH was 85.0 ± 13.9 %. The temperatures in December 2022 and January 2023 were 26.9 ± 3.2 ℃ and 25.0 ± 2.6 ℃, and the corresponding RH were 78.8 ± 14.4 % and 89.9 ± 11. 6 %, respectively. Long-term measurements have shown that temperatures peaked in dry season, with an average of 27.5 °C in September, while the lowest temperature (25.9 °C) occurred in wet season in March (Andreae et al., 2015). **Figure 2c** displays the combined particle number size distribution derived from NAIS and the ATTO long-term SMPS. We observed several "Amazonian bananas", where particle growth typically started with a peak diameter between 20 and 40 nm, consistent with the findings by Franco et al., (2022). In most previous studies, the reported lower size limit for the measured particles was generally around 10 nm (Franco et al., 2022; Rizzo et al., 2018; Martin et al., 2010a). Here, we further present the number size distribution information of particles below 10 nm. **Figure 2d** shows the total number concentrations in different size ranges. For the whole measurement period, the total particle number concentration ranged from 350 to 4110 $cm^{-3}$and the median concentration was 969 cm^{-3}. There was a large number of particles between 1.5 nm and 3.5 nm, accounting for up to 59 % of the measured total number concentration. Note that, due to their different working principles, the size measured by NAIS is the mobility size, whereas the PSM measures the Kelvin size (Kangasluoma et al., 2020).

As illustrated in **Fig. 2c**, there were multiple instances of needle-shaped bursts in NAIS measurement during the observation period. The bursts exhibited a good correlation with precipitation events, as evidenced by the RH and rainfall data. **Figure S3** shows that the median values remained within the 330-400 cm^{-3} range across different RH ranges. The high RH range (90-100 %) had significantly more outlier values, up to 12000 cm^{-3}. Previous studies have also shown that heavy rainfall can cause bursts in the measured ion and particle concentrations by

NAIS (Wimmer et al., 2018; Manninen et al., 2016; Tammet et al., 2009; Hirsikko et al., 2007). The proposed explanation is that the splashing of water during heavy rainfall can generate balloelectric intermediate ions, which exist as singly charged water nanoparticles (Tammet et al., 2009). Therefore, all the data suspected to be influenced by precipitation were excluded from our NAIS data analysis.

No typical NPF events were observed during the entire measurement period, as indicated by the measured particle number size distribution in **Fig. 2c**. Typical NPF involves a rapid increase in the concentration of sub-3 nm particles in the atmosphere, followed by a continuous growth to larger particle sizes (Kulmala et al., 2012). Previous ground-based measurements have consistently demonstrated the absence of typical NPF events within the Amazon rainforest PBL (Franco et al., 2022; Wimmer et al., 2018; Rizzo et al., 2018). Although a few NPF events were observed, they were attributed to either the influence of urban pollution plumes (Wimmer et al., 2018), or the initial growth from particles larger than 10 nm (Franco et al., 2022; Rizzo et al., 2018). The growth of particles between 10 and 50 nm in the PBL were found to be closely linked to precipitation events, especially deep convective processes, which served as potential sources to increase the number concentration of nucleation mode particles (Franco et al., 2022; Machado et al., 2021; Andreae et al., 2018; Wang et al., 2016).

It still remains unclear why there is no typical NPF within the Amazon PBL. During our measurement period, although typical NPF was absent, a high number concentration of particles below 6 nm was constantly observed (**Fig. 2c** and **2d**). Field measurements in the boreal forest during nighttime have indicated that the clusters formed from highly oxygenated organic molecules (HOMs) typically do not exceed a few nanometers in diameter (Bianchi et al., 2019). The proposed reason for this is the lack of photochemistry and essential vapors (Rose et al., 2018). These vapors are most likely HOMs resulting from the oxidation of volatile organic compounds (Rose et al., 2018; Ehn et al., 2014). The contribution of HOMs to particle nucleation and growth is strongly dependent on the volatility of HOMs and the particle size, with compounds of lower volatility being more important in the early growth (Tröstl et al., 2016). Other studies have concluded that isoprene can interfere with NPFs associated with monoterpene oxidation, and high levels of isoprene generally inhibit particle formation (Stolzenburg et al., 2023; Lee et al., 2019). The involved mechanisms include: (1) scavenging of OH radicals by isoprene , thus reducing the rate of monoterpene oxidation (Mcfiggans et al., 2019); (2) the increased reaction probability between the RO_2 radicals generated during α-pinene and isoprene oxidation processes could result in a higher production rate of more

volatile C_{15} dimers compared to condensable C_{20} dimers, thus suppressing nucleation and early growth (Heinritzi et al., 2020).

Table 1 gives an overview of the observed number concentrations of particles and ions across different size ranges for our measurement period. Based on the particle size classification method proposed by Wimmer et al. (2018), the median concentrations of intermediate (2-4 nm) and large (4-12 nm) particles during the entire measurement period were 749 and 403 cm^{-3}, respectively (Table 1). The corresponding concentrations in December were 931 and 491 cm^{-3}, much higher than 558 and 306 cm^{-3} observed in January. The study by Wimmer et al. (2018) at another site of the Amazon reported concentrations of 404 and 141 cm^{-3} respectively for the intermediate and large particles during the dry season, and 358 and 115 cm^{-3} during the wet season. In contrast to their ground-based observations, the ATTO measurements were made above the rainforest canopy and therefore are supposed to be more representative of the boundary layer conditions. Both Wimmer et al. (2018) and our study showed higher concentrations for intermediate and large particles in the dry season than the wet season. During wet season, airborne particles tend to be washed out by more frequent rain events (Wimmer et al., 2018; Rizzo et al., 2018).

Figure 3 compares the number concentrations of particles in different size ranges between December and January, based on PSM measurements. The median total particle number concentrations ($N_{1.5\text{-}1000\ nm}$) at the ATTO site were 963 cm^{-3} and 972 cm^{-3} for December and January, respectively. No significant difference was observed between these two months. In December, the median concentration of particles with diameters from 1.5 to 3.5 nm was 371 cm^{-3}; while in January it increased to 573 cm^{-3}, indicating a prominent increase in concentration during the pre-wet season compared to the late dry season.

In contrast to particles with diameters below 3.5 nm, particles larger than 3.5 nm exhibited higher median concentrations in December (481 cm^{-3}) than in January (335 cm^{-3}). Zhou et al. (2002) performed measurements on particles in a similar size range (3-850 nm) during the wet season (March and April) at the Balbina site in the Amazon region using a differential mobility particle sizer (DMPS), and their results yielded a mean concentration around 450 cm^{-3}. Further multi-year observations at another site in the Amazon rainforest showed that the median particle number concentration (10-600 nm) was significantly higher in the dry season (1254 cm^{-3}) than in the wet season (403 cm^{-3}) (Rizzo et al., 2018). Long-term SMPS measurements also revealed that the total number concentrations of particles in the size range of 10-400 nm were, on average, higher in December than in January at the ATTO site (Franco et al., 2022).

During the dry season, biomass burning and anthropogenic emissions strongly impact the abundance of larger size particles in the Amazon region (Artaxo et al., 2022).

Figure 4 shows the abundances of sub-3 nm particles across diverse environments. Here, we use sub-3 nm to denote diameters from 1.5 to 3.5 nm for comparison with previous studies. Table S1 lists their specific concentrations, size ranges, and site types. Under pristine conditions in the Amazon region, the particle number concentration (397 cm^{-3}) was notably lower than in megacities (> 8500 cm^{-3}) such as Nanjing, Shanghai and San Pietro Capo Fiume (Kontkanen et al., 2017; Xiao et al., 2015). Sub-3 nm particle number concentration in the Amazon rainforest was also slightly lower compared to those observed in specific rural areas, such as Long Island, USA (590 cm^{-3}) (Yu et al., 2014) and Mt. Puy de Dôme mountain, France (500 cm^{-3}) (Rose et al., 2015). As for the boreal forest site in Hyytiälä (Kontkanen et al., 2017), its concentrations (580-2900 cm^{-3}) are higher than that of the other rural sites, indicating that human activities close to the forest site have an essential impact on the aerosol particle properties(Artaxo et al., 2022).

3.2 Number size distribution of naturally charged ions

Naturally charged ions are present in the atmosphere and their average concentrations globally range from 200 to 2500 cm^{-3} depending on the type of measurement sites (Hirsikko et al., 2011). The ion number size distribution obtained from NAIS is shown in **Fig. S4**. According to the classification criteria by Manninen et al. (2016), naturally charged ions can be classified into cluster, intermediate and large ions, with equivalent mobility diameters of 0.8-2, 2-7 and 7-20 nm, respectively. As shown in **Fig. 5**, median concentrations of the cluster ions in December and January were 610 cm^{-3} and 639 cm^{-3}, respectively. These numbers are slightly lower than previous measurements in the Amazon rainforest, where the authors reported median concentrations up to 856 cm^{-3} and 952 cm^{-3} in the wet and dry seasons, respectively (Wimmer et al., 2018). In contrast, the median concentrations of intermediate and large ions at the ATTO site remained relatively lower, with their respective concentrations quite comparable, i.e., 40 cm^{-3} versus 35 cm^{-3} for December and 23 cm^{-3} versus 24 cm^{-3} for January. These values, however, are 2-3 times higher than those found by Wimmer et al. (2018). This discrepancy may be related to the different measurement locations/sites. In the previous study, the NAIS was placed inside the canopy in a hut with the sampling inlet 2 meters above the ground (Wimmer et al., 2018). In our study, the NAIS was sampling via the original 50 cm long metal inlet positioned above canopy on the 54-meter-high platform of the ATTO tower.

3.3 Diurnal variation patterns of particles and ions

Figure 6 presents the diurnal variation patterns of the number concentrations of particles of different sizes obtained from the PSM measurements. For both months, the particles within the size range of 1.5-1000 nm showed a clear diurnal trend. After sunrise (around 06:00 local time, LT), the total concentration of particles started to increase, reaching its maximum around 14:00, and then began to decrease steadily until midnight, with the lowest levels occurring around 01:00-03:00. The concentration of particles with diameters above 3.5 nm also increased slightly in the morning in December, and their minimum and maximum values occurred around 5:00 and 17:00, respectively. The latter group of particles, however, showed less pronounced diurnal variation in January.

The particle concentrations in the size range of 1.5-3.5 nm also increased around sunrise for both measurement periods. Their peak concentrations occurred in the morning (08:00 -10:00), and the minimum concentrations were found in the night (around 3:00). The more significant variation in their diurnal pattern was observed for January 2023. This could indicate a sustained growth over a longer period for smaller particles under cleaner conditions. The study at a pasture site in the Amazon during the dry season showed an increase in the median concentrations of sub 3 nm particles before sunrise (03:00-06:00), followed by a decrease in the early afternoon (12:00-15:00) and finally an increase in the evening (18:00-24:00) (Wimmer et al., 2018). The authors attributed these patterns to a so-called Carnegie curve, which reflects the diurnal variation pattern of the ionospheric potential (Wimmer et al., 2018). Other studies have also reported daytime maxima in the concentrations of particles smaller than 3 nm, which were commonly associated with NPF events (Sulo et al., 2021; Yu et al., 2014; Kulmala et al., 2013). For the daytime maximum of sub-3 nm particle concentrations observed on non-event days, it was likely associated with the photochemical processing of low volatile gas precursors (Kontkanen et al., 2017).

Figure. 7 illustrates the daily variation in the size distribution of particles within the 2-40 nm range measured by NAIS. The concentration of particles larger than 15 nm ($D_{15\text{-}40\ nm}$) showed an increase around midnight, reaching a peak concentration in the early morning hours. Subsequently, a gradual decrease in their number concentration was observed until the afternoon. A further increase in the $D_{15\text{-}40\ nm}$ particles was observed following sunset. Meanwhile, a comparable diurnal variation pattern was also identified for the number concentrations of sub-50 nm particles at the same site, based on long-term measurements conducted over more than six years (Franco et al., 2022). The authors attributed the observed

decrease in number concentration in the late morning to the increased mixing following the destruction of the nocturnal boundary layer and the subsequent formation of a well-mixed boundary layer (Franco et al., 2022). In December 2022, the concentration of nucleation mode particles ($D_{6\text{-}15\ nm}$) showed a significant increase before sunset. A similar distribution peak within the 6-15 nm range was also observed by Rissler et al. (2004).

Figure. 8 displays the diurnal patterns of naturally charged ions within different size ranges. The concentration of cluster ions showed a similar daily pattern in both months, with the highest concentrations observed in the morning (~8:00-11:00 LT). Throughout the day, the concentrations were relatively stable with minor fluctuations. The overall range of cluster ion concentration was between 500 cm^{-3} and 700 cm^{-3} and was constantly higher than intermediate and large ions. The concentrations of intermediate and large ions increased slightly during the day and remained at relatively constant levels throughout the night, with their maximum concentrations appeared in the afternoon.

3.4 Comparisons of diurnal variation patterns between plume and non-plume days

Black carbon (BC) can serve as a unique marker to estimate and track the potential contributions from biomass burning activities in the Amazon Basin and long-term transport of African smoke (Holanda et al., 2023; Pöhlker et al., 2018). To assess the background particle levels in the pristine environment, we divided the entire observation period into two scenarios: polluted days affected by short- and long-distance transported plumes, and clean days with extremely clean conditions. Following the approach described in Pöhlker et al. (2018), a threshold of 0.01 μg m^{-3} for the mass concentration of BC was used to distinguish pristine and plume-affected conditions. Accordingly, a day was considered pristine if the BC mass concentration was continuously below 0.01 μg m^{-3} for more than 6 hours; otherwise, it was categorized as a polluted day.

The measurement period was divided into 38 polluted days and 7 clean days. Only 18 % of the total measurement days were truly pollution-free, with two days in December and five days in January. The median concentration of particles below 3.5 nm were 441 and 1153 cm^{-3} on polluted and clean days, respectively. However, particles larger than 3.5 nm were more abundant on polluted days, with a median concentration of 388 cm^{-3}, compared to 315 cm^{-3} on clean days. The higher concentrations of large particles on polluted days could be related to biomass burning or long-term transport. On the other hand, these large particles provided more aerosol surfaces to act as a sink for condensable gas precursors (condensation) and

nanoparticles (coagulation), resulting in lower concentrations of sub-3 nm particles on polluted days.

The diurnal patterns of the number concentrations of particles measured by PSM are presented in **Fig. 9**. The sub-3 nm particles exhibited much more pronounced variations on clean days compared to polluted days. During clean days, the number concentration of sub-3 nm particles increased significantly in the morning, reaching a peak value around 12:00 LT, and then steadily decreased until midnight. For particles with diameters between 3.5 nm and 1000 nm, their concentrations were rather flat on both clean days and polluted days. The number concentration of sub-3 nm particles was significantly higher during the daytime on clean days. This indicates that photochemistry has a significant impact on the production of particles below 3 nm. During the night, the difference between the two scenarios was less pronounced, although the concentration of sub-3 nm particles on clean days was still slightly higher than that on polluted days. Previous observation in Hyytiälä reported high concentrations of sub-3 nm particle in the evening, and this phenomenon has been proposed to be related to ozonolysis products of monoterpenes (Lehtipalo et al., 2009).

Figure 10 illustrates the diurnal patterns of the particle size distributions on days with and without plumes. As shown in Figure 10a, there was a larger number of nucleation mode particles on clear days. The diurnal variation observed during plume days (**Fig. 10b**) exhibited a pattern similar to that described in **Fig. 7**. It can be inferred that the more pronounced increase of nucleation mode particles is linked to the low coagulation sinks during clean days. Nevertheless, the potential formation mechanisms of these nucleation particles remain to be elucidated through further investigation.

Conclusion

The Amazon rainforest provides a unique pristine environment that offers the opportunity to investigate atmospheric aerosol particles during episodes that are free of anthropogenic pollution. In this study, state-of-the-art aerosol instruments including PSM, NAIS, and SMPS were deployed at the ATTO site for an intensive field measurement as part of the "CAFE-Brazil" campaign from December 2022 to January 2023. The size distributions of particles and ions smaller than 40 nm were obtained. During these two months of measurements, a large number of sub-3 nm particles and cluster ions were constantly observed in the Amazonian PBL. Based on the PSM measurements, we found that the median concentrations of particles below 3.5 nm were 371 and 573 cm^{-3} in December and January, respectively. These values

represented 38 % and 59 % of the total number concentrations of particles in the size range of 1.5 nm to 1 μm. The NAIS measurements revealed that the median concentration of naturally charged ions in the range of 0.8-40 nm (equivalent mobility diameter) was 761 cm^{-3}. In addition, the median concentrations of cluster (0.8-2 nm), intermediate (2-7 nm) and large (7-20 nm) ions were 624, 33, and 30 cm^{-3}, respectively. NAIS also measured the median concentration of particles with diameters between 2 and 40 nm as 1462 cm^{-3}. These results highlight the significant contribution of nucleation mode particles to the total particle number concentration in the Amazon rainforest.

Although a large number of sub-3 nm particles and naturally charged ions were present in the Amazonia boundary layer, typical NPF events were not observed throughout the entire measurement period. However, the particles and ions below 3 nm showed a clear diurnal variation. Their concentrations started to increase around sunrise, peaked around midday, and then slowly decreased until midnight. This pattern is an indication that the photochemistry that converts the biogenic VOCs into low volatility vapors may be responsible for the formation of these nanoclusters. In addition, boundary layer convective mixing and rainfall events might also contribute to the diurnal variation to some extent. Particles with diameters larger than 3.5 nm and intermediate/large ions only displayed small diurnal variations. Under pristine conditions, we observed higher number concentrations and more pronounced diurnal patterns for sub-3 nm particles and ions. However, when influenced by biomass burning and other transported plumes, their diurnal patterns were significantly suppressed.

The present study provides for the first-time detailed information on the number size distributions and variation patterns of nanometer-sized particles and ions, in particular for the nanoclusters smaller than 10 nm at the central Amazon region. In future work, we aim to elucidate whether these clusters in the PBL of the Amazon rainforest originate from biogenic VOC precursors, by integrating the gas-phase measurement data obtained from chemical ionization mass spectrometry (CIMS). By investigating the potential links between those gas species that favor NPF (e.g., HOMs and sulfuric acid) and the nanoclusters, we will further unravel the underlying mechanisms that drive the appearance and/or initial growth of nanoparticles, as well as the reasons why their subsequent growth could not be sustained. All this information will contribute to gain a more comprehensive understanding of the air chemistry in this particular pristine environment, and also provide insights into the atmospheric processes in the areas where the influences of human activities is most pronounced.

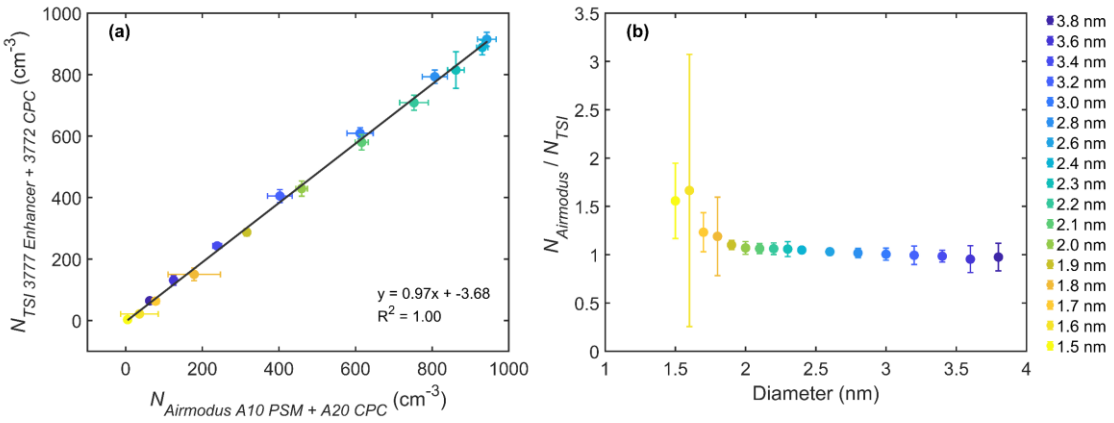

Figure 1. (a) Comparison between the median particle number concentrations measured by two systems, namely the Airmodus (A10 PSM + A20 CPC) and the TSI (Nano-enhancer 3777 + CPC 3772) systems, for the selected different sizes (diameters ranging from 1.5 to 3.8 nm). The solid line represents the linear fitting result with an R^2 value of 1. (b) The ratio of the particle concentration measured by the two systems at different sizes. All error bars denote the standard error.

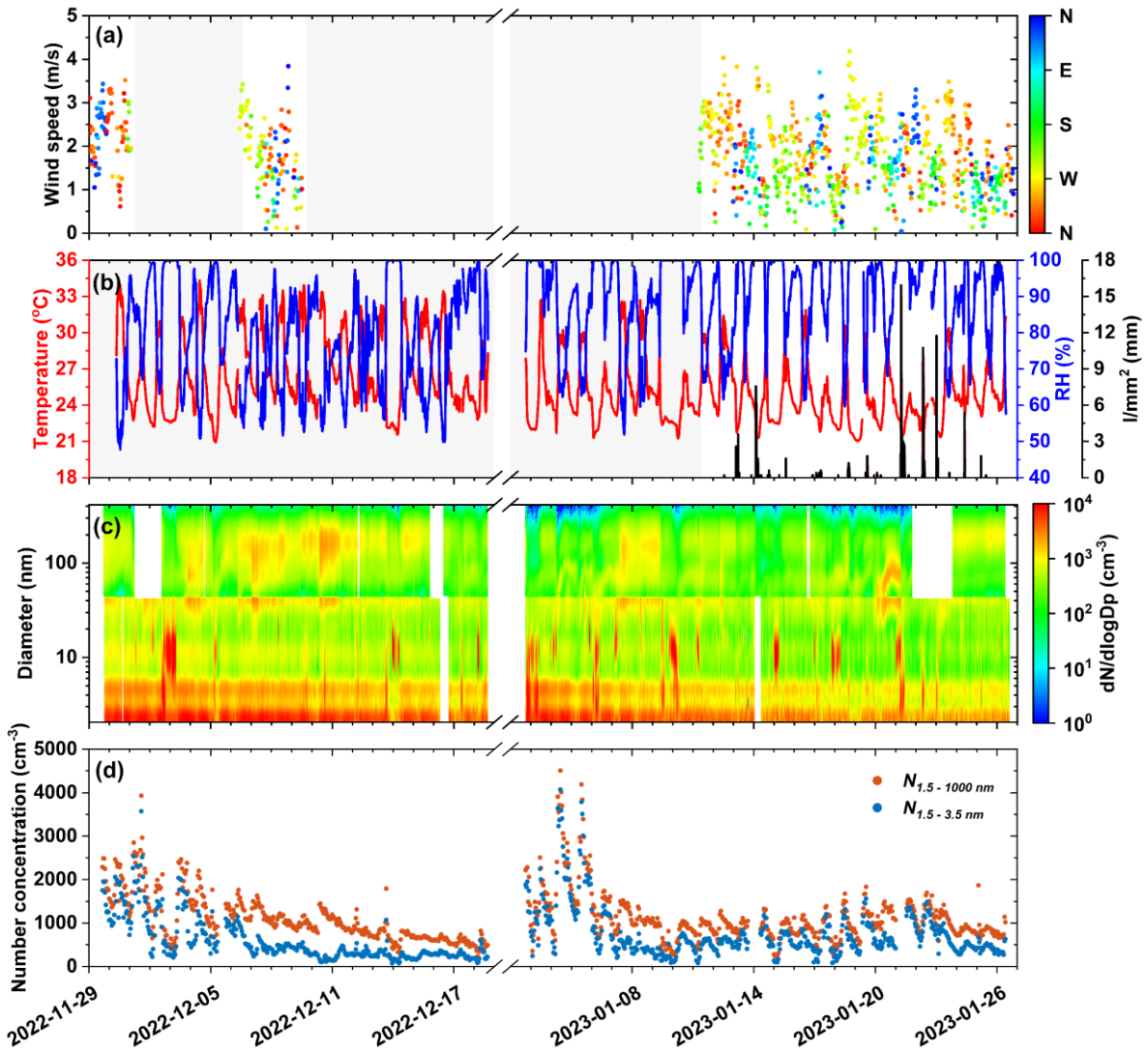

Figure 2. The time series plot of (a) Wind speed and wind direction; (b) Ambient relative humidity (RH), temperature, and rainfall; (c) Particle number size distribution combined from the NAIS (2-40 nm, negative particle mode) and the SMPS system (40-414 nm); (d) Total number concentration of particles with diameter ranges of 1.5-1000 nm and 1.5-3.5 nm from the PSM measurement. Note that the grey parts in panels (a) and (b) and the white part in panel (c) indicate that no data are available. The timestamps used here are synchronized with the local time in Manaus, called Local Time (LT), which is equal to Coordinated Universal Time (UTC) minus 4 hours.

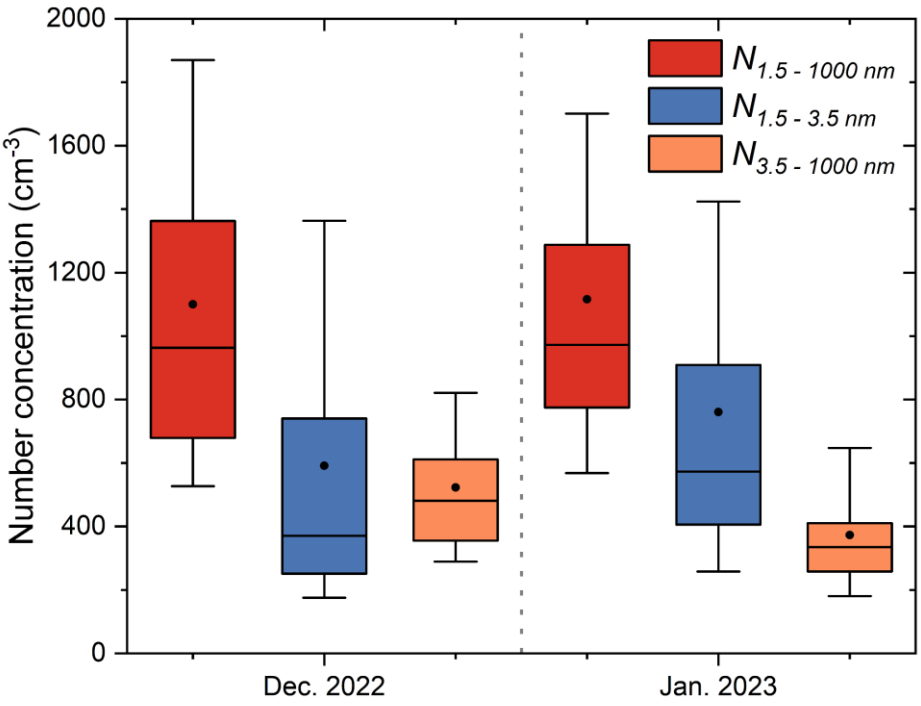

Figure 3. Comparison of particle number concentrations in December 2022 and January 2023 for different size ranges based on PSM measurements. The lower/upper boundaries of the box and the vertical whiskers indicate the 25th/75th and 10th/90th percentiles, respectively. Horizontal lines and black dots within the boxes indicate median and mean values, respectively.

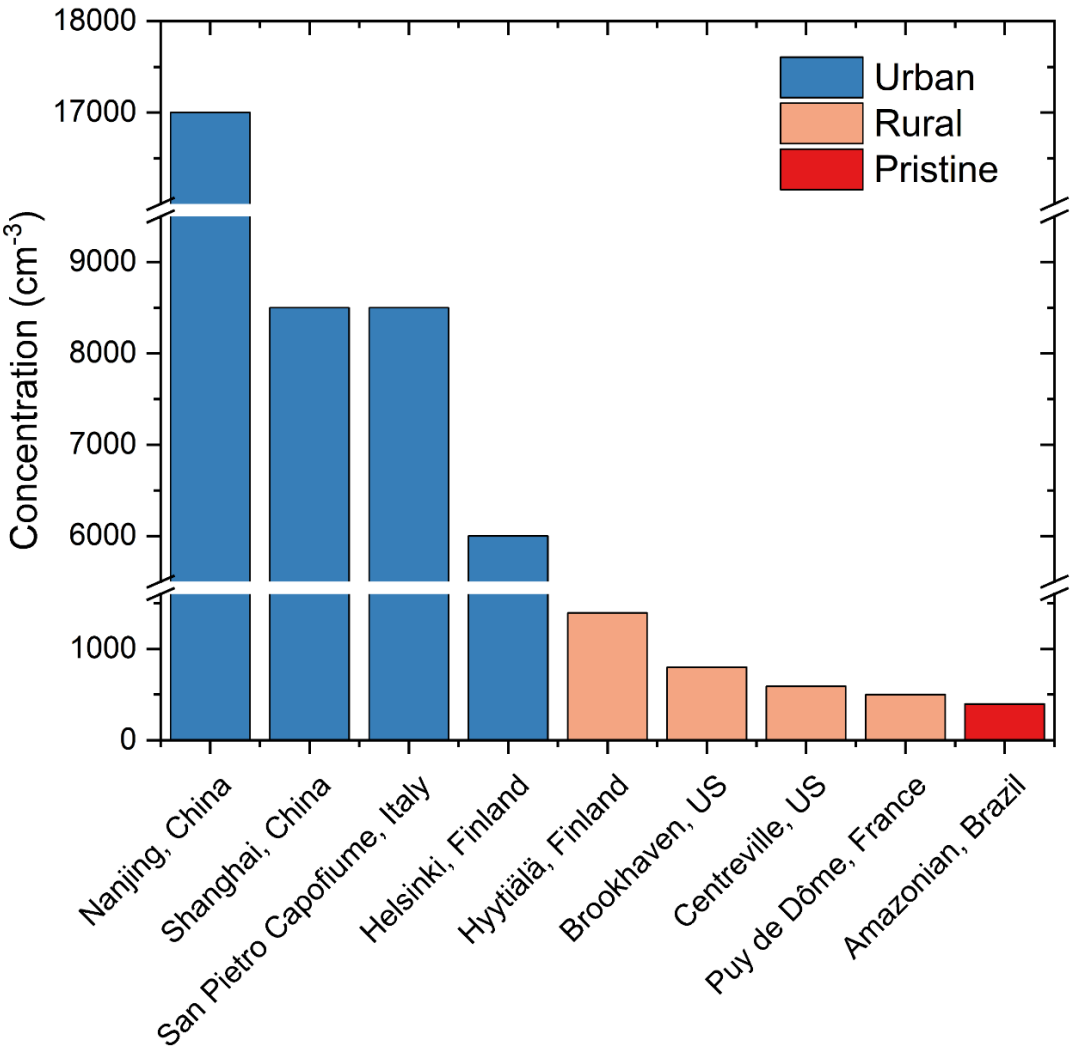

Figure 4. Summary of PSM measurements of particle number concentrations below 3 nm in different environments around the globe. All data are from previous studies, except for the results from the Amazonian region, see Table S1 for details.

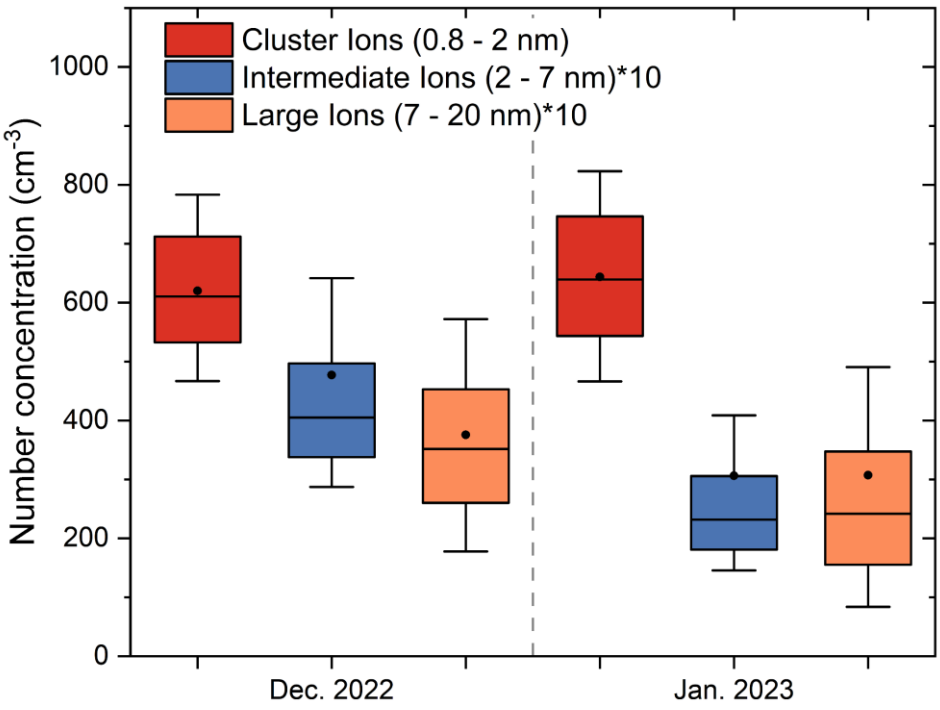

Figure 5. Comparison of negative ion number concentrations in December 2022 and January 2023 for different size ranges based on NAIS measurements. The 25th and 75th percentiles are indicated by the bottom and top edges of the box, while the 5th and 95th percentiles are indicated by vertical whiskers. The horizontal line in the box indicates the median value and the black dot indicates the mean value.

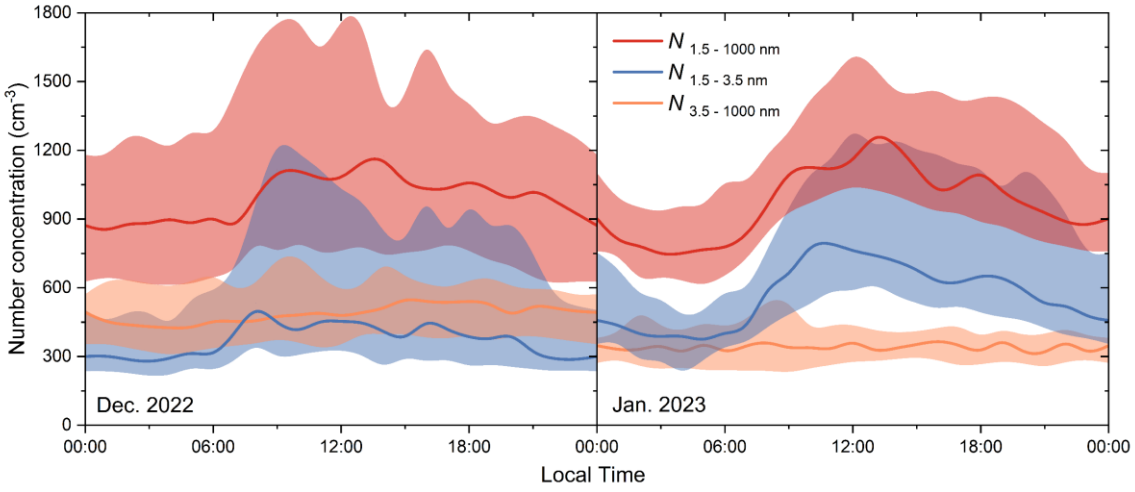

Figure 6. Diurnal variation of particle number concentrations in December 2022 (left panel) and January 2023 (right panel), based on PSM measurements of the size ranges of 1.5-1000 nm (in red line), 1.5-3.5 nm (in blue line), and 3.5-1000 nm (in orange line). The left panel shows the December 2022 results and the right panel shows the January 2023 results. Solid lines indicate median values and shaded areas indicate the 25th-75th percentiles.

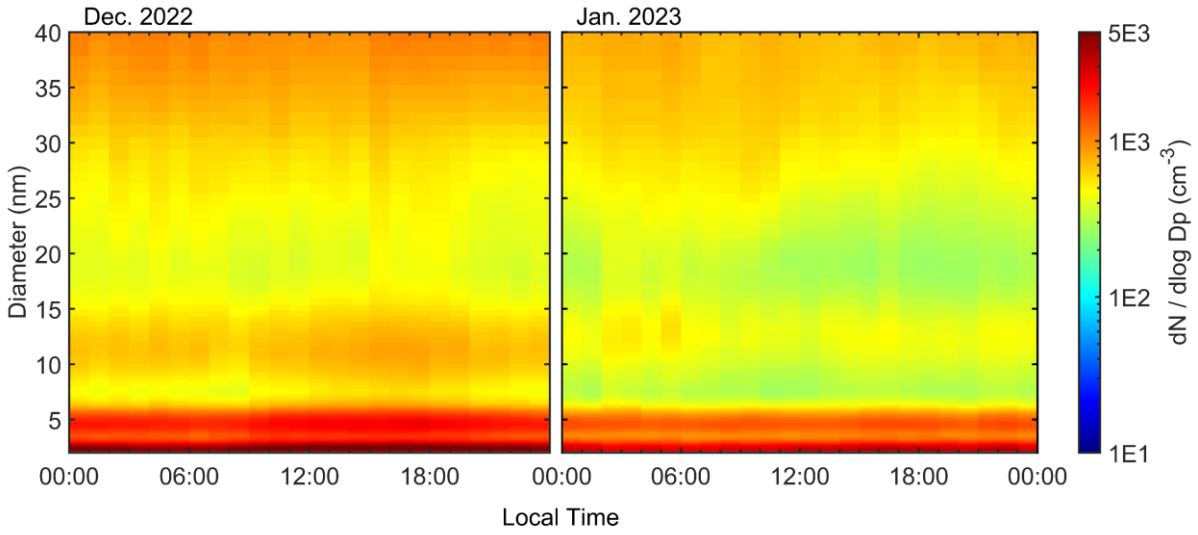

Figure 7. Diurnal variation of the particle number size distribution measured by NAIS during December 2022 (left panel) and January 2023 (right panel). The plot data represent the median values.

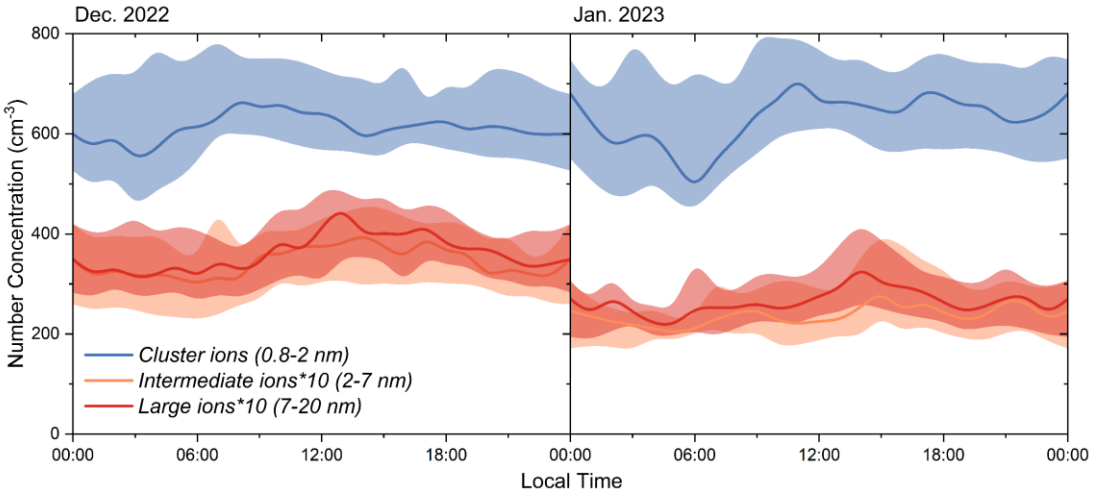

Figure 8. Diurnal patterns of cluster ions in the 0.8-2 nm size range (blue), medium ions in the 2-7 nm range (orange), and large ions in the 7-20 nm range (red) based on NAIS measurements. The left panel indicates results for December 2022 and the right panel indicates results for January 2023. The solid lines indicate the median values and the shaded areas indicate the 25th-75th percentile.

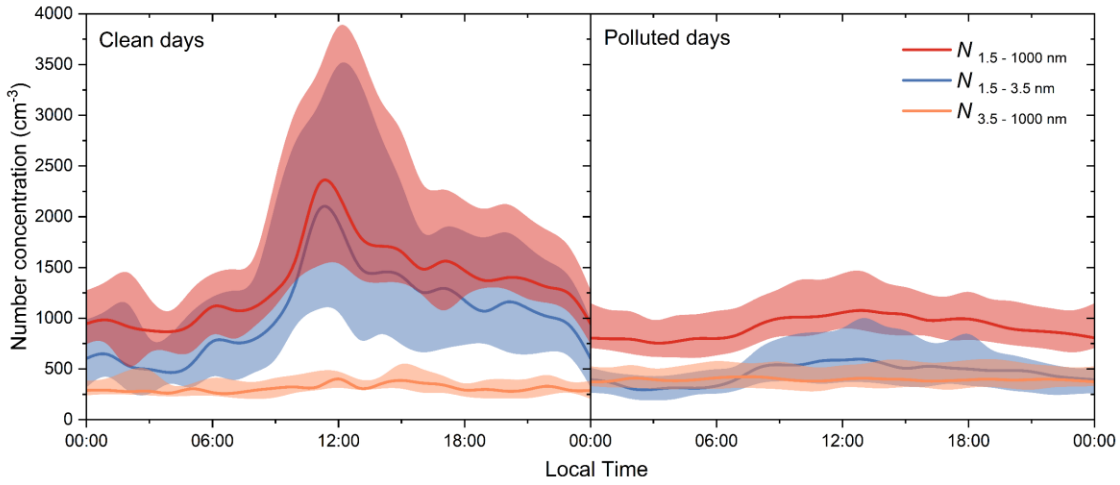

Figure 9. Diurnal variation in number concentrations on clean (left panel) and polluted days (right panel) based on PSM measurements for particles with diameters between 1.5 and 1000 nm (red), 1.5 and 3.5 nm (blue) and 3.5 and 1000 nm (orange). The Lines indicate median values and the shaded areas indicate the 25th-75th percentiles.

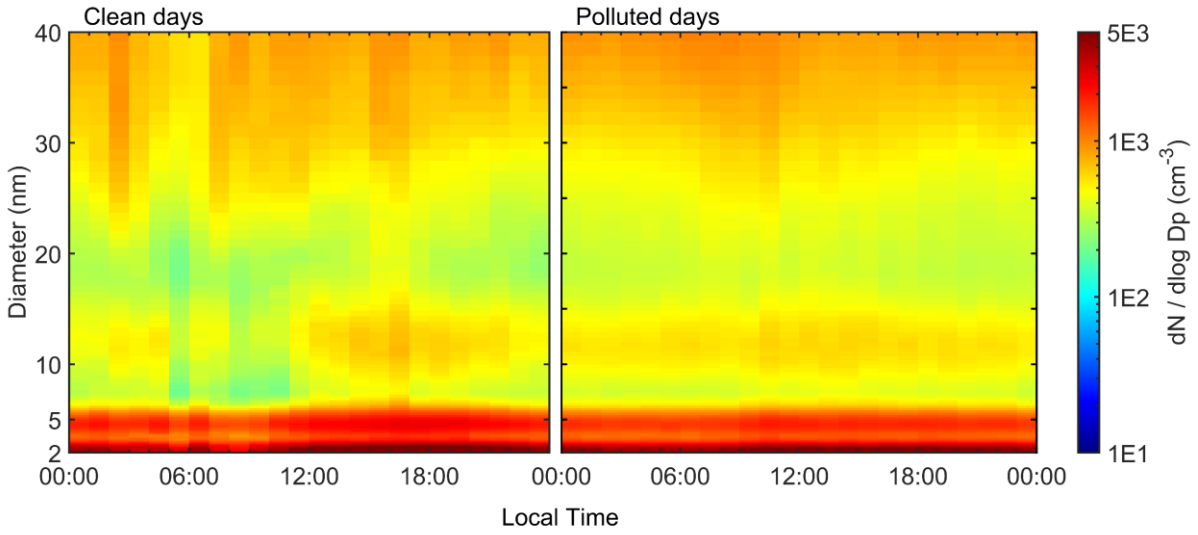

Figure 10. Diurnal variation of the particle number size distribution measured by NAIS during clean days (left panel) and polluted days (right panel). The plot data represents the median values.

Table 1. A summary of the particle number concentration for each instrument in different size ranges. Numbers represent median values, with the 25th-75th percentiles in parentheses.

Instrument	Size range (nm)	Concentration		
		2022.12	2023.01	All period
PSM	1.5-1000	963 (678-1362)	972 (775-1287)	969 (735-1320)
	1.5-3.5	371 (251-741)	573 (406-908)	491 (305-851)
	3.5-1000	481 (355-611)	335 (258-410)	380 (295-539)
NAIS (particle)	2-40	1799 (1427-2195)	1141 (883-1489)	1462 (1076-1944)
	2-4	931 (715-1177)	558 (393-778)	749 (509-1032)
	4-12	497 (400-614)	306 (233-401)	403 (290-538)
NAIS (Ion)	0.8-40	769 (677-876)	751 (644-866)	761 (661-872)
	0.8-2	610 (532-712)	639 (543-746)	624 (537-728)
	2-7	40 (34-50)	23 (18-31)	33 (23-43)
	7-20	35 (26-45)	24 (16-35)	30 (20-41)
SMPS	10-40	17 (9-47)	35 (18-73)	27 (13-63)

Supplementary Material

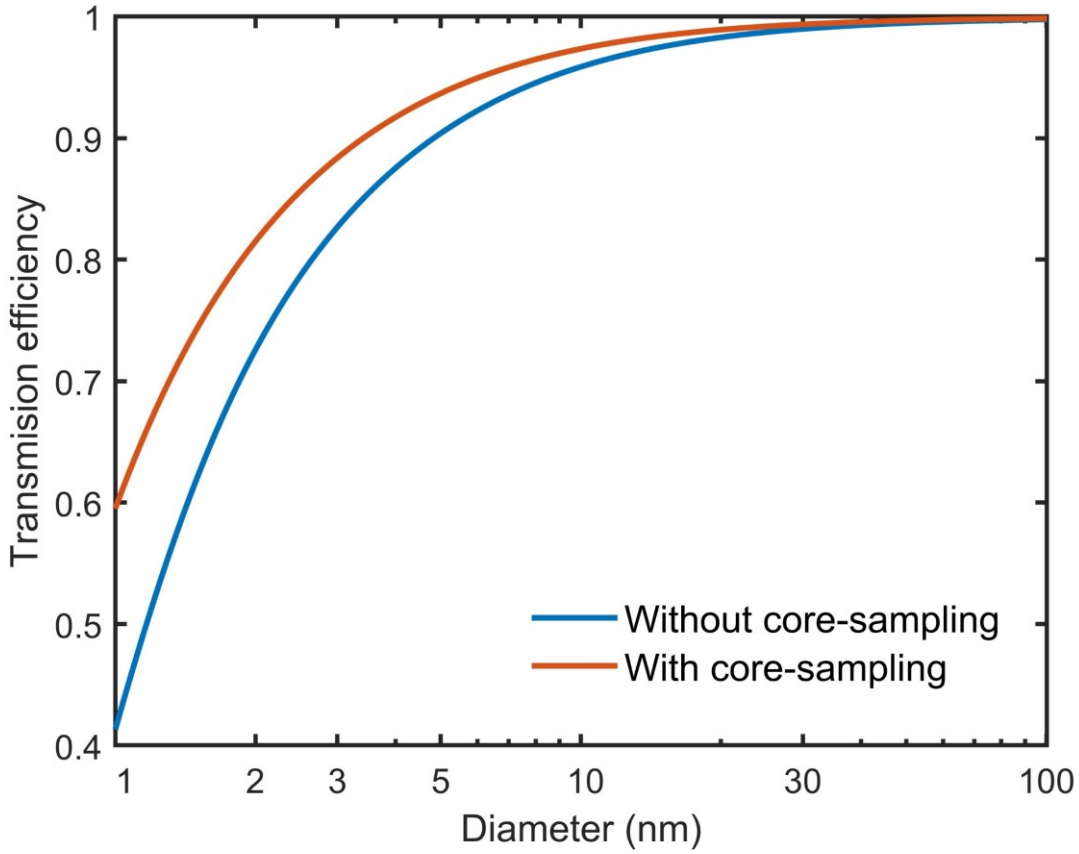

Figure S1. The transmission efficiency for inlet systems with and without core-sampling.

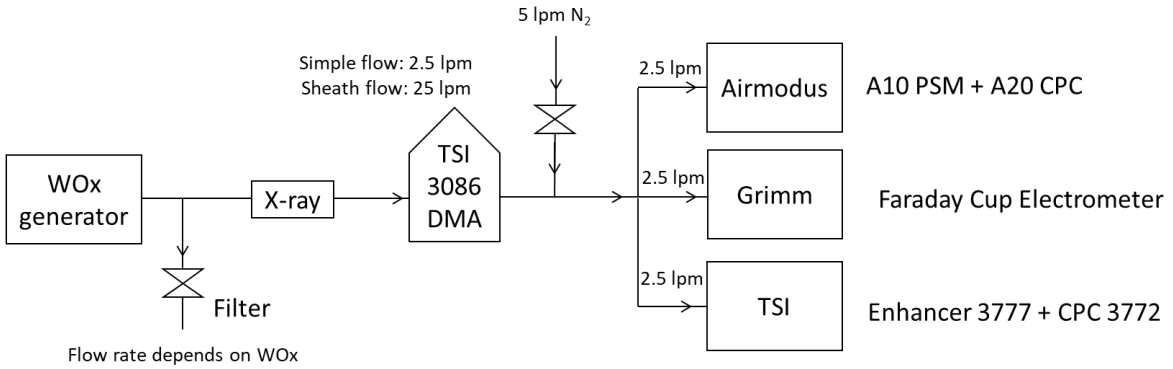

Figure S2. Sketch of the experimental setup for the intercomparison experiments between the Airmodus (A10 PSM + A20 CPC) and the TSI instruments (3777 Enhancer + 3772 CPC).

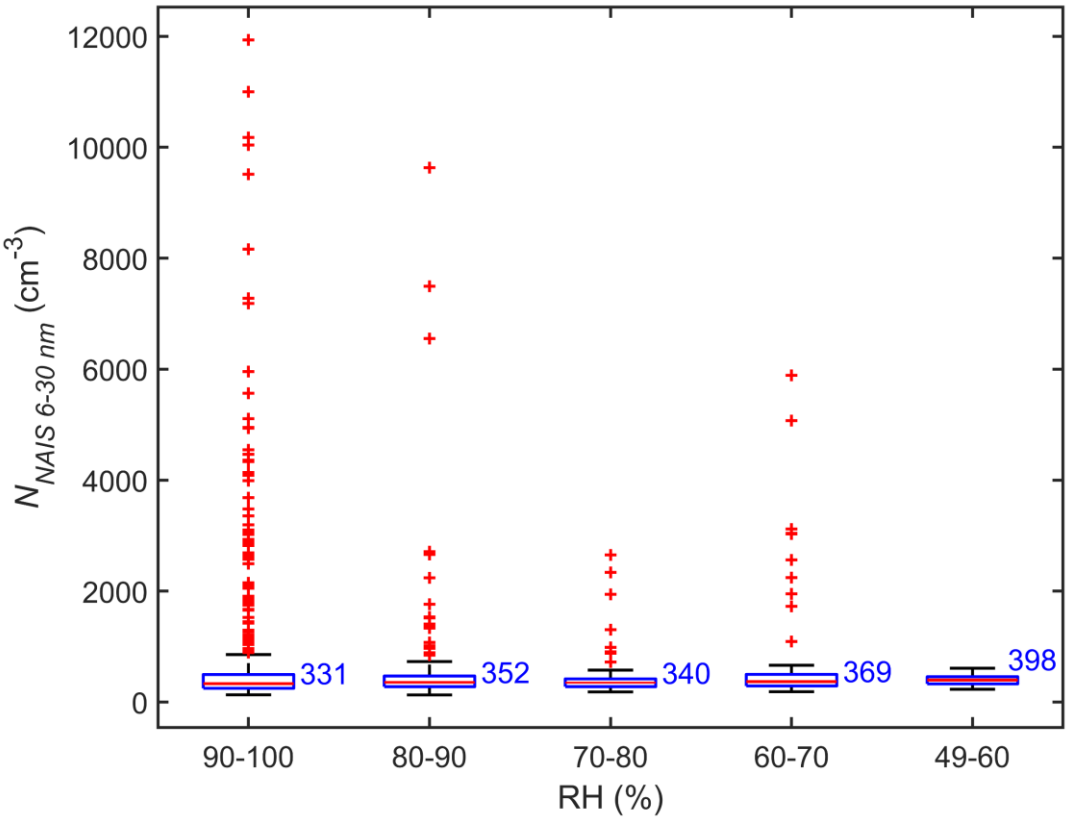

Figure S3. Ambient relative humidity at different range bins versus particle number concentration (size range 6-30 nm) measured by NAIS. The boxes represent the interquartile range (IQR), with the 25th percentile (Q1) at the bottom and the 75th percentile (Q3) at the top. The whiskers extend to the furthest points within Q1 - 1.5 * IQR (lower whisker) and Q3 + 1.5 * IQR (upper whisker). The red points beyond the whiskers are considered outliers and are marked individually. The red lines inside each box represent the median values given next to the boxes (cm^{-3}).

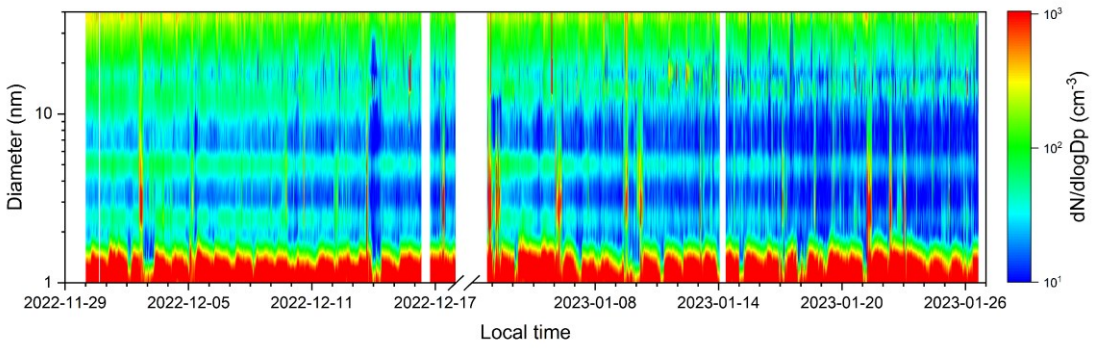

Figure S4. The negative ion number size distribution throughout the measurement period.

Table S1. The summary of the sub-3 nm particle number concentration measurements using PSM across different global environments

Location	Time period	Size range (nm)	Concentration* (cm^{-3})	Environmental type	Literature
Helsinki, Finland	Jan 2015 - Dec 2015	1.1-3.0	6.0E+03	Urban, city	(Kontkanen et al., 2017)
Nanjing, China	Dec 2014 - Jan 2015	1.1-3.0	1.7E+04	Urban, city	(Qi et al., 2015)
Shanghai, China	Nov 2013 - Jan 2014	1.3-3.0	8.5E+03	Urban, city	(Xiao et al., 2015)
San Pietro Capo Fiume, Italy	Jun 2012 - Jul 2012	1.5-3.0	8.5E+03	Urban, city	(Kontkanen et al., 2016)
Centreville, US	Jun 2013 - Jul 2013	1.1-2.1	5.9E+02	Urban, farm/forest	(Yu et al., 2014)
Kent, US	Dec 2011 - Jan 2012	1.3-3.0	4.7E+02	Urban, town	
Brookhaven, US	Jul 2011 - Aug 2011	1.3-3.0	8.0E+02	Rural, coast	
Puy de Dôme, France	Jan 2012 - Feb 2012	1.3- 2.5	5.0E+02	Rural, mountain	(Rose et al., 2015)
Hyytiälä, Finland	Aug 2010 Mar 2011 - Apr 2011 Aug 2011 - Sep 2011 Apr 2012 - May 2012 May 2013 - Jul 2013 May 2015 - Apr 2016	(1.1/1.3)-3.0	1.6E+03	Rural, forest	(Kontkanen et al., 2017)
	April 2014 - April 2020	1.1-2.5	4.1E+02	Rural, forest	(Sulo et al., 2021)
Amazonian, Brazil	Dec 2022	1.5-3.5	4.5E+02	Rural, forest	This study
Amazonian, Brazil	Jan 2023	1.5-3.5	6.1E+02	Rural, forest	This study

* Median values”

Chapter 5

5. Low Sensitivity of Particle Size Distribution to Relative Humidity in a Highly Polluted Environment

This work is to be submitted as Zhu et al. (2025):

I am the first-author of this work and my contributions include performing data analysis, generating all the figures and tables, interpreting and discussing the findings with co-authors, and drafting the manuscript.

The following text, figures, and tables quoted (within"") from page 99 to page 120 are exactly the same as the manuscript which is cited on page 98.

"**Abstract**

The size distribution of atmospheric aerosol particles represents a crucial physical characteristic, intimately associated with a number of key processes, including primary particle emissions, aging processes, air quality, cloud condensation nuclei formation, and human health. Even though a considerable number of studies have demonstrated that the chemical composition of aerosol particles differs significantly under varying relative humidity (RH) conditions, this research focuses on the relationship between chemical composition and particle number size distribution under different humidity conditions. During the autumn-winter of 2018, as part of the Multiphase Chemistry Experiment in Fogs and Aerosols in the North China Plain (McFAN), the size distribution was measured using a scanning mobility particle sizer (SMPS), and the chemical composition was measured using an aerosol mass spectrometer (AMS). By dividing the observation period into high and low humidity periods, it was found that the particle number concentration exhibited a strong correlation with RH, with the concentration in the accumulation mode displaying a greater sensitivity to humidity. In contrast, the diameter of the particles appeared to be less dependent on RH. The mean geometric diameter and the size-resolved particle diameter (Aitken and accumulation mode diameter) demonstrated comparable diurnal fluctuations under both high and low humidity conditions. Our findings indicate that particle size remains relatively constant despite changes in particle composition due to variations in RH. While multiphase reactions play a significant role in chemical composition variation during high humidity conditions, they have less of an impact on particle size distribution. The findings of this study highlight the stability of particle size distribution in highly polluted environments, offering valuable insights into the physical properties of aerosols and the development of pollution mitigation policies.

Introduction

A considerable number of aerosol particles are present in the atmosphere, with diameters ranging over four to five orders of magnitude, from a few nanometers to approximately 100 micrometers (Seinfeld and Pandis, 2016; Pöschl and Shiraiwa, 2015). Furthermore, the concentration of aerosol particles exhibits significant spatial variability, ranging from a few tens of particles per cubic centimeter under Arctic background conditions to several hundred thousand of particles per cubic centimeter in polluted urban environments (Seinfeld and Pandis,

2016; Pöschl, 2005). Particle number size distributions (PNSD) are typically multimodal, comprising the nucleation mode (particles diameter D < 20 nm), the Aitken mode (20 nm < D < 100 nm), the accumulation mode (100 nm < D < 1 μm) and the coarse mode (D > 1 μm) (Hussein, 2005; Whitby, 1978). Fresh aerosols are produced in situ from the gas phase by nucleation and typically consist of nucleation mode particles. Measurements of the PNSD of nucleation mode particles have demonstrated that new particle formation is a global phenomenon (Seinfeld and Pandis, 2016; Kulmala et al., 2012). The majority of Aitken mode particles are initially produced by primary emission, and secondary material condensation during atmospheric transport (Wu and Boor, 2021). The formation of accumulation mode particles occurs through three processes: primary emission from fossil fuel combustion and transportation, condensation of secondary sulfates, nitrates, and organic species in the gas phase, and coagulation of small particles (Seinfeld and Pandis, 2016). The PNSD is a principal parameter for characterizing the microphysical properties of particles. On the one hand, the distribution of particle sizes may be a significant factor influencing the concentration of activated CCN (Dusek et al., 2006). On the other hand, the effects of different particle sizes on human health vary, smaller particles are typically more toxic (Schraufnagel, 2020; Pöschl, 2005).

A substantial number of PNSD measurements have been conducted in various geographical areas, including urban, rural, forest, coastal and remote regions. The mean particle number concentrations were found to range from 12000-18000 cm^{-3} at several measurement stations across different European cities (Reche et al., 2011). The median particle number concentration in the dry season in the Amazonia rain forest was reported to be only 1254 cm^{-3} (Rizzo et al., 2018), whereas the average particle number concentration in Delhi in winter was found to be as high as 52500 cm^{-3} (Gani et al., 2020), and in Beijing in winter it was 37400 cm^{-3} (Liu et al., 2016). Despite the ongoing challenges regarding air pollution in China, the winter haze is still prevailing in the North China Plain (NCP) (Le et al., 2020; Zheng et al., 2015; Guo et al., 2014). The severe pollution not only causes adverse health effects, such as severe respiratory-related symptoms and diseases (Zheng et al., 2015; Pöschl and Shiraiwa, 2015), but is also associated with extremely poor visibility and air quality (Huang et al., 2014). This has implications for the health of more than 400 million inhabitants. Guo et al. (2014) demonstrated that the formation of new particles and subsequent growth through sufficient secondary aerosol formation could significantly contribute to the size distribution during the haze (Guo et al., 2014). A number of recent studies have demonstrated that anomalously high humidity has

facilitated heterogeneous and multiphase chemical processes, which have been identified as a significant contributor to the formation of severe haze in China (Le et al., 2020; Su et al., 2020; Elser et al., 2016).

The chemical composition has a significant impact on the hygroscopicity of aerosols, which in turn affects the radiative forcing, aerosol pH and climate (Wu et al., 2022; Zheng et al., 2020; Jimenez et al., 2009; Pöschl, 2005). In order to obtain the chemical compositions under a range of atmosphere conditions, an aerosol mass spectrometer (AMS) is a particularly well-suited instrument. The AMS is capable of quantifying the mass concentration of non-refractory (NR) species, including sulfate, nitrate, ammonium, chloride, and total organic matter, through thermal vaporization (Zhang et al., 2011; Canagaratna et al., 2007). In highly polluted ambient conditions, significant differences in the PM1/PM2.5 ratios were observed between primary and secondary aerosol at varying RH (Sun et al., 2020b). At higher humidity, the ratio of secondary organic aerosols (OA) is greater than that of primary organic aerosol, and the oxidation capacity of sulfur and nitrogen is higher, indicating stronger multiphase chemistry and secondary chemical transformation (Sun et al., 2020a; Cheng et al., 2016). Previous PNSD studies in North China have demonstrated that particles are commonly formed through new particle formation and subsequent growth through sufficient secondary aerosol formation (Deng et al., 2020; Guo et al., 2014). Despite evidence suggesting that relative humidity can have a significant impact on chemical composition during haze events (Sun et al., 2020b). It was also observed that the particle size distribution is responsible for the majority of the variation in CCN concentration, independent of the chemical composition (Dusek et al., 2006). Further analysis of PNSD is required to provide additional insight into the source and secondary formation processes (Tang et al., 2021).

A comparison of the PNSD measured during the two fog events in 2018 by Wu et al. (2022) revealed that particles with a diameter exceeding 200 nm underwent partial growth into droplets with diameters spanning from 1 to 10 μm during the fog period. This phenomenon elucidated the markedly reduced particle number concentrations observed in the PM1 inlet samples and the absence of a notable decline in the particle number concentration in the PM10 inlet samples. In contrast to previous studies during the McFAN, which focused on the chemical and κ explanation of the fog droplet evolution. The present study focuses on the evolution of PNSD under both low-RH and high-RH conditions, employing the multi-log-normal distribution function to obtain the size-resolved PNSD under different conditions. We aim to present a different perspective on the relationship between PNSD and chemical

composition. Our findings could contribute to more comprehensive understanding of haze formation under background pollution in the North China Plain.

Method

The Multiphase Chemistry Experiment on Fog and Aerosols in the North China Plain (McFAN) campaign was conducted from 12 November to 24 December in winter. The experimental site was located at the Ecological and Agricultural Meteorological Experimental Station of Gucheng, Hebei Province (39°09′ N, 115°44′ E), situated 110 km southeast of Beijing and 35 km northeast of the nearest city, Baoding. The station is surrounded by cultivated land, and there were no agricultural activities in the vicinity of the station during the observation period. This station is minimally affected by urban pollution and can therefore represent background pollution conditions for the NCP regime. Continuous measurements were made of all meteorological parameters (including temperature, RH, wind direction, and speed), trace gases, and aerosol particle number size distributions. A detailed description of the instruments and an overview of this campaign can be found in Li et al. (2021).

During the campaign, a scanning mobility particle sizer (SMPS) was employed to measure the PNSD. The SMPS consists of an electrostatic classifier (Model 3082, TSI, USA), an X-ray neutralizer, a differential mobility analyzer (DMA, Model 3081, TSI, USA), and a condensation particle counter (CPC, Model 3772, TSI, USA) capable of measuring mobility-equivalent diameters from 15 to 750 nm. A custom-built automatic sampling system could achieve continuous switch of the impactors between PM1 and PM10 (sampling aerodynamic diameter less than 1 μm and 10 μm, respectively) every 15 minutes. In addition, a sample dryer system consisting of a 1.2 m long Nafion dryer was employed. The dryer was positioned downstream of the PM inlet to ensure that the relative humidity of the aerosol particle after the dryer was below 15 %. This PM1 and PM10 inlet system advantageously allows for the measurement of particles with dry diameters of less than 1 μm and actual diameters larger than 1 μm under ambient RH conditions. A detailed discussion on this system can be found in the literature (Wu et al., 2022).

An idealized schematic of these particle number size distributions can be characterized by multiple modes, since the basic trimodal distribution described in terms of three additive log-normal distributions was used to interpret particle size distribution (Whitby, 1978). The multi-log-normal distribution function has been widely used to parameterize aerosol particle size distributions (Hussein, 2005). The multi-log-normal distribution function can be described as:

$$n_N^o(\log D_p) = \sum_{i=1}^{n} \frac{N_i}{(2\pi)^{1/2} log\sigma_i} \exp\left(-\frac{(logD_p - log\bar{D}_{pi})^2}{2log^2\sigma_i}\right) \quad (1)$$

Where N_i is the number concentration, $\bar{D}_{pi}$ is the geometric mean diameter, and σ_i is the geometric standard deviation of the ith lognormal mode. D_p is the measured diameter of each aerosol particle, and n is the number of individual log-normal modes. An idealized schematic of these particle number size distributions can be characterized by multiple modes. In this study, the particle sizes range from 15 to 750 nm. Given the range of particle size measured, the nucleation mode is not included in our study. Therefore, the fitted model employed in this paper consists of up to two log-normal modes with a similar fitting methodology (Hussein, 2005). Initial values of the log-normal parameters were fitted by iteration: σ_i for all modes interacted between 1.2 and 2.1. The Aitken and cumulative modes have diameters ranging from 15 to 100 nm and 100 to 750 nm, respectively. In a log-normally distributed particle population, $\bar{D}$pi indicates that most particles are close to $\bar{D}_{pi}$ in size.

Results and Discussion

3.1 Measurement overview

Figure 1 presents the time series of meteorological parameters, including wind speed, wind direction, ambient relative humidity (RH) and temperature, as well as the total particle number concentration, PNSD measured with the PM1 inlet, and the calculated geometric mean diameter of each measurement scan by the SMPS system. During the observation period, the average wind speed was approximately 0.5 m s^{-1}, occasionally exceeding 2.5 m s^{-1}. The prevailing winds were from the southwest, while the strongest winds were mainly from the north. The ambient temperature throughout the observation ranged from -14 to 18 °C and the averaged value was 0.8 ℃. The ambient RH exhibited a range of 12 % to 100 %, with an average value of 58 ± 23 %. The mean total particle number concentration measured with the PM1 inlet over the entire observation period was (1.94 ± 0.67) x 10^4 cm^{-3} and the corresponding geometric mean diameter was determined to be 109 ± 26 nm. Figure S1 illustrates the PNSD and the geometric mean diameter derived for the PM10 inlet. The mean total particle number concentration for the PM10 inlet was (2.08 ± 0.75) x 10^4 cm^{-3}, which was slightly higher than that observed for the PM1 inlet. The geometric mean diameter for the PM10 inlet was identified as 111 ± 29 nm.

Within a similar size range, the above measured particle number concentrations are comparable to those found in some megacities around the world. For example Delhi, the average particle

number concentrations in winter (December to mid-February) and autumn (mid-September to November) can reach 5.25 x 10^4 and 3.8 x 10^4 cm^{-3}, respectively (Gani et al., 2020). Several other cities in China, such as Beijing, Guangzhou and Shanghai, have the mean number concentrations in the particle size range from 20 to 680 nm of 1.6 x 10^4 , 1.4 x 10^4 and 1.3 x 10^4 cm^{-3}, respectively (Cai et al., 2020). In Paris, the mean number concentrations of particles larger than 2.5 nm during summer and winter were 6.9 x 10^4 and 12.1 x 10^4 cm^{-3}, respectively, with significant seasonal variations (Pikridas et al., 2015). In striking contrast, concentrations in extremely clean regions such as the Amazon rainforest were significantly lower, at 403 cm^{-3} in the wet season and 1254 cm^{-3} in the dry season (Rizzo et al., 2018).

3.2 Comparison between high-RH and low RH scenarios

According to the changes in meteorology, mainly the ambient RH, the entire observation period can be divided into two distinct phases. From 12 November to 7 December, the average RH value was 68 ± 23 %, defined as the high RH period. From 7 December to 24 December, the average RH value was 45 ± 16 %, considered as the low RH period. In the following sections, the particle number size distributions during these two periods are further compared and analyzed.

3.2.1 Number/mass concentration and geometric mean diameter

The variation ranges of the meteorological parameters and the measured aerosol properties for the entire measurement period and the two different RH periods are shown in Table 1. The total particle number concentrations at the PM_1 inlet for the high- and low-RH periods were (1.73 ± 0.63) x 10^4 cm^{-3} and (2.29 ± 0.64) x 10^4 cm^{-3}, respectively. For the PM_{10} inlet, the values were (1.84 ± 0.65) x 10^4 cm^{-3} and (2.47 ± 0.77) x 10^4 cm^{-3}, respectively. The difference in particle number concentration between the two inlets was less than 9 % and the slight difference could be due to their distinct aerosol collection efficiencies. Measurements with both inlets showed approximately 20 % higher particle number concentrations during the low RH period compared to the high RH period. The same phenomenon has been shown in previous studies, such as in the Amazon, where values of particle number concentration values were twice as higher in the dry season compared to the wet season (Rizzo et al., 2018). Long-term measurements in South Africa also showed higher concentrations in the dry season (Hirsikko et al., 2012). In addition to potential differences in emission sources, relative humidity has a significant effect on particle number concentration.

The particle mass concentrations were calculated based on the SMPS measurements, assuming that the particles are spherical with a shape factor of 1.0. Additionally, the mean density of the particles was assumed to be approximately 1.2 g cm^{-3}, which is the mean value of the ambient aerosol (Hallquist et al., 2009). As a consequence of the elevated particle number concentration, the total mass concentration at the PM1 inlet was observed to be higher under low RH conditions, at (115 ± 65) μg m^{-3}. Similarly, the mass concentration value can reach to 133 μg m-3 under low RH conditions, as observed at the PM10 inlet. However, the AMS results indicated higher mass concentrations during periods of high humidity (Sun et al., 2020b). The discrepancy may be attributed to the exclusion of black carbon from the AMS results (Zhou et al., 2022; Zhang et al., 2011).

The geometric mean diameter of the PM1 inlet exhibited minimal variation across different RH stages, with mean values of 109 ± 27 nm at high RH and 109 ± 25 nm at low RH conditions. For the PM10 inlet, the geometric mean diameter was observed to be slightly larger at the high RH stage (112 ± 30 nm) in comparison to the low RH stage (109 ± 26 nm). At the low RH, the geometric mean diameters for both inlets were found to be almost identical, indicating a higher proportion of submicron aerosol during this period. This result was also obtained by AMS, which demonstrated that the PM1 fraction was higher within PM2.5 during the low RH stage (Sun et al., 2020b). The chemical composition of the particles revealed a notable increase in the proportion of organic matter in NR-PM1 from 47 % to 64 % during the low RH phase. Concurrently there was a reduction in the mass fraction of all the inorganic species (SO_4, NO_3 and NH_4) (Sun et al., 2020b). Nevertheless, our findings suggest that despite the observed differences in chemical composition, the variation in the geometric mean diameters across different RH stages was relatively minimal.

3.2.2 Log-normal distribution

The size-resolved particle number size distributions are illustrated in in Figure 2. As shown in Fig. 2a, the averaged particle number concentrations in the Aitken and accumulation modes for the entire observation period were 1526 and 15780 cm^{-3}, with the corresponding lognormal mean diameters of 32 and 123 nm, respectively. Figure 2b and 2c present the fitting results for the high- and low- RH periods, respectively. The particle number concentration in the accumulation mode was observed to be 38 % higher in the low RH period (average: 19240 cm^{-3}) compared to the high RH period (13589 cm^{-3}). However, during the period with low humidity, the Aitken mode exhibited lower particle number concentrations (1246 cm^{-3}) than the high humidity period (1691 cm^{-3}). The lognormal mean diameters of the Aitken mode showed a

slight shift from the high RH (31 nm) to the low RH period (33 nm). And the diameters of the accumulation mode were also quite similar for the high- and low-humidity conditions (125 nm vs. 120 nm). Table 1 provides a summary of all the obtained average concentration and diameter values, and all the best-fitting parameters are listed in Table S1.

The log-normal distributions of the data derived using the PM10 inlet are illustrated in Figure S3. The particle number concentration in the Aitken and accumulation modes was found to be 1312 and 17348 cm^{-3}, respectively. In comparison to the findings for the PM1 inlet, the particle concentration at the PM10 inlet exhibited a slight decrease in the Aitken mode and an increase in the accumulation mode. For the PM10 inlet, the log-normal diameters in the Aitken mode were observed to be 30 and 32 nm, respectively, during the periods of high and low humidity periods. The corresponding diameters in the accumulation mode were 124 and 121 nm, respectively. In contrast to the number concentration, no notable discrepancy was observed in the log-normal mean diameter of the two inlets concerning the number concentration.

The study by Sun et al. (2020b) has revealed notable discrepancies in the chemical composition of PM1 between the two different RH scenarios. Under high RH conditions, the mass fraction of inorganic species (i.e., the sum of nitrate, sulfate, ammonium and chloride) was found to be comparable to that of organic species (53 % vs. 47 %). However, during the low RH period, organic aerosols were observed to predominate with a mass fraction of 64 % (Sun et al., 2020b). These differences could be mainly explained by the enhanced formation of secondary inorganic species such as sulfate, nitrate and ammonium in aerosol water facilitated by high RH (Jin et al., 2020; Cheng et al., 2016). Note that, among the organic species, the oxygenated organic aerosols (OOA) were also observed to form rapidly due to daytime photochemical aqueous-phase reactions at the same site during our campaign (Kuang et al., 2020). Despite these clear differences in the chemical composition of PM1 between the two RH scenarios, the particle size distributions were found to be markedly analogous.

3.3 Diurnal variation

3.3.1 Diurnal variation of number, mass concentration and geometric mean diameter

Figure 3 shows the diurnal cycles of the ambient relative humidity (RH), temperature, and the total number/mass concentration and geometric mean diameter of submicron aerosols measured with the PM1 inlet for the entire campaign and at different RH periods. Clearly, the RH and temperature (Fig. 3a and 3b) displayed opposite variation patterns. The RH reached the maximum in the early morning (around 06:00) and the minimum in the late afternoon

(around 18:00). In contrast, the temperature reached its lowest point in the early afternoon and started to increase during morning hours and peaked at late afternoon. Both RH and temperature showed higher values during the high RH period compared to the low RH period.

As shown in Fig. 3c, a pronounced diurnal variation trend was observed in the particle total number concentration. For all the three scenarios, higher number concentrations occurred in the morning (08:00-09:00) and evening (19:00-20:00) and the lowest concentrations were observed in the afternoon (14:00-15:00). The number concentration, however, showed constantly the highest values for the low RH scenario than the other two cases, which could reach up to around 28000 cm^{-3} both in the morning (08:00-09:00) and the evening (19:00-20:00). The lowest concentrations were observed during the high humidity period, with the minimum values of approximately 10000 cm^{-3} appeared in the afternoon (14:00-15:00). Generally, the averaged particle concentration (on an hourly basis) exhibited a 33 % increase during the low RH period compared to the high RH period. Similar diurnal variations in particle number concentration were also found in Beijing, with higher concentrations during low RH periods, particularly during the morning and evening rush hours (Wu et al., 2007).

The diurnal variation of the geometric mean diameter is shown in Fig. 4d. Overall, the geometric mean diameters for the three RH scenarios displayed quite similar daily variation patterns within a narrow size range of ~ 95-125 nm. Two peaks were observed in the early morning (04:00-05:00) and around midday (11:00-13:00), while two troughs were found in the late morning (08:00-09:00) and evening (17:00-19:00). The morning peaks were frequently attributed to the accumulation of emissions during rush hours, in conjunction with the reduced atmospheric mixing heights (Zheng et al., 2015; Wu et al., 2007). The occurrence of midday peaks could be caused by enhanced photochemical reactions, which result in the growth of existing particles (Guo et al., 2014). For the valley around 08:00-09:00, it coincided with the total number concentration peak in Fig. 3c. The coincidence indicates that a large number of small-size particles were generated, which increased the total number concentration yet reduced the mean particle diameter. This phenomenon is probably associated with the new particle formation events normally observed during this time window at the site, as reported by Hong et al. (2023). Figure S4 illustrates the same diurnal variation in the number concentration of PM10 inlet. The geometric mean diameter of the PM1 and PM10 inlets exhibited minimal discrepancy between the low and high humidity stages. Furthermore, the chemical composition of the aerosol exhibited a diurnal variation, with the concentrations of SOA and inorganic species increasing in the afternoon (Li et al., 2021). The geometric mean particle diameter

displayed minimal variation between high and low RH conditions, whereas SOA and inorganic species exhibited a notable increase during periods of high RH.

The trend of the converted mass concentration is shown in Figure 4 panel (e), with the lowest value in the afternoon (14:00-15:00) under all conditions. During the night, the mass concentration demonstrated a consistent and elevated profile. During the night and morning, a notable discrepancy was observed in mass concentration between the high and low RH conditions, with the low RH stage showing approximately 20 % higher mass concentration than the high RH stage. Given that the particle sizes were similar between the high and low RH conditions, it can be observed that the number concentration is significantly higher during the low RH periods. As shown in Figure S4, the diurnal variation of the mass concentration in the PM10 inlet exhibited a similar pattern to that observed in the PM1 inlet.

The overall particle size distribution exhibited minimal sensitivity to RH, with the exception of the total number concentration, which demonstrated a clear correlation with RH. Previous studies have demonstrated a notable increase in the mass fraction of inorganic species and an upward trend in the SOA fraction from low to high RH phases (Li et al., 2021; Sun et al., 2020b). Although multiphase processes played an important role in the increase of secondary species composition under high RH conditions, our findings indicate that the diverse chemical compositions do not represent the primary driver influencing the diurnal cycles of particle diameter.

3.3.2 Size-resolved diurnal variation of particle diameter

The diurnal cycle of fitted particle diameters with PM1 inlet in the Aitken and accumulation modes are illustrated in Figure 5. In the Aitken mode, a distinct minimum in particle diameter was observed (~37 nm) during the morning period (07:00-09:00), after which there was a notable increase in diameter to a maximum (~86 nm) at midnight. The particles in the accumulation mode exhibited a maximum diameter peak in the afternoon (approximately 13:00) and a minimum diameter in the evening (approximately 19:00). From morning to early afternoon, there was a consistent increase in particle diameter in both the Aitken and accumulation modes. However, there was a subsequent divergence in the trend between the two modes for the remainder of the day. A similar diurnal pattern was observed for particle size distributions in Beijing, with an increase in particle size during the morning due to traffic and other anthropogenic activities (Wu et al., 2007). The discrepancies in particle diameter between the high and low RH periods were insignificant, particularly during the night and

morning. However, some fluctuations in particle diameter were observed between the high and low RH periods in the afternoon and evening. As previously stated, there are discrepancies in the chemical composition observed in the afternoon (Li et al., 2021). Such differentiation between modes may also be attributed to intricate interactions between photochemical reactions, coagulation processes and condensation. Additionally, the drying process employed during sampling may also influence particle morphology and mixing state, potentially contributing to slight variations in size distributions (Riemer et al., 2019).

Figure S4 illustrates the diurnal variation of the fitted Aitken and accumulation modes using the PM10 inlet. In comparison to the PM1 inlet, both the Aitken and accumulation mode diameters demonstrated comparable trends. Nevertheless, a slight discrepancy was observed in the Aitken mode between 03:00 and 08:00: the PM1 inlet indicated a continuous decrease in diameter, whereas the PM10 inlet demonstrated a nearly constant diameter. During this period, when the relative humidity is at its highest for the day, the inclusion of larger particles in the PM10 inlet served to buffer the changes in particle size, resulting in a constant Aitken mode diameter. Furthermore, the chemical composition remains constant for all particles throughout the night (Li et al., 2021). In comparison to the daytime, the primary emission sources (such as traffic and cooking) and photochemical processes contributed less significantly to particle diameter in both modes during the night. A number of studies have demonstrated that a greater proportion of inorganic species is present in the accumulation mode particle, and that external mixing is also a common occurrence (Wu et al., 2022; Lee et al., 2017). These two properties may result in the behavior of large particles differing from that of small particles.

Conclusion

The PNSD and chemical composition are two key parameters of the physicochemical properties of aerosol particles, with implications for both climate impacts and human health. In this work, detailed characterizations of submicron particles during the November-December 2018 McFAN campaign are presented. Considerably high number concentrations (18900 cm^{-3}) were observed, with an average mass concentration of 100 $\mu g\ m^{-3}$, which was significantly higher than in other regions.

The observation period was divided into two comparative periods based on relative humidity (RH), with the high and low RH conditions serving as the basis for the division. The particle size distribution showed almost identical patterns with geometric mean diameters of 109 nm under high and low RH conditions. The size-resolved diameter values indicated that the Aitken

mode particles exhibited a lower sensitivity to RH than the accumulation mode particles. Specifically, the diameters of the Aitken mode particles were found to be 31 nm and 33 nm under high and low RH stages, respectively, whereas the diameters of the accumulation mode particles were 125 nm and 120 nm, respectively. In terms of diurnal variation, the particle number concentration was influenced by RH, with higher particle number concentration during the low RH period than during the high RH period, as indicated by the diurnal variation. The diurnal cycle of particle size for both Aitken and accumulation modes had a comparable pattern between two different RH stages, and all the results related to particle size indicated that the particle size distributions were less sensitive to RH.

The chemical compositions showed significant differences under different RH conditions, with high humidity increasing the amount of secondary inorganic and organic materials in aerosol particles under low RH conditions (Sun et al., 2020b). Regarding cloud nucleation capacity, a previous study demonstrated that size is more important than chemistry (Dusek et al., 2006). In this study, we emphasized the size distribution for submicron particles was less sensitive to different RH compared to the chemical composition. The driving forces behind this phenomenon remain to be discovered. These results contribute to a better understanding of haze events in China and help to formulate emission control policies.

Table and Figures

Table. 1 Comparison of parameters across different RH periods (i.e., the entire period, high RH period, and low RH period) and with two sampling inlets (PM1and PM10). Entire period: 12 November - 24 December; High RH period: 12 November - 6 December; Low RH period: 7 December - 24 December. The numbers represent median values, with the 25th-75th percentiles shown in brackets.

	Entire period		High RH		Low RH	
	PM1	PM10	PM1	PM10	PM1	PM10
RH (%)	57.5 (40.8-74.9)		67.7 (50.5-87.9)		45.4 (32.4-59.5)	
Temperature (℃)	0.8 (-3.1-4.9)		3.4 (-0.1-4.9)		-3.3 (-6.2-0.8)	
Total number concentration ($1/cm^3$)	19371 (14664-24206)	20878 (15467-26106)	17281 (13305-21561)	18370 (13928-23017)	22912 (18209-26062)	24728 (19301-28412)
Total mass concentration ($\mu g/m^3$)	99.0 (59.0-143.1)	120.6 (72.2-179.3)	90.8 (58.0-130.4)	115.4 (74.8-176.4)	115.1 (60.4-157.2)	132.6 (65.5-185.4)
Aitken mode number concentration ($1/cm^3$)	1526 (1343-1708)	1312 (1181-1442)	1691 (1526-1856)	1357 (1247-1466)	1246 (1040-1452)	1263 (1067-1459)
Accumulation mode number concentration ($1/cm^3$)	15780 (15557-16002)	17348 (17177-17519)	13589 (13390-13787)	14925 (14782-15069)	19240 (18979-19502)	21138 (20880-21396)
Geometric mean diameter (nm)	109 (94-125)	111 (95-128)	109 (95-124)	112 (97-128)	109 (93-126)	110 (93-127)
Lognormal diameter for Aitken mode (nm)	32 (31-33)	31 (30-32)	31 (31-32)	30 (30-31)	33 (32-34)	32 (31-33)
Lognormal diameter for Accumulation mode (nm)	123 (121-124)	123 (122-124)	125 (123-126)	124 (124-126)	120 (119-122)	121 (120-122)

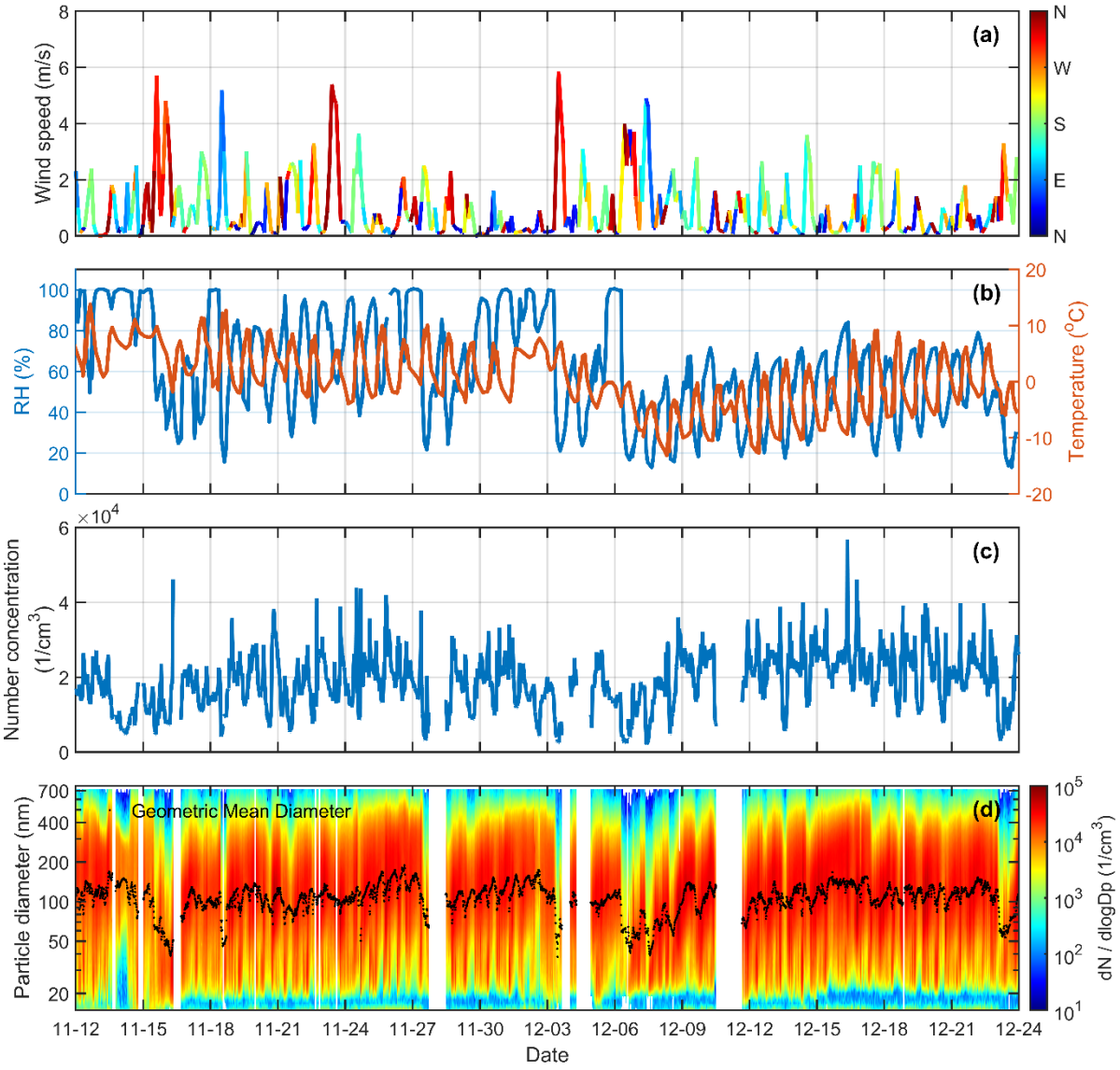

Figure 1. Time series of (a) wind speed and direction; (b) relative humidity (RH) and temperature (T); (c) total particle number concentration derived from PNSD data; (d) measured PNSD within the 15-750 nm size range, with black dots representing the geometric mean diameter derived from each measurement scan throughout the entire measurement period (12 November – 24 December 2018). The white areas indicate periods without measurement data.

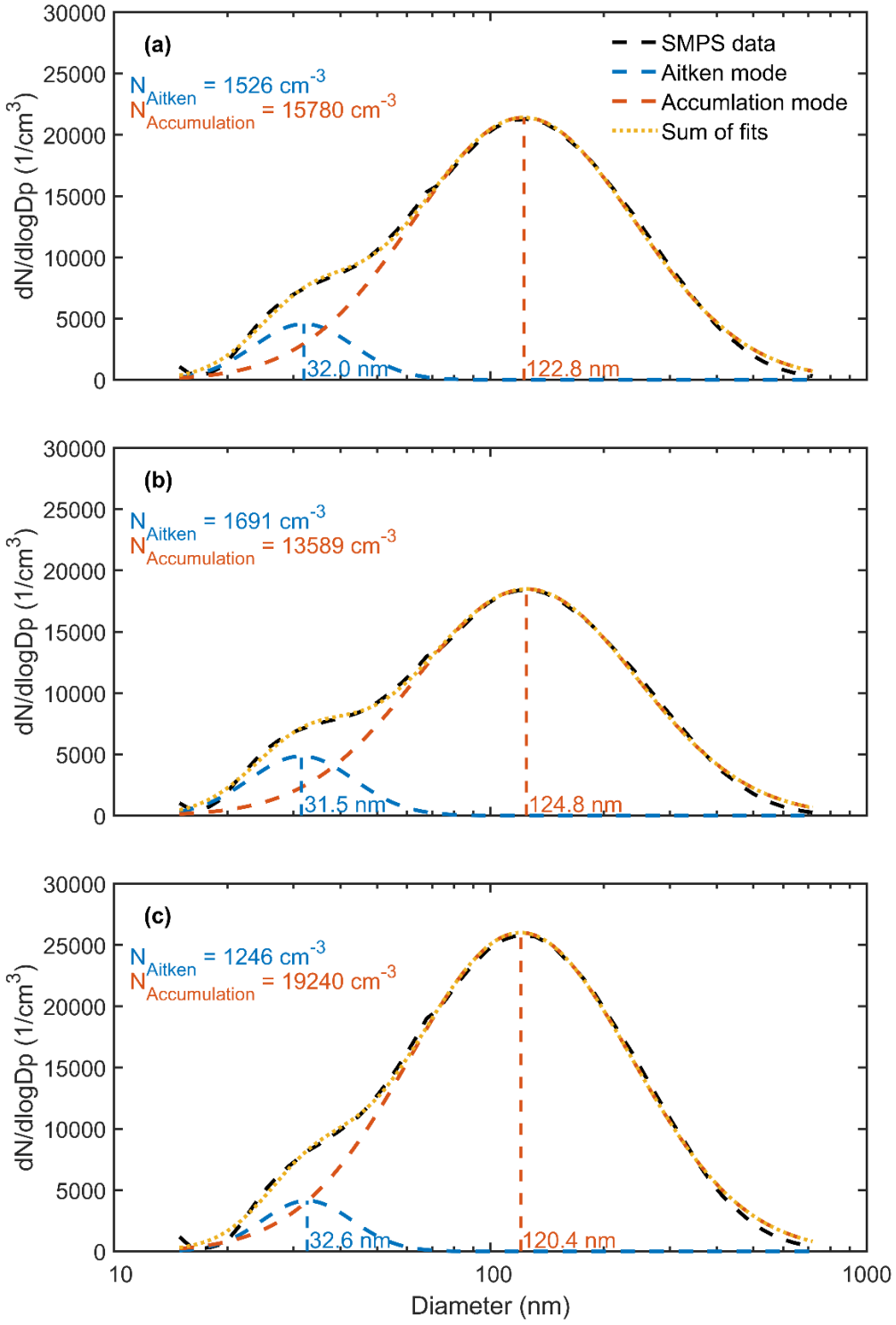

Figure 2. Size-resolved particle number size distribution obtained with the PM1 inlet under different conditions: (a) the entire measurement period (12 November to 24 December), (b) the high humidity period (12 November to 7 December), and (c) the low humidity period (7 December to 24 December). The best-fitted particle diameter and number concentration are shown in each panel. Black, blue, and orange dashed lines represent SMPS measurements, the fitted Aitken mode, and the fitted accumulation mode, respectively.

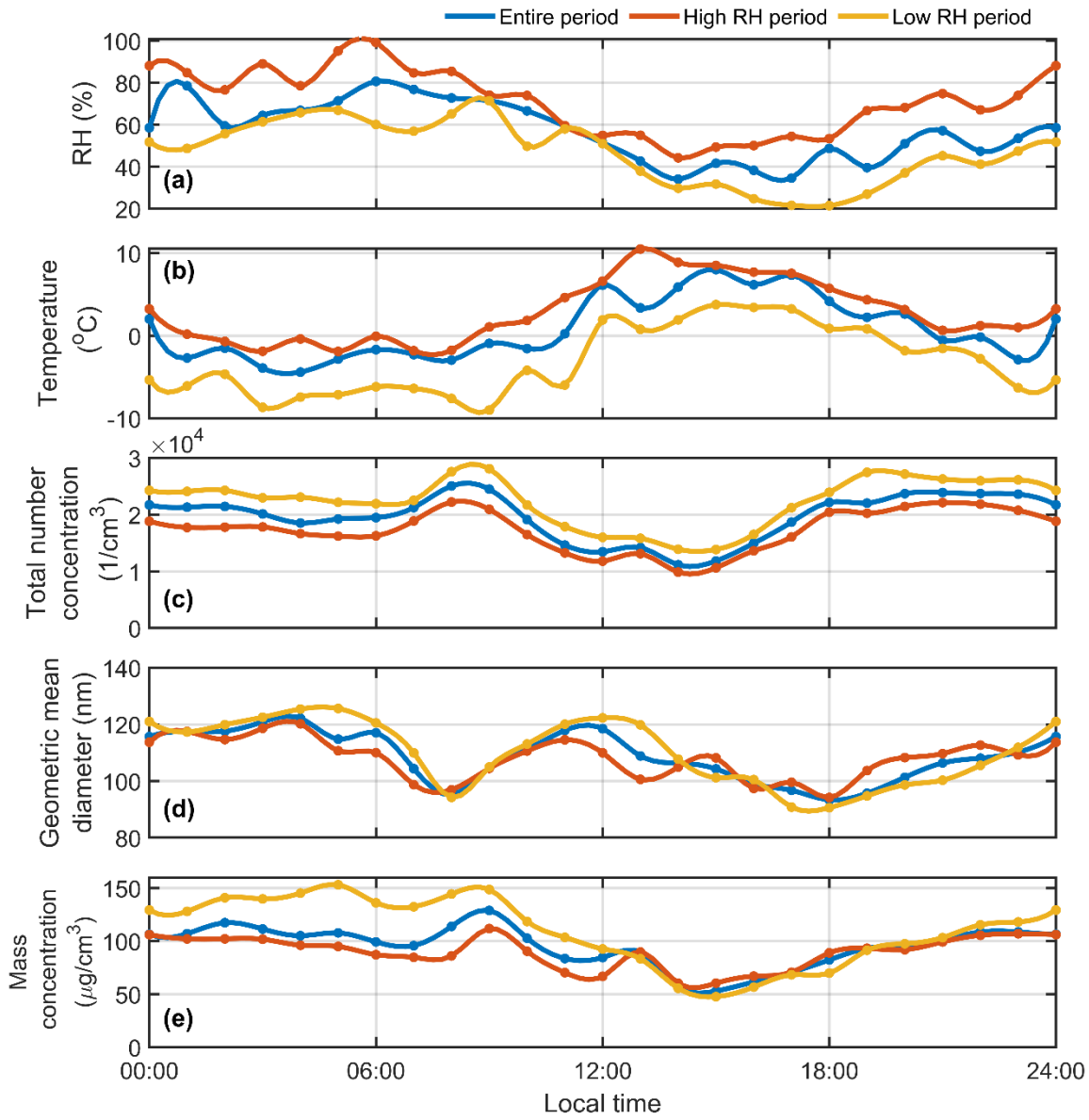

Figure 3. Diurnal cycles of (a) ambient relative humidity; (b) ambient temperature; (c) total number concentration; (d) geometric mean diameter, and (e) mass concentration of the aerosol measured with the PM1 inlet. The blue, red and orange lines represent the entire measurement period (12 November to 24 December), the high humidity period (12 November to 7 December), and the low humidity period (7 December to 24 December), respectively.

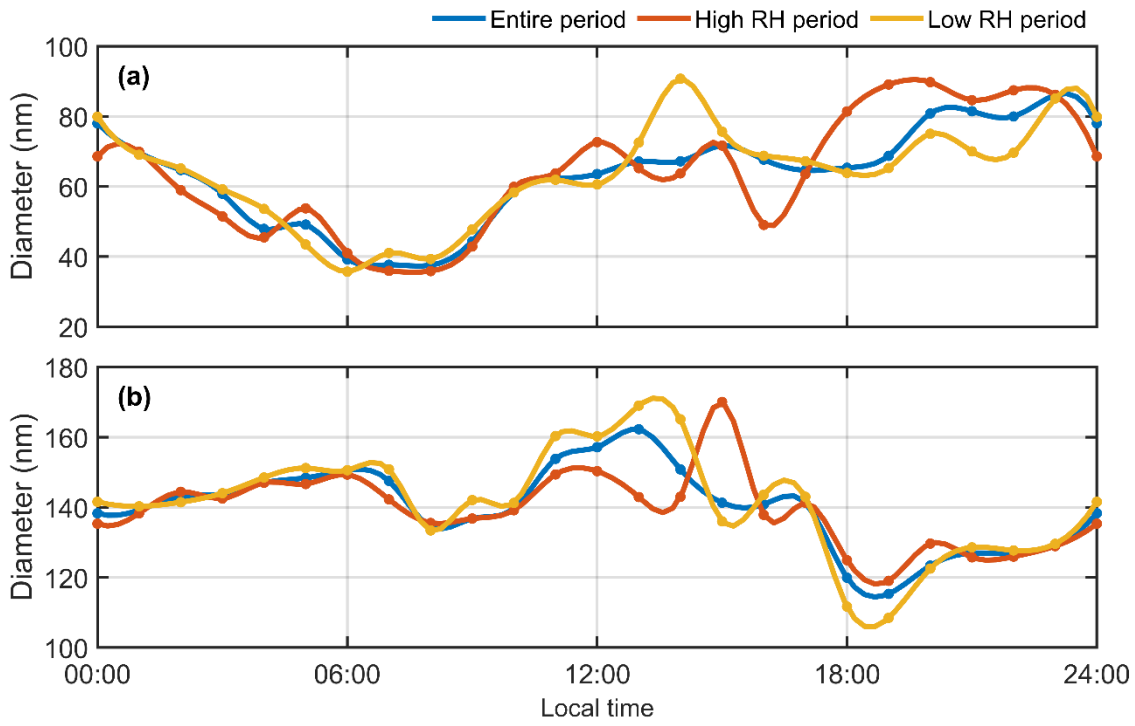

Figure 4. Diurnal variation of (a) fitted Aitken mode particle diameter and (b) fitted accumulation mode particle diameter with the PM1 inlet across different RH periods. The blue line represents the entire measurement period (12 November to 24 December), the red line represents the high RH period (12 November to 7 December), and the orange line represents the low RH period (7 December to 24 December).

Supplementary Material

Table S1. Best-fit parameters of the log-normal distribution applied to the observed PNSD, as shown in Figure. 3. Parameters include geometric standard deviation (σ_g) and R squared coefficient (R^2).

Period	Mode	σ_g	R^2
Entire period	Aitken	1.36 ± 0.05	0.99794
	Accumulation	1.97 ± 0.03	
High RH period	Aitken	1.39 ± 0.05	0.99787
	Accumulation	1.95 ± 0.03	
Low RH period	Aitken	1.30 ± 0.06	0.99784
	Accumulation	1.99 ± 0.03	

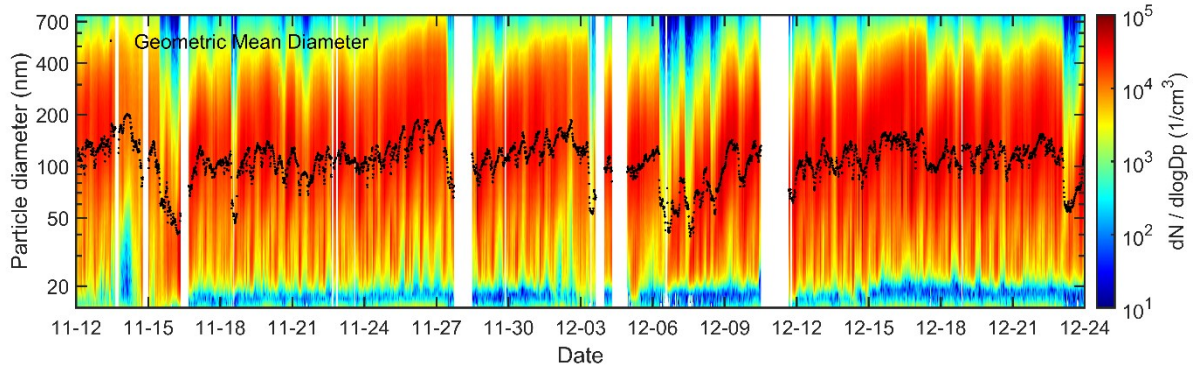

Figure S1. The particle number size distribution with the PM10 inlet during the observation period (from 12 November to 24 December 2018). The black dots indicated the geometric mean diameter for each scan.

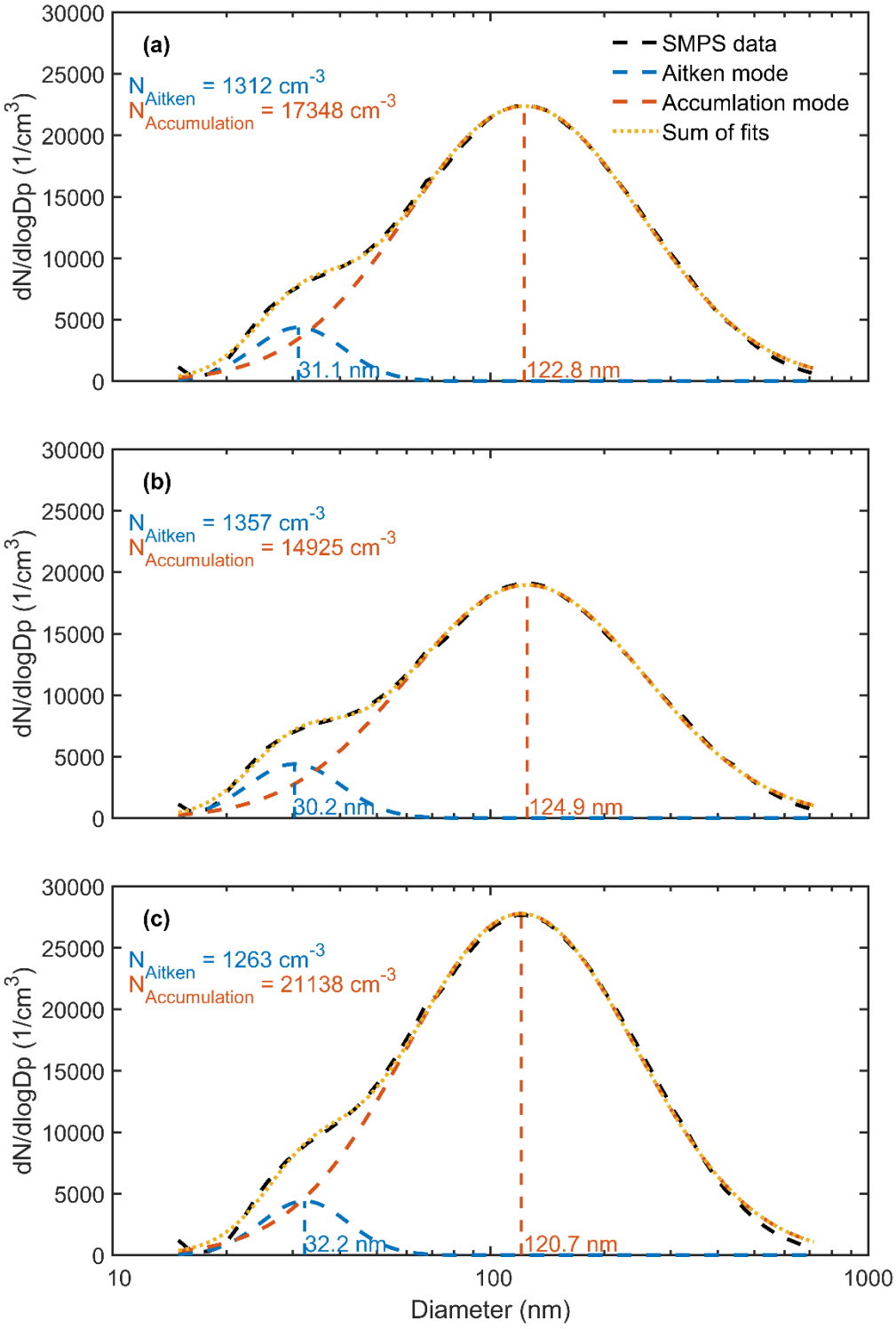

Figure S2. Size-resolved particle number size distribution obtained with the PM10 inlet under different conditions: (a) the entire measurement period (12 November to 24 December), (b) the high humidity period (12 November to 7 December), and (c) the low humidity period (7 December to 24 December). The best-fitted particle diameter and number concentration are indicated in each panel. Black, blue, and orange dashed lines represent SMPS measurements, the fitted Aitken mode, and the fitted accumulation mode, respectively.

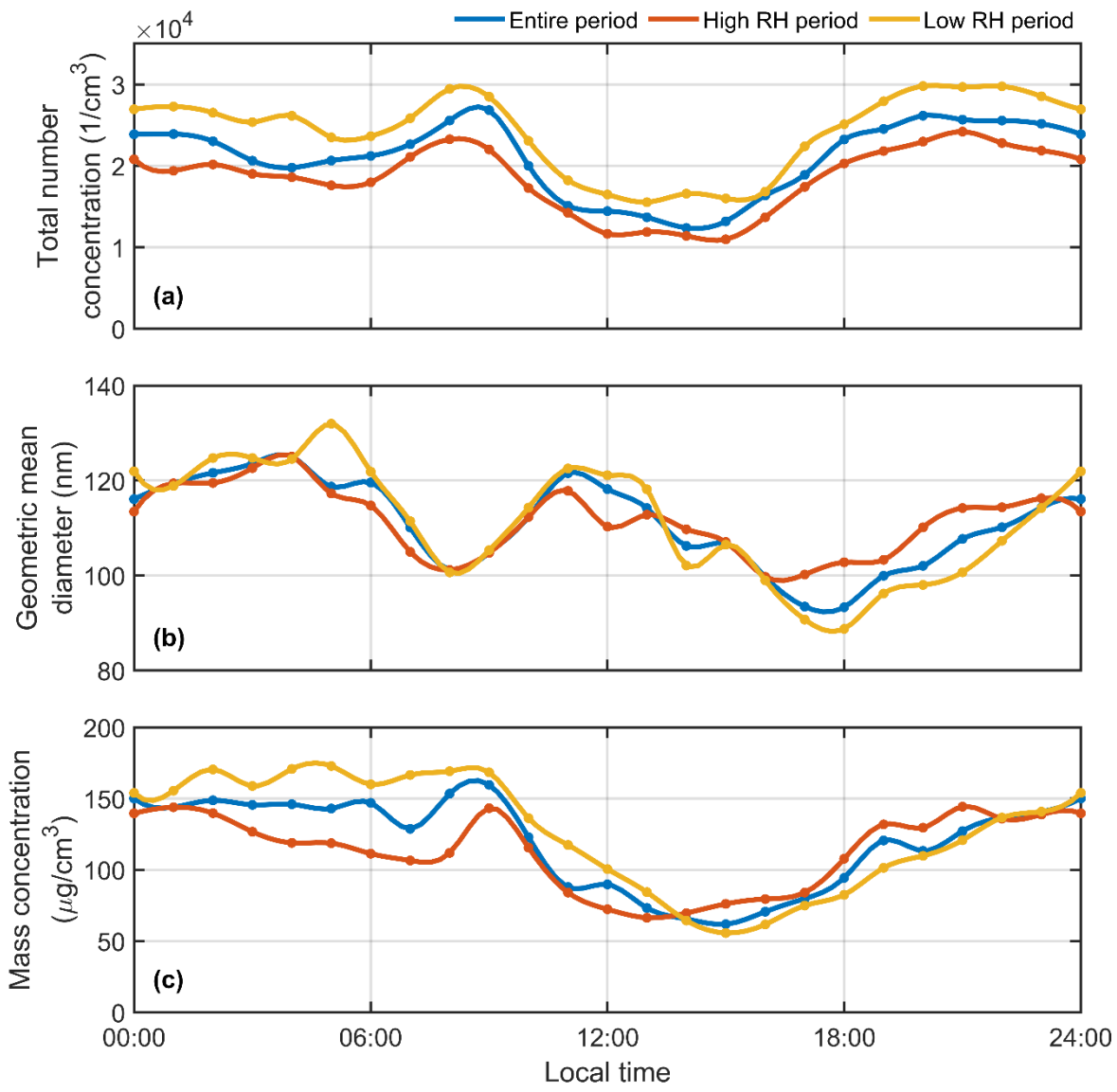

Figure S3. Diurnal cycles of (a) total number concentration; (b) geometric mean diameter, and (c) mass concentration with the PM10 inlet. The blue, red and orange lines represent the entire measurement period (12 November to 24 December), the high humidity period (12 November to 7 December), and the low humidity period (7 December to 24 December), respectively.

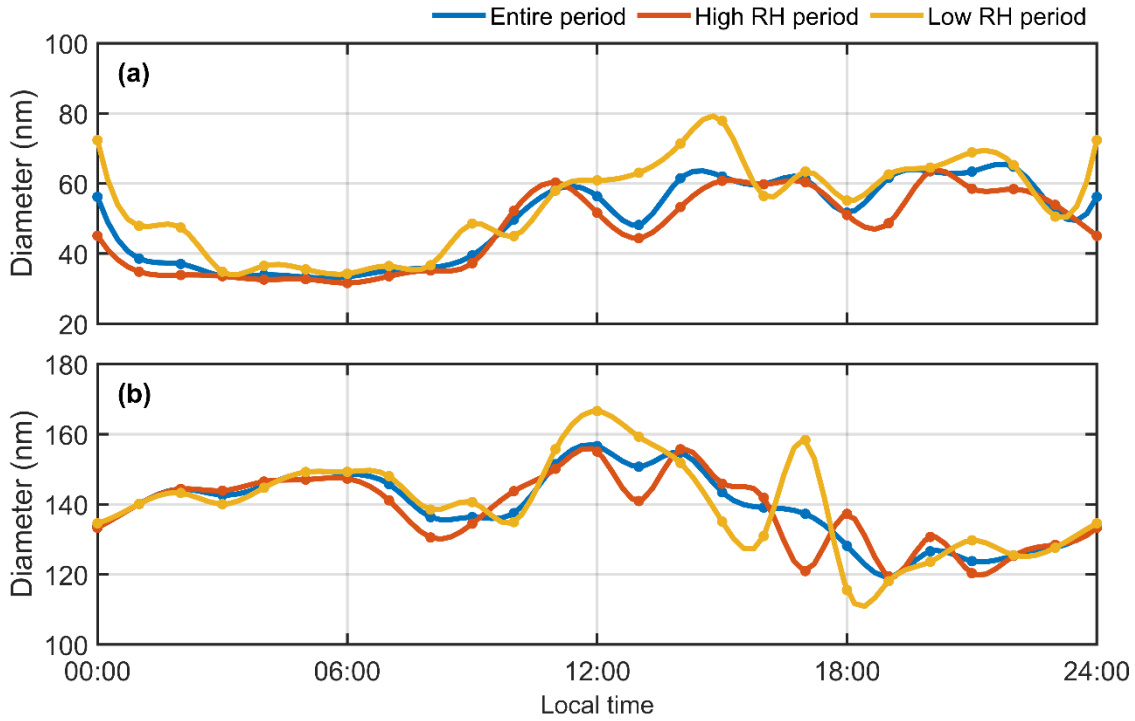

Figure S4. Diurnal variation of PM10 inlet (a) fitted to the Aitken mode particle diameter and (b) fitted to the accumulation mode particle diameter. The blue, red and orange lines represent the entire measurement period (12 November to 24 December), the high humidity period (12 November to 7 December), and the low humidity period (7 December to 24 December), respectively."

Chapter 6

6. Conclusion and outlook

Aerosol particles are an integral part of cloud formation and precipitation, and also have a significant impact on local air quality, the energy balance of the Earth's surface, the global climate system and human health. A deeper understanding of the sources and processes of aerosol particles in urban and pristine environments is essential for improving our understanding of the natural atmosphere and for accurately quantifying the impact of anthropogenic sources on atmospheric composition and radiative forcing. In addition, this knowledge is essential for predicting the dynamics of aerosols from natural and anthropogenic sources, thereby improving the accuracy of climate models and predictions in urban and pristine areas.

The objective of this thesis was to characterize aerosol particles in distinct environmental settings, including urban areas in Germany, the pristine Amazon rainforest, and the polluted atmosphere of the North China Plain (NCP). The key insights into NPF processes and aerosol dynamics included the PNSD and diurnal variations. The ultimate goal was to improve understanding of aerosol dynamics and NPF processes across diverse environments, thereby enhancing the accuracy of air quality models and refining climate impact assessments. These objectives were addressed by three measurement campaigns, in the Mainz (Germany), ATTO (Brazil) and Gucheng (China).

The objective of the measurements conducted in Mainz, Germany was to investigate the NPF and aerosol dynamics in an urban environment, as detailed in Chapter 3. The study employed state-of-the-art aerosol instruments, including the TSI Nano-SMPS, Airmodus PSM, and Ariel NAIS, to quantify particle number size distributions and evaluate NPF frequency and parameters over a period from 1 March to 10 July 2022. The findings indicated that 8 % of the days were identified as NPF event days. During event periods, the formation rate ($J \leq 1.5$ nm) ranged from 0.3 to 11.3 cm^{-3} s^{-1}, and the growth rate (particle size range 1.5-20 nm) ranged from 1.9 to 6.6 nm h^{-1}. In addition, the CS values ranged from (1.8-6.9) × 10^{-3} s^{-1}. The particle concentrations and growth rates were observed to be generally lower than those documented in megacities but higher than in remote areas. A comprehensive analysis of meteorological conditions revealed that low relative humidity, low wind speeds, and high solar radiation were conducive to the occurrence of NPF events. At the same time, these findings highlight the importance of employing a variety of instruments to accurately characterize aerosol dynamics, particularly within the sub-10 nm size range, where significant uncertainties frequently exist.

The study offers valuable insights into the behavior of ultrafine particles in urban environments and highlights the necessity for further research to enhance understanding of NPF processes and their implications for air quality and climate.

The measurements conducted at ATTO in the Amazon rainforest as part of the CAFE-Brazil campaign (December 2022 to January 2023) were undertaken with the objective of exploring aerosol dynamics and NPF in a pristine environment (Chapter 4). The findings for the first time indicated the significant presence of sub-3 nm particles and cluster ions in the Amazon boundary layer, with their concentrations exhibiting distinct diurnal variations. The diurnal patterns of sub-3 nm particles were particularly pronounced during the clean days. No typical regional NPF events were observed during the measurement period. These findings indicate that, although NPF events did not occur, the formation of nanoclusters in the pristine Amazon environment is influenced by biogenic processes rather than anthropogenic factors. The study provides valuable data into nanocluster dynamics, paving the way for future investigations into the gas-phase precursors that drive aerosol formation in the Amazon and other pristine regions.

The measurements conducted in Gucheng, China, during the McFAN campaign (November-December 2018) yielded pivotal insights into the relationship between aerosol dynamics and chemical composition in the heavily polluted NCP (Chapter 5). The study observed exceptionally high particle number concentrations (median 20800 cm^{-3}) and mass concentrations (median 121 $\mu g\ m^{-3}$), which greatly exceeded the levels typically observed in other regions. The particle size distributions under different RH conditions demonstrated that the Aitken and accumulation mode particles exhibited a minimal change in particle size (log-normal fitting) with humidity. However, notable differences were observed in the chemical composition of the aerosols between high and low RH conditions, with high humidity favoring the formation of secondary inorganic and organic species (Sun et al., 2020b). These findings highlight that the particle size distribution is less dependent on RH than the chemical composition. While the underlying mechanisms remain to be elucidated through further research, this new perspective contributes to a more comprehensive understanding of haze events in China.

Despite our best efforts to guarantee the precise measurement of particles below 10 nm in size and concentration, including regular instrument calibration, optimization of the sampling tube, and accurate loss calculations. The discrepancies were noted in the measurements obtained from the various instruments during the field observations. Accurately quantifying of sub-10 nm particles, particularly those sub-3 nm particles, is a major challenge in the field of aerosol

science. Previous comprehensive comparisons have also reported discrepancies in particle number concentrations and size distributions between instruments, especially in the sub-10 nm range (Kangasluoma et al., 2020). This emphasizes the challenge of obtaining consistent and reliable data regarding nucleation mode particles under ambient conditions. One of main reasons for this discrepancy is the low charge efficiency of these nanoparticles, which results in an underestimation of the particle concentration. Moreover, nanoparticles, particularly those sub-3 nm, have a high loss rate, which also leads to in inaccurate measurement outcomes. The aforementioned particles are also highly susceptible to changes in environmental conditions (such as temperature, humidity, and chemical composition) during the measurement process. Furthermore, the low concentrations of these particles in many environments enhance the challenge of measurement, as the low signal-to-noise ratio hinders the capacity to distinguish the signal of small particles from background noise. The combination of these factors renders the measurement of particles below 10 nm (especially below 3 nm) a challenging process that demands precise calibration and the utilization of multiple techniques to ensure the reliability of the obtained data.

Another limitation of this study is the lack of detailed chemical composition data for the gas-phase precursors, clusters, and particle phases. This prevents a comprehensive understanding of the formation mechanisms underlying NPF events. Although measurements of particle size distributions and ion concentrations provide valuable insights, the formation mechanisms of these nanoclusters remain unclear due to the lack of sufficient chemical information about the gaseous precursors involved in NPF. For instance, key species such as sulfuric acid, HOMs, and ammonia are known to play critical roles in NPF. However, the specific contributions of these species to particle formation under varying atmospheric conditions remain unclear. Moreover, although the ATTO campaign has yielded some chemical data through CIMS measurements, these data are still undergoing analysis. Gaining insight into the mechanisms behind NPF events represents a significant challenge within the field of atmospheric research, particularly in the context of complex environments where multiple factors, including photochemistry, biogenic emissions, and atmospheric mixing, interact in a nonlinear manner. Thus, there is a pressing need for more detailed investigations into the chemical composition of both the gas-phase precursors and the particle phases. This will facilitate the unravelling of the underlying processes that govern NPF and, in turn, lead to more accurate predictions of aerosol dynamics in a range of atmospheric contexts.

Further research is required to gain a deeper understanding of the complex interactions between aerosol formation, chemical composition, and environmental factors, especially in regions with diverse levels of anthropogenic influence. In urban environments, there is a need for more comprehensive studies on the drivers of NPF, particularly in areas with frequent pollution episodes, in order to refine the understanding of growth rates, condensation sinks, and the role of various precursors in particle formation. Furthermore, future studies in the North China Plain should seek to investigate the multiphase chemistry of aerosols in greater detail, taking into account the dual impacts of high pollution levels and varying RH conditions on particle growth and composition. In the case of the Amazon rainforest, future research will focus on integrating gas-phase measurements in order to gain insight into the relationship between biogenic VOCs, sulfuric acid, and nanocluster formation. This will facilitate the discovery of the mechanisms that drive nanoparticle formation in this pristine environment, thereby enhancing our comprehension of NPF processes in the absence of anthropogenic influences. In conclusion, these studies will contribute to a more comprehensive understanding of aerosol dynamics across different environments, thereby providing critical insights into air quality management and climate change modeling.

7. References

Agarwal, J. K. and Sem, G. J.: Continuous flow, single-particle-counting condensation nucleus counter, Journal of Aerosol Science, 11, 343-357, https://doi.org/10.1016/0021-8502(80)90042-7, 1980.

Ahlm, L., Nilsson, E. D., Krejci, R., aring, rtensson, E. M., Vogt, M., and Artaxo, P.: Aerosol number fluxes over the Amazon rain forest during the wet season, Atmos. Chem. Phys., 9, 9381-9400, 10.5194/acp-9-9381-2009, 2009.

Almeida, J., Schobesberger, S., Kürten, A., Ortega, I. K., Kupiainen-Määttä, O., Praplan, A. P., Adamov, A., Amorim, A., Bianchi, F., Breitenlechner, M., David, A., Dommen, J., Donahue, N. M., Downard, A., Dunne, E., Duplissy, J., Ehrhart, S., Flagan, R. C., Franchin, A., Guida, R., Hakala, J., Hansel, A., Heinritzi, M., Henschel, H., Jokinen, T., Junninen, H., Kajos, M., Kangasluoma, J., Keskinen, H., Kupc, A., Kurtén, T., Kvashin, A. N., Laaksonen, A., Lehtipalo, K., Leiminger, M., Leppä, J., Loukonen, V., Makhmutov, V., Mathot, S., McGrath, M. J., Nieminen, T., Olenius, T., Onnela, A., Petäjä, T., Riccobono, F., Riipinen, I., Rissanen, M., Rondo, L., Ruuskanen, T., Santos, F. D., Sarnela, N., Schallhart, S., Schnitzhofer, R., Seinfeld, J. H., Simon, M., Sipilä, M., Stozhkov, Y., Stratmann, F., Tomé, A., Tröstl, J., Tsagkogeorgas, G., Vaattovaara, P., Viisanen, Y., Virtanen, A., Vrtala, A., Wagner, P. E., Weingartner, E., Wex, H., Williamson, C., Wimmer, D., Ye, P., Yli-Juuti, T., Carslaw, K. S., Kulmala, M., Curtius, J., Baltensperger, U., Worsnop, D. R., Vehkamäki, H., and Kirkby, J.: Molecular understanding of sulphuric acid–amine particle nucleation in the atmosphere, Nature, 502, 359-363, 10.1038/nature12663, 2013.

Andreae, M. O., Artaxo, P., Brandão, C., Carswell, F. E., Ciccioli, P., da Costa, A. L., Culf, A. D., Esteves, J. L., Gash, J. H. C., Grace, J., Kabat, P., Lelieveld, J., Malhi, Y., Manzi, A. O., Meixner, F. X., Nobre, A. D., Nobre, C., Ruivo, M. d. L. P., Silva-Dias, M. A., Stefani, P., Valentini, R., von Jouanne, J., and Waterloo, M. J.: Biogeochemical cycling of carbon, water, energy, trace gases, and aerosols in Amazonia: The LBA-EUSTACH experiments, Journal of Geophysical Research: Atmospheres, 107, LBA 33-31-LBA 33-25, https://doi.org/10.1029/2001JD000524, 2002.

Andreae, M. O., Afchine, A., Albrecht, R., Holanda, B. A., Artaxo, P., Barbosa, H. M. J., Borrmann, S., Cecchini, M. A., Costa, A., Dollner, M., Fütterer, D., Järvinen, E., Jurkat, T., Klimach, T., Konemann, T., Knote, C., Krämer, M., Krisna, T., Machado, L. A. T., Mertes, S., Minikin, A., Pöhlker, C., Pöhlker, M. L., Pöschl, U., Rosenfeld, D., Sauer, D., Schlager, H., Schnaiter, M., Schneider, J., Schulz, C., Spanu, A., Sperling, V. B., Voigt, C., Walser, A., Wang, J., Weinzierl, B., Wendisch, M., and Ziereis, H.: Aerosol characteristics and particle production in the upper troposphere over the Amazon Basin, Atmos. Chem. Phys., 18, 921-961, 10.5194/acp-18-921-2018, 2018.

Andreae, M. O., Acevedo, O. C., Araùjo, A., Artaxo, P., Barbosa, C. G. G., Barbosa, H. M. J., Brito, J., Carbone, S., Chi, X., Cintra, B. B. L., da Silva, N. F., Dias, N. L., Dias-Júnior, C. Q., Ditas, F., Ditz, R., Godoi, A. F. L., Godoi, R. H. M., Heimann, M., Hoffmann, T., Kesselmeier, J., Könemann, T., Krüger, M. L., Lavric, J. V., Manzi, A. O., Lopes, A. P., Martins, D. L., Mikhailov, E. F., Moran-Zuloaga, D., Nelson, B. W., Nölscher, A. C., Santos Nogueira, D., Piedade, M. T. F., Pöhlker, C., Pöschl, U., Quesada, C. A., Rizzo, L. V., Ro, C. U., Ruckteschler, N., Sá, L. D. A., de Oliveira Sá, M., Sales, C. B., dos Santos, R. M. N., Saturno, J., Schöngart, J., Sörgel, M., de Souza, C. M., de Souza, R. A. F., Su, H., Targhetta, N., Tóta, J., Trebs, I., Trumbore, S., van Eijck, A., Walter, D., Wang, Z., Weber, B., Williams, J., Winderlich, J., Wittmann, F., Wolff, S., and Yáñez-Serrano, A. M.: The Amazon Tall Tower Observatory (ATTO): overview of

pilot measurements on ecosystem ecology, meteorology, trace gases, and aerosols, Atmos. Chem. Phys., 15, 10723-10776, 10.5194/acp-15-10723-2015, 2015.

Arffman, A., Yli-Ojanperä, J., Kalliokoski, J., Harra, J., Pirjola, L., Karjalainen, P., Rönkkö, T., and Keskinen, J.: High-resolution low-pressure cascade impactor, Journal of Aerosol Science, 78, 97-109, https://doi.org/10.1016/j.jaerosci.2014.08.006, 2014.

Artaxo, P., Hansson, H.-C., Andreae, M. O., Bäck, J., Alves, E. G., Barbosa, H. M. J., Bender, F., Bourtsoukidis, E., Carbone, S., Chi, J., Decesari, S., Després, V. R., Ditas, F., Ezhova, E., Fuzzi, S., Hasselquist, N. J., Heintzenberg, J., Holanda, B. A., Guenther, A., Hakola, H., Heikkinen, L., Kerminen, V.-M., Kontkanen, J., Krejci, R., Kulmala, M., Lavric, J. V., de Leeuw, G., Lehtipalo, K., Machado, L. A. T., McFiggans, G., Franco, M. A. M., Meller, B. B., Morais, F. G., Mohr, C., Morgan, W., Nilsson, M. B., Peichl, M., Petäjä, T., Praß, M., Pöhlker, C., Pöhlker, M. L., Pöschl, U., Von Randow, C., Riipinen, I., Rinne, J., Rizzo, L. V., Rosenfeld, D., Silva Dias, M. A. F., Sogacheva, L., Stier, P., Swietlicki, E., Sörgel, M., Tunved, P., Virkkula, A., Wang, J., Weber, B., Yáñez-Serrano, A. M., Zieger, P., Mikhailov, E., Smith, J. N., and Kesselmeier, J.: Tropical and Boreal Forest – Atmosphere Interactions: A Review, Tellus B: Chemical and Physical Meteorology, 10.16993/tellusb.34, 2022.

Baalbaki, R., Pikridas, M., Jokinen, T., Laurila, T., Dada, L., Bezantakos, S., Ahonen, L., Neitola, K., Maisser, A., Bimenyimana, E., Christodoulou, A., Unga, F., Savvides, C., Lehtipalo, K., Kangasluoma, J., Biskos, G., Petäjä, T., Kerminen, V. M., Sciare, J., and Kulmala, M.: Towards understanding the characteristics of new particle formation in the Eastern Mediterranean, Atmos. Chem. Phys., 21, 9223-9251, 10.5194/acp-21-9223-2021, 2021.

Baccarini, A., Karlsson, L., Dommen, J., Duplessis, P., Vüllers, J., Brooks, I. M., Saiz-Lopez, A., Salter, M., Tjernström, M., Baltensperger, U., Zieger, P., and Schmale, J.: Frequent new particle formation over the high Arctic pack ice by enhanced iodine emissions, Nature Communications, 11, 4924, 10.1038/s41467-020-18551-0, 2020.

Bellouin, N., Quaas, J., Gryspeerdt, E., Kinne, S., Stier, P., Watson-Parris, D., Boucher, O., Carslaw, K. S., Christensen, M., Daniau, A.-L., Dufresne, J.-L., Feingold, G., Fiedler, S., Forster, P., Gettelman, A., Haywood, J. M., Lohmann, U., Malavelle, F., Mauritsen, T., McCoy, D. T., Myhre, G., Mülmenstädt, J., Neubauer, D., Possner, A., Rugenstein, M., Sato, Y., Schulz, M., Schwartz, S. E., Sourdeval, O., Storelvmo, T., Toll, V., Winker, D., and Stevens, B.: Bounding Global Aerosol Radiative Forcing of Climate Change, Reviews of Geophysics, 58, e2019RG000660, https://doi.org/10.1029/2019RG000660, 2020.

Bianchi, F., Kurtén, T., Riva, M., Mohr, C., Rissanen, M. P., Roldin, P., Berndt, T., Crounse, J. D., Wennberg, P. O., Mentel, T. F., Wildt, J., Junninen, H., Jokinen, T., Kulmala, M., Worsnop, D. R., Thornton, J. A., Donahue, N., Kjaergaard, H. G., and Ehn, M.: Highly Oxygenated Organic Molecules (HOM) from Gas-Phase Autoxidation Involving Peroxy Radicals: A Key Contributor to Atmospheric Aerosol, Chemical Reviews, 119, 3472-3509, 10.1021/acs.chemrev.8b00395, 2019.

Bianchi, F., Tröstl, J., Junninen, H., Frege, C., Henne, S., Hoyle, C. R., Molteni, U., Herrmann, E., Adamov, A., Bukowiecki, N., Chen, X., Duplissy, J., Gysel, M., Hutterli, M., Kangasluoma, J., Kontkanen, J., Kürten, A., Manninen, H. E., Münch, S., Peräkylä, O., Petäjä, T., Rondo, L., Williamson, C., Weingartner, E., Curtius, J., Worsnop, D. R., Kulmala, M., Dommen, J., and Baltensperger, U.: New particle formation in the free troposphere: A question of chemistry and timing, Science, 352, 1109-1112, doi:10.1126/science.aad5456, 2016.

Birmili, W., Weinhold, K., Rasch, F., Sonntag, A., Sun, J., Merkel, M., Wiedensohler, A., Bastian, S., Schladitz, A., Löschau, G., Cyrys, J., Pitz, M., Gu, J., Kusch, T., Flentje,

H., Quass, U., Kaminski, H., Kuhlbusch, T. A. J., Meinhardt, F., Schwerin, A., Bath, O., Ries, L., Gerwig, H., Wirtz, K., and Fiebig, M.: Long-term observations of tropospheric particle number size distributions and equivalent black carbon mass concentrations in the German Ultrafine Aerosol Network (GUAN), Earth Syst. Sci. Data, 8, 355-382, 10.5194/essd-8-355-2016, 2016.

Boulon, J., Sellegri, K., Venzac, H., Picard, D., Weingartner, E., Wehrle, G., Collaud Coen, M., Bütikofer, R., Flückiger, E., Baltensperger, U., and Laj, P.: New particle formation and ultrafine charged aerosol climatology at a high altitude site in the Alps (Jungfraujoch, 3580 m a.s.l., Switzerland), Atmos. Chem. Phys., 10, 9333-9349, 10.5194/acp-10-9333-2010, 2010.

Bousiotis, D., Dall'Osto, M., Beddows, D. C. S., Pope, F. D., and Harrison, R. M.: Analysis of new particle formation (NPF) events at nearby rural, urban background and urban roadside sites, Atmos. Chem. Phys., 19, 5679-5694, 10.5194/acp-19-5679-2019, 2019.

Bousiotis, D., Brean, J., Pope, F. D., Dall'Osto, M., Querol, X., Alastuey, A., Perez, N., Petäjä, T., Massling, A., Nøjgaard, J. K., Nordstrøm, C., Kouvarakis, G., Vratolis, S., Eleftheriadis, K., Niemi, J. V., Portin, H., Wiedensohler, A., Weinhold, K., Merkel, M., Tuch, T., and Harrison, R. M.: The effect of meteorological conditions and atmospheric composition in the occurrence and development of new particle formation (NPF) events in Europe, Atmos. Chem. Phys., 21, 3345-3370, 10.5194/acp-21-3345-2021, 2021a.

Bousiotis, D., Pope, F. D., Beddows, D. C. S., Dall'Osto, M., Massling, A., Nøjgaard, J. K., Nordstrøm, C., Niemi, J. V., Portin, H., Petäjä, T., Perez, N., Alastuey, A., Querol, X., Kouvarakis, G., Mihalopoulos, N., Vratolis, S., Eleftheriadis, K., Wiedensohler, A., Weinhold, K., Merkel, M., Tuch, T., and Harrison, R. M.: A phenomenology of new particle formation (NPF) at 13 European sites, Atmos. Chem. Phys., 21, 11905-11925, 10.5194/acp-21-11905-2021, 2021b.

Brean, J., Beddows, D. C. S., Shi, Z., Temime-Roussel, B., Marchand, N., Querol, X., Alastuey, A., Minguillón, M. C., and Harrison, R. M.: Molecular insights into new particle formation in Barcelona, Spain, Atmos. Chem. Phys., 20, 10029-10045, 10.5194/acp-20-10029-2020, 2020.

Brean, J., Beddows, D. C. S., Harrison, R. M., Song, C., Tunved, P., Ström, J., Krejci, R., Freud, E., Massling, A., Skov, H., Asmi, E., Lupi, A., and Dall'Osto, M.: Collective geographical ecoregions and precursor sources driving Arctic new particle formation, Atmos. Chem. Phys., 23, 2183-2198, 10.5194/acp-23-2183-2023, 2023.

Burnett, R., Chen, H., Szyszkowicz, M., Fann, N., Hubbell, B., Pope, C. A., Apte, J. S., Brauer, M., Cohen, A., Weichenthal, S., Coggins, J., Di, Q., Brunekreef, B., Frostad, J., Lim, S. S., Kan, H., Walker, K. D., Thurston, G. D., Hayes, R. B., Lim, C. C., Turner, M. C., Jerrett, M., Krewski, D., Gapstur, S. M., Diver, W. R., Ostro, B., Goldberg, D., Crouse, D. L., Martin, R. V., Peters, P., Pinault, L., Tjepkema, M., van Donkelaar, A., Villeneuve, P. J., Miller, A. B., Yin, P., Zhou, M., Wang, L., Janssen, N. A. H., Marra, M., Atkinson, R. W., Tsang, H., Quoc Thach, T., Cannon, J. B., Allen, R. T., Hart, J. E., Laden, F., Cesaroni, G., Forastiere, F., Weinmayr, G., Jaensch, A., Nagel, G., Concin, H., and Spadaro, J. V.: Global estimates of mortality associated with long-term exposure to outdoor fine particulate matter, Proceedings of the National Academy of Sciences, 115, 9592-9597, 10.1073/pnas.1803222115, 2018.

Cai, J., Chu, B., Yao, L., Yan, C., Heikkinen, L. M., Zheng, F., Li, C., Fan, X., Zhang, S., Yang, D., Wang, Y., Kokkonen, T. V., Chan, T., Zhou, Y., Dada, L., Liu, Y., He, H., Paasonen, P., Kujansuu, J. T., Petäjä, T., Mohr, C., Kangasluoma, J., Bianchi, F., Sun, Y., Croteau, P. L., Worsnop, D. R., Kerminen, V. M., Du, W., Kulmala, M., and Daellenbach, K. R.: Size-segregated particle number and mass concentrations from different emission

sources in urban Beijing, Atmos. Chem. Phys., 20, 12721-12740, 10.5194/acp-20-12721-2020, 2020.

Cai, R., Yan, C., Yang, D., Yin, R., Lu, Y., Deng, C., Fu, Y., Ruan, J., Li, X., Kontkanen, J., Zhang, Q., Kangasluoma, J., Ma, Y., Hao, J., Worsnop, D. R., Bianchi, F., Paasonen, P., Kerminen, V. M., Liu, Y., Wang, L., Zheng, J., Kulmala, M., and Jiang, J.: Sulfuric acid–amine nucleation in urban Beijing, Atmos. Chem. Phys., 21, 2457-2468, 10.5194/acp-21-2457-2021, 2021.

Canagaratna, M. R., Jayne, J. T., Jimenez, J. L., Allan, J. D., Alfarra, M. R., Zhang, Q., Onasch, T. B., Drewnick, F., Coe, H., Middlebrook, A., Delia, A., Williams, L. R., Trimborn, A. M., Northway, M. J., DeCarlo, P. F., Kolb, C. E., Davidovits, P., and Worsnop, D. R.: Chemical and microphysical characterization of ambient aerosols with the aerodyne aerosol mass spectrometer, Mass Spectrometry Reviews, 26, 185-222, https://doi.org/10.1002/mas.20115, 2007.

Chan, T., Cai, R., Ahonen, L. R., Liu, Y., Zhou, Y., Vanhanen, J., Dada, L., Chao, Y., Liu, Y., Wang, L., Kulmala, M., and Kangasluoma, J.: Assessment of particle size magnifier inversion methods to obtain the particle size distribution from atmospheric measurements, Atmos. Meas. Tech., 13, 4885-4898, 10.5194/amt-13-4885-2020, 2020.

Charlson, R. J., Schwartz, S. E., Hales, J. M., Cess, R. D., Coakley, J. A., Hansen, J. E., and Hofmann, D. J.: Climate Forcing by Anthropogenic Aerosols, Science, 255, 423-430, doi:10.1126/science.255.5043.423, 1992.

Cheng, Y., Zheng, G., Wei, C., Mu, Q., Zheng, B., Wang, Z., Gao, M., Zhang, Q., He, K., Carmichael, G., Pöschl, U., and Su, H.: Reactive nitrogen chemistry in aerosol water as a source of sulfate during haze events in China, Science Advances, 2, e1601530, doi:10.1126/sciadv.1601530, 2016.

Chu, B., Kerminen, V. M., Bianchi, F., Yan, C., Petäjä, T., and Kulmala, M.: Atmospheric new particle formation in China, Atmos. Chem. Phys., 19, 115-138, 10.5194/acp-19-115-2019, 2019.

Costabile, F., Birmili, W., Klose, S., Tuch, T., Wehner, B., Wiedensohler, A., Franck, U., König, K., and Sonntag, A.: Spatio-temporal variability and principal components of the particle number size distribution in an urban atmosphere, Atmos. Chem. Phys., 9, 3163-3195, 10.5194/acp-9-3163-2009, 2009.

Crumeyrolle, S., Kontkanen, J. S. S., Rose, C., Velazquez Garcia, A., Bourrianne, E., Catalfamo, M., Riffault, V., Tison, E., Ferreira de Brito, J., Visez, N., Ferlay, N., Auriol, F., and Chiapello, I.: Measurement report: Atmospheric new particle formation at a peri-urban site in Lille, northern France, Atmos. Chem. Phys., 23, 183-201, 10.5194/acp-23-183-2023, 2023.

Dada, L., Chellapermal, R., Buenrostro Mazon, S., Paasonen, P., Lampilahti, J., Manninen, H. E., Junninen, H., Petäjä, T., Kerminen, V. M., and Kulmala, M.: Refined classification and characterization of atmospheric new-particle formation events using air ions, Atmos. Chem. Phys., 18, 17883-17893, 10.5194/acp-18-17883-2018, 2018.

Dai, L., Wang, H., Zhou, L., An, J., Tang, L., Lu, C., Yan, W., Liu, R., Kong, S., Chen, M., Lee, S., and Yu, H.: Regional and local new particle formation events observed in the Yangtze River Delta region, China, Journal of Geophysical Research: Atmospheres, 122, 2389-2402, https://doi.org/10.1002/2016JD026030, 2017.

Deng, C., Fu, Y., Dada, L., Yan, C., Cai, R., Yang, D., Zhou, Y., Yin, R., Lu, Y., Li, X., Qiao, X., Fan, X., Nie, W., Kontkanen, J., Kangasluoma, J., Chu, B., Ding, A., Kerminen, V.-M., Paasonen, P., Worsnop, D. R., Bianchi, F., Liu, Y., Zheng, J., Wang, L., Kulmala, M., and Jiang, J.: Seasonal Characteristics of New Particle Formation and Growth in Urban Beijing, Environmental Science & Technology, 54, 8547-8557, 10.1021/acs.est.0c00808, 2020.

Dubtsov, S., Ovchinnikova, T., Valiulin, S., Chen, X., Manninen, H. E., Aalto, P. P., and Petäjä, T.: Laboratory verification of Aerosol Diffusion Spectrometer and the application to ambient measurements of new particle formation, Journal of Aerosol Science, 105, 10-23, https://doi.org/10.1016/j.jaerosci.2016.10.015, 2017.

Dusek, U., Frank, G. P., Hildebrandt, L., Curtius, J., Schneider, J., Walter, S., Chand, D., Drewnick, F., Hings, S., Jung, D., Borrmann, S., and Andreae, M. O.: Size Matters More Than Chemistry for Cloud-Nucleating Ability of Aerosol Particles, Science, 312, 1375-1378, 10.1126/science.1125261, 2006.

Ehn, M., Junninen, H., Schobesberger, S., Manninen, H. E., Franchin, A., Sipilä, M., Petäjä, T., Kerminen, V.-M., Tammet, H., Mirme, A., Mirme, S., Hõrrak, U., Kulmala, M., and Worsnop, D. R.: An Instrumental Comparison of Mobility and Mass Measurements of Atmospheric Small Ions, Aerosol Science and Technology, 45, 522-532, 10.1080/02786826.2010.547890, 2011.

Ehn, M., Thornton, J. A., Kleist, E., Sipilä, M., Junninen, H., Pullinen, I., Springer, M., Rubach, F., Tillmann, R., Lee, B., Lopez-Hilfiker, F., Andres, S., Acir, I.-H., Rissanen, M., Jokinen, T., Schobesberger, S., Kangasluoma, J., Kontkanen, J., Nieminen, T., Kurtén, T., Nielsen, L. B., Jørgensen, S., Kjaergaard, H. G., Canagaratna, M., Maso, M. D., Berndt, T., Petäjä, T., Wahner, A., Kerminen, V.-M., Kulmala, M., Worsnop, D. R., Wildt, J., and Mentel, T. F.: A large source of low-volatility secondary organic aerosol, Nature, 506, 476-479, 10.1038/nature13032, 2014.

Elser, M., Huang, R. J., Wolf, R., Slowik, J. G., Wang, Q., Canonaco, F., Li, G., Bozzetti, C., Daellenbach, K. R., Huang, Y., Zhang, R., Li, Z., Cao, J., Baltensperger, U., El-Haddad, I., and Prévôt, A. S. H.: New insights into PM2.5 chemical composition and sources in two major cities in China during extreme haze events using aerosol mass spectrometry, Atmos. Chem. Phys., 16, 3207-3225, 10.5194/acp-16-3207-2016, 2016.

Farmer, D. K., Cappa, C. D., and Kreidenweis, S. M.: Atmospheric Processes and Their Controlling Influence on Cloud Condensation Nuclei Activity, Chemical Reviews, 115, 4199-4217, 10.1021/cr5006292, 2015.

Franco, M. A., Ditas, F., Kremper, L. A., Machado, L. A. T., Andreae, M. O., Araújo, A., Barbosa, H. M. J., de Brito, J. F., Carbone, S., Holanda, B. A., Morais, F. G., Nascimento, J. P., Pöhlker, M. L., Rizzo, L. V., Sá, M., Saturno, J., Walter, D., Wolff, S., Pöschl, U., Artaxo, P., and Pöhlker, C.: Occurrence and growth of sub-50 nm aerosol particles in the Amazonian boundary layer, Atmos. Chem. Phys., 22, 3469-3492, 10.5194/acp-22-3469-2022, 2022.

Fu, G. Q., Xu, W. Y., Yang, R. F., Li, J. B., and Zhao, C. S.: The distribution and trends of fog and haze in the North China Plain over the past 30 years, Atmos. Chem. Phys., 14, 11949-11958, 10.5194/acp-14-11949-2014, 2014.

Fuchs, N. A.: On the stationary charge distribution on aerosol particles in a bipolar ionic atmosphere, Geofisica pura e applicata, 56, 185-193, 10.1007/BF01993343, 1963.

Gani, S., Bhandari, S., Patel, K., Seraj, S., Soni, P., Arub, Z., Habib, G., Hildebrandt Ruiz, L., and Apte, J. S.: Particle number concentrations and size distribution in a polluted megacity: the Delhi Aerosol Supersite study, Atmos. Chem. Phys., 20, 8533-8549, 10.5194/acp-20-8533-2020, 2020.

Ghassoun, Y., Ruths, M., Löwner, M.-O., and Weber, S.: Intra-urban variation of ultrafine particles as evaluated by process related land use and pollutant driven regression modelling, Science of The Total Environment, 536, 150-160, https://doi.org/10.1016/j.scitotenv.2015.07.051, 2015.

Gonzalez Carracedo, L., Lehtipalo, K., Ahonen, L. R., Sarnela, N., Holm, S., Kangasluoma, J., Kulmala, M., Winkler, P. M., and Stolzenburg, D.: On the relation between apparent

ion and total particle growth rates in the boreal forest and related chamber experiments, Atmos. Chem. Phys., 22, 13153-13166, 10.5194/acp-22-13153-2022, 2022.

Größ, J., Hamed, A., Sonntag, A., Spindler, G., Manninen, H. E., Nieminen, T., Kulmala, M., Hõrrak, U., Plass-Dülmer, C., Wiedensohler, A., and Birmili, W.: Atmospheric new particle formation at the research station Melpitz, Germany: connection with gaseous precursors and meteorological parameters, Atmos. Chem. Phys., 18, 1835-1861, 10.5194/acp-18-1835-2018, 2018.

Gunthe, S. S., Rose, D., Su, H., Garland, R. M., Achtert, P., Nowak, A., Wiedensohler, A., Kuwata, M., Takegawa, N., Kondo, Y., Hu, M., Shao, M., Zhu, T., Andreae, M. O., and Pöschl, U.: Cloud condensation nuclei (CCN) from fresh and aged air pollution in the megacity region of Beijing, Atmos. Chem. Phys., 11, 11023-11039, 10.5194/acp-11-11023-2011, 2011.

Guo, S., Hu, M., Zamora, M. L., Peng, J., Shang, D., Zheng, J., Du, Z., Wu, Z., Shao, M., Zeng, L., Molina, M. J., and Zhang, R.: Elucidating severe urban haze formation in China, Proceedings of the National Academy of Sciences, 111, 17373-17378, 10.1073/pnas.1419604111, 2014.

Guyon, P., Graham, B., Beck, J., Boucher, O., Gerasopoulos, E., Mayol-Bracero, O. L., Roberts, G. C., Artaxo, P., and Andreae, M. O.: Physical properties and concentration of aerosol particles over the Amazon tropical forest during background and biomass burning conditions, Atmos. Chem. Phys., 3, 951-967, 10.5194/acp-3-951-2003, 2003.

Guyon, P., Frank, G. P., Welling, M., Chand, D., Artaxo, P., Rizzo, L., Nishioka, G., Kolle, O., Fritsch, H., Silva Dias, M. A. F., Gatti, L. V., Cordova, A. M., and Andreae, M. O.: Airborne measurements of trace gas and aerosol particle emissions from biomass burning in Amazonia, Atmos. Chem. Phys., 5, 2989-3002, 10.5194/acp-5-2989-2005, 2005.

Hallquist, M., Wenger, J. C., Baltensperger, U., Rudich, Y., Simpson, D., Claeys, M., Dommen, J., Donahue, N. M., George, C., Goldstein, A. H., Hamilton, J. F., Herrmann, H., Hoffmann, T., Iinuma, Y., Jang, M., Jenkin, M. E., Jimenez, J. L., Kiendler-Scharr, A., Maenhaut, W., McFiggans, G., Mentel, T. F., Monod, A., Prévôt, A. S. H., Seinfeld, J. H., Surratt, J. D., Szmigielski, R., and Wildt, J.: The formation, properties and impact of secondary organic aerosol: current and emerging issues, Atmos. Chem. Phys., 9, 5155-5236, 10.5194/acp-9-5155-2009, 2009.

HALO-Research: CAFE Brazil, https://halo-research.de/sience/previous-missions/cafe-brazil/, 2022.

Hamed, A., Korhonen, H., Sihto, S.-L., Joutsensaari, J., Järvinen, H., Petäjä, T., Arnold, F., Nieminen, T., Kulmala, M., Smith, J. N., Lehtinen, K. E. J., and Laaksonen, A.: The role of relative humidity in continental new particle formation, Journal of Geophysical Research: Atmospheres, 116, https://doi.org/10.1029/2010JD014186, 2011.

Hansen, M. C., Wang, L., Song, X.-P., Tyukavina, A., Turubanova, S., Potapov, P. V., and Stehman, S. V.: The fate of tropical forest fragments, Science Advances, 6, eaax8574, 10.1126/sciadv.aax8574, 2020.

He, X.-C., Tham, Y. J., Dada, L., Wang, M., Finkenzeller, H., Stolzenburg, D., Iyer, S., Simon, M., Kürten, A., Shen, J., Rörup, B., Rissanen, M., Schobesberger, S., Baalbaki, R., Wang, D. S., Koenig, T. K., Jokinen, T., Sarnela, N., Beck, L. J., Almeida, J., Amanatidis, S., Amorim, A., Ataei, F., Baccarini, A., Bertozzi, B., Bianchi, F., Brilke, S., Caudillo, L., Chen, D., Chiu, R., Chu, B., Dias, A., Ding, A., Dommen, J., Duplissy, J., El Haddad, I., Gonzalez Carracedo, L., Granzin, M., Hansel, A., Heinritzi, M., Hofbauer, V., Junninen, H., Kangasluoma, J., Kemppainen, D., Kim, C., Kong, W., Krechmer, J. E., Kvashin, A., Laitinen, T., Lamkaddam, H., Lee, C. P., Lehtipalo, K., Leiminger, M., Li, Z., Makhmutov, V., Manninen, H. E., Marie, G., Marten, R., Mathot,

S., Mauldin, R. L., Mentler, B., Möhler, O., Müller, T., Nie, W., Onnela, A., Petäjä, T., Pfeifer, J., Philippov, M., Ranjithkumar, A., Saiz-Lopez, A., Salma, I., Scholz, W., Schuchmann, S., Schulze, B., Steiner, G., Stozhkov, Y., Tauber, C., Tomé, A., Thakur, R. C., Väisänen, O., Vazquez-Pufleau, M., Wagner, A. C., Wang, Y., Weber, S. K., Winkler, P. M., Wu, Y., Xiao, M., Yan, C., Ye, Q., Ylisirniö, A., Zauner-Wieczorek, M., Zha, Q., Zhou, P., Flagan, R. C., Curtius, J., Baltensperger, U., Kulmala, M., Kerminen, V.-M., Kurtén, T., Donahue, N. M., Volkamer, R., Kirkby, J., Worsnop, D. R., and Sipilä, M.: Role of iodine oxoacids in atmospheric aerosol nucleation, Science, 371, 589-595, 10.1126/science.abe0298, 2021.

Heinritzi, M., Dada, L., Simon, M., Stolzenburg, D., Wagner, A. C., Fischer, L., Ahonen, L. R., Amanatidis, S., Baalbaki, R., Baccarini, A., Bauer, P. S., Baumgartner, B., Bianchi, F., Brilke, S., Chen, D., Chiu, R., Dias, A., Dommen, J., Duplissy, J., Finkenzeller, H., Frege, C., Fuchs, C., Garmash, O., Gordon, H., Granzin, M., El Haddad, I., He, X., Helm, J., Hofbauer, V., Hoyle, C. R., Kangasluoma, J., Keber, T., Kim, C., Kürten, A., Lamkaddam, H., Laurila, T. M., Lampilahti, J., Lee, C. P., Lehtipalo, K., Leiminger, M., Mai, H., Makhmutov, V., Manninen, H. E., Marten, R., Mathot, S., Mauldin, R. L., Mentler, B., Molteni, U., Müller, T., Nie, W., Nieminen, T., Onnela, A., Partoll, E., Passananti, M., Petäjä, T., Pfeifer, J., Pospisilova, V., Quéléver, L. L. J., Rissanen, M. P., Rose, C., Schobesberger, S., Scholz, W., Scholze, K., Sipilä, M., Steiner, G., Stozhkov, Y., Tauber, C., Tham, Y. J., Vazquez-Pufleau, M., Virtanen, A., Vogel, A. L., Volkamer, R., Wagner, R., Wang, M., Weitz, L., Wimmer, D., Xiao, M., Yan, C., Ye, P., Zha, Q., Zhou, X., Amorim, A., Baltensperger, U., Hansel, A., Kulmala, M., Tomé, A., Winkler, P. M., Worsnop, D. R., Donahue, N. M., Kirkby, J., and Curtius, J.: Molecular understanding of the suppression of new-particle formation by isoprene, Atmos. Chem. Phys., 20, 11809-11821, 10.5194/acp-20-11809-2020, 2020.

Herrmann, E., Ding, A. J., Kerminen, V. M., Petäjä, T., Yang, X. Q., Sun, J. N., Qi, X. M., Manninen, H., Hakala, J., Nieminen, T., Aalto, P. P., Kulmala, M., and Fu, C. B.: Aerosols and nucleation in eastern China: first insights from the new SORPES-NJU station, Atmos. Chem. Phys., 14, 2169-2183, 10.5194/acp-14-2169-2014, 2014.

Hirsikko, A., Bergman, T., Laakso, L., Dal Maso, M., Riipinen, I., Hõrrak, U., and Kulmala, M.: Identification and classification of the formation of intermediate ions measured in boreal forest, Atmos. Chem. Phys., 7, 201-210, 10.5194/acp-7-201-2007, 2007.

Hirsikko, A., Vakkari, V., Tiitta, P., Manninen, H. E., Gagné, S., Laakso, H., Kulmala, M., Mirme, A., Mirme, S., Mabaso, D., Beukes, J. P., and Laakso, L.: Characterisation of sub-micron particle number concentrations and formation events in the western Bushveld Igneous Complex, South Africa, Atmos. Chem. Phys., 12, 3951-3967, 10.5194/acp-12-3951-2012, 2012.

Hirsikko, A., Nieminen, T., Gagné, S., Lehtipalo, K., Manninen, H. E., Ehn, M., Hõrrak, U., Kerminen, V. M., Laakso, L., McMurry, P. H., Mirme, A., Mirme, S., Petäjä, T., Tammet, H., Vakkari, V., Vana, M., and Kulmala, M.: Atmospheric ions and nucleation: a review of observations, Atmos. Chem. Phys., 11, 767-798, 10.5194/acp-11-767-2011, 2011.

Holanda, B. A., Franco, M. A., Walter, D., Artaxo, P., Carbone, S., Cheng, Y., Chowdhury, S., Ditas, F., Gysel-Beer, M., Klimach, T., Kremper, L. A., Krüger, O. O., Lavric, J. V., Lelieveld, J., Ma, C., Machado, L. A. T., Modini, R. L., Morais, F. G., Pozzer, A., Saturno, J., Su, H., Wendisch, M., Wolff, S., Pöhlker, M. L., Andreae, M. O., Pöschl, U., and Pöhlker, C.: African biomass burning affects aerosol cycling over the Amazon, Communications Earth & Environment, 4, 154, 10.1038/s43247-023-00795-5, 2023.

Holanda, B. A., Pöhlker, M. L., Walter, D., Saturno, J., Sörgel, M., Ditas, J., Ditas, F., Schulz, C., Franco, M. A., Wang, Q., Donth, T., Artaxo, P., Barbosa, H. M. J., Borrmann, S.,

Braga, R., Brito, J., Cheng, Y., Dollner, M., Kaiser, J. W., Klimach, T., Knote, C., Krüger, O. O., Fütterer, D., Lavrič, J. V., Ma, N., Machado, L. A. T., Ming, J., Morais, F. G., Paulsen, H., Sauer, D., Schlager, H., Schneider, J., Su, H., Weinzierl, B., Walser, A., Wendisch, M., Ziereis, H., Zöger, M., Pöschl, U., Andreae, M. O., and Pöhlker, C.: Influx of African biomass burning aerosol during the Amazonian dry season through layered transatlantic transport of black carbon-rich smoke, Atmos. Chem. Phys., 20, 4757-4785, 10.5194/acp-20-4757-2020, 2020.

Hong, J., Tang, M., Wang, Q., Ma, N., Zhu, S., Zhang, S., Pan, X., Xie, L., Li, G., Kuhn, U., Yan, C., Tao, J., Kuang, Y., He, Y., Xu, W., Cai, R., Zhou, Y., Wang, Z., Zhou, G., Yuan, B., Cheng, Y., and Su, H.: Measurement Report: Wintertime new particle formation in the rural area of the North China Plain – influencing factors and possible formation mechanism, Atmos. Chem. Phys., 23, 5699-5713, 10.5194/acp-23-5699-2023, 2023.

Huang, R.-J., Zhang, Y., Bozzetti, C., Ho, K.-F., Cao, J.-J., Han, Y., Daellenbach, K. R., Slowik, J. G., Platt, S. M., Canonaco, F., Zotter, P., Wolf, R., Pieber, S. M., Bruns, E. A., Crippa, M., Ciarelli, G., Piazzalunga, A., Schwikowski, M., Abbaszade, G., Schnelle-Kreis, J., Zimmermann, R., An, Z., Szidat, S., Baltensperger, U., Haddad, I. E., and Prévôt, A. S. H.: High secondary aerosol contribution to particulate pollution during haze events in China, Nature, 514, 218-222, 10.1038/nature13774, 2014.

Huang, W., Junninen, H., Garmash, O., Lehtipalo, K., Stolzenburg, D., Lampilahti, J. L. P., Ezhova, E., Schallhart, S., Rantala, P., Aliaga, D., Ahonen, L., Sulo, J., Quéléver, L. L. J., Cai, R., Alekseychik, P., Mazon, S. B., Yao, L., Blichner, S. M., Zha, Q., Mammarella, I., Kirkby, J., Kerminen, V.-M., Worsnop, D. R., Kulmala, M., and Bianchi, F.: Potential pre-industrial–like new particle formation induced by pure biogenic organic vapors in Finnish peatland, Science Advances, 10, eadm9191, 10.1126/sciadv.adm9191, 2024.

Hubau, W., Lewis, S. L., Phillips, O. L., Affum-Baffoe, K., Beeckman, H., Cuní-Sanchez, A., Daniels, A. K., Ewango, C. E. N., Fauset, S., Mukinzi, J. M., Sheil, D., Sonké, B., Sullivan, M. J. P., Sunderland, T. C. H., Taedoumg, H., Thomas, S. C., White, L. J. T., Abernethy, K. A., Adu-Bredu, S., Amani, C. A., Baker, T. R., Banin, L. F., Baya, F., Begne, S. K., Bennett, A. C., Benedet, F., Bitariho, R., Bocko, Y. E., Boeckx, P., Boundja, P., Brienen, R. J. W., Brncic, T., Chezeaux, E., Chuyong, G. B., Clark, C. J., Collins, M., Comiskey, J. A., Coomes, D. A., Dargie, G. C., de Haulleville, T., Kamdem, M. N. D., Doucet, J.-L., Esquivel-Muelbert, A., Feldpausch, T. R., Fofanah, A., Foli, E. G., Gilpin, M., Gloor, E., Gonmadje, C., Gourlet-Fleury, S., Hall, J. S., Hamilton, A. C., Harris, D. J., Hart, T. B., Hockemba, M. B. N., Hladik, A., Ifo, S. A., Jeffery, K. J., Jucker, T., Yakusu, E. K., Kearsley, E., Kenfack, D., Koch, A., Leal, M. E., Levesley, A., Lindsell, J. A., Lisingo, J., Lopez-Gonzalez, G., Lovett, J. C., Makana, J.-R., Malhi, Y., Marshall, A. R., Martin, J., Martin, E. H., Mbayu, F. M., Medjibe, V. P., Mihindou, V., Mitchard, E. T. A., Moore, S., Munishi, P. K. T., Bengone, N. N., Ojo, L., Ondo, F. E., Peh, K. S. H., Pickavance, G. C., Poulsen, A. D., Poulsen, J. R., Qie, L., Reitsma, J., Rovero, F., Swaine, M. D., Talbot, J., Taplin, J., Taylor, D. M., Thomas, D. W., Toirambe, B., Mukendi, J. T., Tuagben, D., Umunay, P. M., van der Heijden, G. M. F., Verbeeck, H., Vleminckx, J., Willcock, S., Wöll, H., Woods, J. T., and Zemagho, L.: Asynchronous carbon sink saturation in African and Amazonian tropical forests, Nature, 579, 80-87, 10.1038/s41586-020-2035-0, 2020.

Hussein, T., Dal Maso, M., Petäjä, T., Koponen, I. K., Paatero, P., Aalto, P. P., Hämeri, K. & Kulmala, M.: Evaluation of an automatic algorithm for fitting the particle number size distributions., Boreal Environment Research, 10, 337–355, 2005.

Iida, K., Stolzenburg, M. R., and McMurry, P. H.: Effect of Working Fluid on Sub-2 nm Particle Detection with a Laminar Flow Ultrafine Condensation Particle Counter, Aerosol Science and Technology, 43, 81-96, 10.1080/02786820802488194, 2009.

IPCC, Okem; Andrew Okem, H.-O. P. D. C. R. M. M. B. T. E. P. K. M. A. A. M. C. S. L. S. L. V. M. A. (Ed.): Climate Change 2022: Impacts, Adaptation and Vulnerability. Contribution of Working Group II to the Sixth Assessment Report of the Intergovernmental Panel on Climate Change, Cambridge University Press, Cambridge, 3056 pp., 10.1017/9781009325844, 2022.

Jayaratne, R., Pushpawela, B., He, C., Li, H., Gao, J., Chai, F., and Morawska, L.: Observations of particles at their formation sizes in Beijing, China, Atmos. Chem. Phys., 17, 8825-8835, 10.5194/acp-17-8825-2017, 2017.

Jen, C. N., Hanson, D. R., and McMurry, P. H.: Toward Reconciling Measurements of Atmospherically Relevant Clusters by Chemical Ionization Mass Spectrometry and Mobility Classification/Vapor Condensation, Aerosol Science and Technology, 49, i-iii, 10.1080/02786826.2014.1002602, 2015.

Jiang, J., Chen, M., Kuang, C., Attoui, M., and McMurry, P. H.: Electrical Mobility Spectrometer Using a Diethylene Glycol Condensation Particle Counter for Measurement of Aerosol Size Distributions Down to 1 nm, Aerosol Science and Technology, 45, 510-521, 10.1080/02786826.2010.547538, 2011a.

Jiang, J., Attoui, M., Heim, M., Brunelli, N. A., McMurry, P. H., Kasper, G., Flagan, R. C., Giapis, K., and Mouret, G.: Transfer Functions and Penetrations of Five Differential Mobility Analyzers for Sub-2 nm Particle Classification, Aerosol Science and Technology, 45, 480-492, 10.1080/02786826.2010.546819, 2011b.

Jimenez, J. L., Canagaratna, M. R., Donahue, N. M., Prevot, A. S. H., Zhang, Q., Kroll, J. H., DeCarlo, P. F., Allan, J. D., Coe, H., Ng, N. L., Aiken, A. C., Docherty, K. S., Ulbrich, I. M., Grieshop, A. P., Robinson, A. L., Duplissy, J., Smith, J. D., Wilson, K. R., Lanz, V. A., Hueglin, C., Sun, Y. L., Tian, J., Laaksonen, A., Raatikainen, T., Rautiainen, J., Vaattovaara, P., Ehn, M., Kulmala, M., Tomlinson, J. M., Collins, D. R., Cubison, M. J., Dunlea, J., Huffman, J. A., Onasch, T. B., Alfarra, M. R., Williams, P. I., Bower, K., Kondo, Y., Schneider, J., Drewnick, F., Borrmann, S., Weimer, S., Demerjian, K., Salcedo, D., Cottrell, L., Griffin, R., Takami, A., Miyoshi, T., Hatakeyama, S., Shimono, A., Sun, J. Y., Zhang, Y. M., Dzepina, K., Kimmel, J. R., Sueper, D., Jayne, J. T., Herndon, S. C., Trimborn, A. M., Williams, L. R., Wood, E. C., Middlebrook, A. M., Kolb, C. E., Baltensperger, U., and Worsnop, D. R.: Evolution of Organic Aerosols in the Atmosphere, Science, 326, 1525-1529, 10.1126/science.1180353, 2009.

Jin, X., Wang, Y., Li, Z., Zhang, F., Xu, W., Sun, Y., Fan, X., Chen, G., Wu, H., Ren, J., Wang, Q., and Cribb, M.: Significant contribution of organics to aerosol liquid water content in winter in Beijing, China, Atmos. Chem. Phys., 20, 901-914, 10.5194/acp-20-901-2020, 2020.

Jokinen, T., Sipilä, M., Junninen, H., Ehn, M., Lönn, G., Hakala, J., Petäjä, T., Mauldin Iii, R. L., Kulmala, M., and Worsnop, D. R.: Atmospheric sulphuric acid and neutral cluster measurements using CI-APi-TOF, Atmos. Chem. Phys., 12, 4117-4125, 10.5194/acp-12-4117-2012, 2012.

Kanakidou, M., Seinfeld, J. H., Pandis, S. N., Barnes, I., Dentener, F. J., Facchini, M. C., Van Dingenen, R., Ervens, B., Nenes, A., Nielsen, C. J., Swietlicki, E., Putaud, J. P., Balkanski, Y., Fuzzi, S., Horth, J., Moortgat, G. K., Winterhalter, R., Myhre, C. E. L., Tsigaridis, K., Vignati, E., Stephanou, E. G., and Wilson, J.: Organic aerosol and global climate modelling: a review, Atmos. Chem. Phys., 5, 1053-1123, 10.5194/acp-5-1053-2005, 2005.

Kangasluoma, J. and Attoui, M.: Review of sub-3 nm condensation particle counters, calibrations, and cluster generation methods, Aerosol Science and Technology, 53, 1277-1310, 10.1080/02786826.2019.1654084, 2019.

Kangasluoma, J. and Kontkanen, J.: On the sources of uncertainty in the sub-3nm particle concentration measurement, Journal of Aerosol Science, 112, 34-51, https://doi.org/10.1016/j.jaerosci.2017.07.002, 2017.

Kangasluoma, J., Ahonen, L. R., Laurila, T. M., Cai, R., Enroth, J., Mazon, S. B., Korhonen, F., Aalto, P. P., Kulmala, M., Attoui, M., and Petäjä, T.: Laboratory verification of a new high flow differential mobility particle sizer, and field measurements in Hyytiälä, Journal of Aerosol Science, 124, 1-9, https://doi.org/10.1016/j.jaerosci.2018.06.009, 2018.

Kangasluoma, J., Attoui, M., Junninen, H., Lehtipalo, K., Samodurov, A., Korhonen, F., Sarnela, N., Schmidt-Ott, A., Worsnop, D., Kulmala, M., and Petäjä, T.: Sizing of neutral sub 3nm tungsten oxide clusters using Airmodus Particle Size Magnifier, Journal of Aerosol Science, 87, 53-62, https://doi.org/10.1016/j.jaerosci.2015.05.007, 2015.

Kangasluoma, J., Franchin, A., Duplissy, J., Ahonen, L., Korhonen, F., Attoui, M., Mikkilä, J., Lehtipalo, K., Vanhanen, J., Kulmala, M., and Petäjä, T.: Operation of the Airmodus A11 nano Condensation Nucleus Counter at various inlet pressures and various operation temperatures, and design of a new inlet system, Atmos. Meas. Tech., 9, 2977-2988, 10.5194/amt-9-2977-2016, 2016.

Kangasluoma, J., Cai, R., Jiang, J., Deng, C., Stolzenburg, D., Ahonen, L. R., Chan, T., Fu, Y., Kim, C., Laurila, T. M., Zhou, Y., Dada, L., Sulo, J., Flagan, R. C., Kulmala, M., Petäjä, T., and Lehtipalo, K.: Overview of measurements and current instrumentation for 1–10 nm aerosol particle number size distributions, Journal of Aerosol Science, 148, 105584, https://doi.org/10.1016/j.jaerosci.2020.105584, 2020.

Kerminen, V.-M., Chen, X., Vakkari, V., Petäjä, T., Kulmala, M., and Bianchi, F.: Atmospheric new particle formation and growth: review of field observations, Environmental Research Letters, 13, 103003, 10.1088/1748-9326/aadf3c, 2018.

Kim, J. H., Mulholland, G. W., Kukuck, S. R., and Pui, D. Y.: Slip Correction Measurements of Certified PSL Nanoparticles Using a Nanometer Differential Mobility Analyzer (Nano-DMA) for Knudsen Number From 0.5 to 83, J Res Natl Inst Stand Technol, 110, 31-54, 10.6028/jres.110.005, 2005.

Kirkby, J., Amorim, A., Baltensperger, U., Carslaw, K. S., Christoudias, T., Curtius, J., Donahue, N. M., Haddad, I. E., Flagan, R. C., Gordon, H., Hansel, A., Harder, H., Junninen, H., Kulmala, M., Kürten, A., Laaksonen, A., Lehtipalo, K., Lelieveld, J., Möhler, O., Riipinen, I., Stratmann, F., Tomé, A., Virtanen, A., Volkamer, R., Winkler, P. M., and Worsnop, D. R.: Atmospheric new particle formation from the CERN CLOUD experiment, Nature Geoscience, 16, 948-957, 10.1038/s41561-023-01305-0, 2023.

Kirkby, J., Curtius, J., Almeida, J., Dunne, E., Duplissy, J., Ehrhart, S., Franchin, A., Gagné, S., Ickes, L., Kürten, A., Kupc, A., Metzger, A., Riccobono, F., Rondo, L., Schobesberger, S., Tsagkogeorgas, G., Wimmer, D., Amorim, A., Bianchi, F., Breitenlechner, M., David, A., Dommen, J., Downard, A., Ehn, M., Flagan, R. C., Haider, S., Hansel, A., Hauser, D., Jud, W., Junninen, H., Kreissl, F., Kvashin, A., Laaksonen, A., Lehtipalo, K., Lima, J., Lovejoy, E. R., Makhmutov, V., Mathot, S., Mikkilä, J., Minginette, P., Mogo, S., Nieminen, T., Onnela, A., Pereira, P., Petäjä, T., Schnitzhofer, R., Seinfeld, J. H., Sipilä, M., Stozhkov, Y., Stratmann, F., Tomé, A., Vanhanen, J., Viisanen, Y., Vrtala, A., Wagner, P. E., Walther, H., Weingartner, E., Wex, H., Winkler, P. M., Carslaw, K. S., Worsnop, D. R., Baltensperger, U., and

Kulmala, M.: Role of sulphuric acid, ammonia and galactic cosmic rays in atmospheric aerosol nucleation, Nature, 476, 429-433, 10.1038/nature10343, 2011.

Kirkby, J., Duplissy, J., Sengupta, K., Frege, C., Gordon, H., Williamson, C., Heinritzi, M., Simon, M., Yan, C., Almeida, J., Tröstl, J., Nieminen, T., Ortega, I. K., Wagner, R., Adamov, A., Amorim, A., Bernhammer, A.-K., Bianchi, F., Breitenlechner, M., Brilke, S., Chen, X., Craven, J., Dias, A., Ehrhart, S., Flagan, R. C., Franchin, A., Fuchs, C., Guida, R., Hakala, J., Hoyle, C. R., Jokinen, T., Junninen, H., Kangasluoma, J., Kim, J., Krapf, M., Kürten, A., Laaksonen, A., Lehtipalo, K., Makhmutov, V., Mathot, S., Molteni, U., Onnela, A., Peräkylä, O., Piel, F., Petäjä, T., Praplan, A. P., Pringle, K., Rap, A., Richards, N. A. D., Riipinen, I., Rissanen, M. P., Rondo, L., Sarnela, N., Schobesberger, S., Scott, C. E., Seinfeld, J. H., Sipilä, M., Steiner, G., Stozhkov, Y., Stratmann, F., Tomé, A., Virtanen, A., Vogel, A. L., Wagner, A. C., Wagner, P. E., Weingartner, E., Wimmer, D., Winkler, P. M., Ye, P., Zhang, X., Hansel, A., Dommen, J., Donahue, N. M., Worsnop, D. R., Baltensperger, U., Kulmala, M., Carslaw, K. S., and Curtius, J.: Ion-induced nucleation of pure biogenic particles, Nature, 533, 521-526, 10.1038/nature17953, 2016.

Knutson, E. O. and Whitby, K. T.: Aerosol classification by electric mobility: apparatus, theory, and applications, Journal of Aerosol Science, 6, 443-451, https://doi.org/10.1016/0021-8502(75)90060-9, 1975.

Kontkanen, J., Järvinen, E., Manninen, H. E., Lehtipalo, K., Kangasluoma, J., Decesari, S., Gobbi, G. P., Laaksonen, A., Petäjä, T., and Kulmala, M.: High concentrations of sub-3nm clusters and frequent new particle formation observed in the Po Valley, Italy, during the PEGASOS 2012 campaign, Atmos. Chem. Phys., 16, 1919-1935, 10.5194/acp-16-1919-2016, 2016.

Kontkanen, J., Lehtipalo, K., Ahonen, L., Kangasluoma, J., Manninen, H. E., Hakala, J., Rose, C., Sellegri, K., Xiao, S., Wang, L., Qi, X., Nie, W., Ding, A., Yu, H., Lee, S., Kerminen, V. M., Petäjä, T., and Kulmala, M.: Measurements of sub-3 nm particles using a particle size magnifier in different environments: from clean mountain top to polluted megacities, Atmos. Chem. Phys., 17, 2163-2187, 10.5194/acp-17-2163-2017, 2017.

Krejci, R., Ström, J., de Reus, M., Hoor, P., Williams, J., Fischer, H., and Hansson, H.-C.: Evolution of aerosol properties over the rain forest in Surinam, South America, observed from aircraft during the LBA-CLAIRE 98 experiment, Journal of Geophysical Research: Atmospheres, 108, https://doi.org/10.1029/2001JD001375, 2003.

Krejci, R., Ström, J., de Reus, M., Williams, J., Fischer, H., Andreae, M. O., and Hansson, H. C.: Spatial and temporal distribution of atmospheric aerosols in the lowermost troposphere over the Amazonian tropical rainforest, Atmos. Chem. Phys., 5, 1527-1543, 10.5194/acp-5-1527-2005, 2005.

Kuang, C., Chen, M., Zhao, J., Smith, J., McMurry, P. H., and Wang, J.: Size and time-resolved growth rate measurements of 1 to 5 nm freshly formed atmospheric nuclei, Atmos. Chem. Phys., 12, 3573-3589, 10.5194/acp-12-3573-2012, 2012.

Kuang, Y., He, Y., Xu, W., Yuan, B., Zhang, G., Ma, Z., Wu, C., Wang, C., Wang, S., Zhang, S., Tao, J., Ma, N., Su, H., Cheng, Y., Shao, M., and Sun, Y.: Photochemical Aqueous-Phase Reactions Induce Rapid Daytime Formation of Oxygenated Organic Aerosol on the North China Plain, Environmental Science & Technology, 54, 3849-3860, 10.1021/acs.est.9b06836, 2020.

Kulmala, M., Vehkamäki, H., Petäjä, T., Dal Maso, M., Lauri, A., Kerminen, V. M., Birmili, W., and McMurry, P. H.: Formation and growth rates of ultrafine atmospheric particles: a review of observations, Journal of Aerosol Science, 35, 143-176, https://doi.org/10.1016/j.jaerosci.2003.10.003, 2004.

Kulmala, M., Petäjä, T., Nieminen, T., Sipilä, M., Manninen, H. E., Lehtipalo, K., Dal Maso, M., Aalto, P. P., Junninen, H., Paasonen, P., Riipinen, I., Lehtinen, K. E. J., Laaksonen, A., and Kerminen, V.-M.: Measurement of the nucleation of atmospheric aerosol particles, Nature Protocols, 7, 1651-1667, 10.1038/nprot.2012.091, 2012.

Kulmala, M., Junninen, H., Dada, L., Salma, I., Weidinger, T., Thén, W., Vörösmarty, M., Komsaare, K., Stolzenburg, D., Cai, R., Yan, C., Li, X., Deng, C., Jiang, J., Petäjä, T., Nieminen, T., and Kerminen, V.-M.: Quiet New Particle Formation in the Atmosphere, Frontiers in Environmental Science, 10, 10.3389/fenvs.2022.912385, 2022.

Kulmala, M., Mordas, G., Petäjä, T., Grönholm, T., Aalto, P. P., Vehkamäki, H., Hienola, A. I., Herrmann, E., Sipilä, M., Riipinen, I., Manninen, H. E., Hämeri, K., Stratmann, F., Bilde, M., Winkler, P. M., Birmili, W., and Wagner, P. E.: The condensation particle counter battery (CPCB): A new tool to investigate the activation properties of nanoparticles, Journal of Aerosol Science, 38, 289-304, https://doi.org/10.1016/j.jaerosci.2006.11.008, 2007.

Kulmala, M., Kontkanen, J., Junninen, H., Lehtipalo, K., Manninen, H. E., Nieminen, T., Petäjä, T., Sipilä, M., Schobesberger, S., Rantala, P., Franchin, A., Jokinen, T., Järvinen, E., Äijälä, M., Kangasluoma, J., Hakala, J., Aalto, P. P., Paasonen, P., Mikkilä, J., Vanhanen, J., Aalto, J., Hakola, H., Makkonen, U., Ruuskanen, T., Mauldin, R. L., Duplissy, J., Vehkamäki, H., Bäck, J., Kortelainen, A., Riipinen, I., Kurtén, T., Johnston, M. V., Smith, J. N., Ehn, M., Mentel, T. F., Lehtinen, K. E. J., Laaksonen, A., Kerminen, V.-M., and Worsnop, D. R.: Direct Observations of Atmospheric Aerosol Nucleation, Science, 339, 943-946, doi:10.1126/science.1227385, 2013.

Le, T., Wang, Y., Liu, L., Yang, J., Yung, Y. L., Li, G., and Seinfeld, J. H.: Unexpected air pollution with marked emission reductions during the COVID-19 outbreak in China, Science, 369, 702-706, doi:10.1126/science.abb7431, 2020.

Lee, B. P., Wang, H., and Chan, C. K.: Diurnal and day-to-day characteristics of ambient particle mass size distributions from HR-ToF-AMS measurements at an urban site and a suburban site in Hong Kong, Atmos. Chem. Phys., 17, 13605-13624, 10.5194/acp-17-13605-2017, 2017.

Lee, S.-H., Gordon, H., Yu, H., Lehtipalo, K., Haley, R., Li, Y., and Zhang, R.: New Particle Formation in the Atmosphere: From Molecular Clusters to Global Climate, Journal of Geophysical Research: Atmospheres, 124, 7098-7146, 10.1029/2018jd029356, 2019.

Lehtipalo, K., Sipilä, M., Riipinen, I., Nieminen, T., and Kulmala, M.: Analysis of atmospheric neutral and charged molecular clusters in boreal forest using pulse-height CPC, Atmos. Chem. Phys., 9, 4177-4184, 10.5194/acp-9-4177-2009, 2009.

Lehtipalo, K., Ahonen, L. R., Baalbaki, R., Sulo, J., Chan, T., Laurila, T., Dada, L., Duplissy, J., Miettinen, E., Vanhanen, J., Kangasluoma, J., Kulmala, M., Petäjä, T., and Jokinen, T.: The standard operating procedure for Airmodus Particle Size Magnifier and nano-Condensation Nucleus Counter, Journal of Aerosol Science, 159, 105896, https://doi.org/10.1016/j.jaerosci.2021.105896, 2022.

Lelieveld, J., Evans, J. S., Fnais, M., Giannadaki, D., and Pozzer, A.: The contribution of outdoor air pollution sources to premature mortality on a global scale, Nature, 525, 367-371, 10.1038/nature15371, 2015.

Lelieveld, J., Klingmüller, K., Pozzer, A., Pöschl, U., Fnais, M., Daiber, A., and Münzel, T.: Cardiovascular disease burden from ambient air pollution in Europe reassessed using novel hazard ratio functions, European Heart Journal, 40, 1590-1596, 10.1093/eurheartj/ehz135, 2019.

Li, G., Su, H., Ma, N., Tao, J., Kuang, Y., Wang, Q., Hong, J., Zhang, Y., Kuhn, U., Zhang, S., Pan, X., Lu, N., Tang, M., Zheng, G., Wang, Z., Gao, Y., Cheng, P., Xu, W., Zhou, G., Zhao, C., Yuan, B., Shao, M., Ding, A., Zhang, Q., Fu, P., Sun, Y., Pöschl, U., and

Cheng, Y.: Multiphase chemistry experiment in Fogs and Aerosols in the North China Plain (McFAN): integrated analysis and intensive winter campaign 2018, Faraday Discussions, 226, 207-222, 10.1039/D0FD00099J, 2021.

Li, Z., Guo, J., Ding, A., Liao, H., Liu, J., Sun, Y., Wang, T., Xue, H., Zhang, H., and Zhu, B.: Aerosol and boundary-layer interactions and impact on air quality, National Science Review, 4, 810-833, 10.1093/nsr/nwx117, 2017.

Liu, B. Y. H., Pui, D. Y. H., Whitby, K. T., Kittelson, D. B., Kousaka, Y., and McKenzie, R. L.: The aerosol mobility chromatograph: A new detector for sulfuric acid aerosols, Atmospheric Environment (1967), 12, 99-104, https://doi.org/10.1016/0004-6981(78)90192-0, 1978.

Liu, Z., Hu, B., Zhang, J., Yu, Y., and Wang, Y.: Characteristics of aerosol size distributions and chemical compositions during wintertime pollution episodes in Beijing, Atmospheric Research, 168, 1-12, https://doi.org/10.1016/j.atmosres.2015.08.013, 2016.

Machado, L. A. T., Franco, M. A., Kremper, L. A., Ditas, F., Andreae, M. O., Artaxo, P., Cecchini, M. A., Holanda, B. A., Pöhlker, M. L., Saraiva, I., Wolff, S., Pöschl, U., and Pöhlker, C.: How weather events modify aerosol particle size distributions in the Amazon boundary layer, Atmos. Chem. Phys., 21, 18065-18086, 10.5194/acp-21-18065-2021, 2021.

Machado, L. A. T., Unfer, G. R., Brill, S., Hildmann, S., Pöhlker, C., Cheng, Y., Williams, J., Hartwig, H., Andreae, M. O., Artaxo, P., Curtius, J., Franco, M. A., Cecchini, M. A., Edtbauer, A., Hoffmann, T., Holanda, B., Khadir, T., Krejci, R., Kremper, L. A., Liu, Y., Meller, B. B., Pöhlker, M. L., Quesada, C. A., Ringsdorf, A., Riipinen, I., Trumbore, S., Wolff, S., Lelieveld, J., and Pöschl, U.: Frequent rainfall-induced new particle formation within the canopy in the Amazon rainforest, Nature Geoscience, 10.1038/s41561-024-01585-0, 2024.

Manisalidis, I., Stavropoulou, E., Stavropoulos, A., and Bezirtzoglou, E.: Environmental and Health Impacts of Air Pollution: A Review, Front Public Health, 8, 14, 10.3389/fpubh.2020.00014, 2020.

Manninen, H. E., Mirme, S., Mirme, A., Petäjä, T., and Kulmala, M.: How to reliably detect molecular clusters and nucleation mode particles with Neutral cluster and Air Ion Spectrometer (NAIS), Atmos. Meas. Tech., 9, 3577-3605, 10.5194/amt-9-3577-2016, 2016.

Manninen, H. E., Nieminen, T., Asmi, E., Gagné, S., Häkkinen, S., Lehtipalo, K., Aalto, P., Vana, M., Mirme, A., Mirme, S., Hõrrak, U., Plass-Dülmer, C., Stange, G., Kiss, G., Hoffer, A., Törő, N., Moerman, M., Henzing, B., de Leeuw, G., Brinkenberg, M., Kouvarakis, G. N., Bougiatioti, A., Mihalopoulos, N., O'Dowd, C., Ceburnis, D., Arneth, A., Svenningsson, B., Swietlicki, E., Tarozzi, L., Decesari, S., Facchini, M. C., Birmili, W., Sonntag, A., Wiedensohler, A., Boulon, J., Sellegri, K., Laj, P., Gysel, M., Bukowiecki, N., Weingartner, E., Wehrle, G., Laaksonen, A., Hamed, A., Joutsensaari, J., Petäjä, T., Kerminen, V. M., and Kulmala, M.: EUCAARI ion spectrometer measurements at 12 European sites – analysis of new particle formation events, Atmos. Chem. Phys., 10, 7907-7927, 10.5194/acp-10-7907-2010, 2010.

Martin, S. T., Artaxo, P., Machado, L. A. T., Manzi, A. O., Souza, R. A. F., Schumacher, C., Wang, J., Andreae, M. O., Barbosa, H. M. J., Fan, J., Fisch, G., Goldstein, A. H., Guenther, A., Jimenez, J. L., Pöschl, U., Silva Dias, M. A., Smith, J. N., and Wendisch, M.: Introduction: Observations and Modeling of the Green Ocean Amazon (GoAmazon2014/5), Atmos. Chem. Phys., 16, 4785-4797, 10.5194/acp-16-4785-2016, 2016.

Martin, S. T., Andreae, M. O., Artaxo, P., Baumgardner, D., Chen, Q., Goldstein, A. H., Guenther, A., Heald, C. L., Mayol-Bracero, O. L., McMurry, P. H., Pauliquevis, T., Pöschl, U., Prather, K. A., Roberts, G. C., Saleska, S. R., Silva Dias, M. A., Spracklen, D. V., Swietlicki, E., and Trebs, I.: Sources and properties of Amazonian aerosol particles, Reviews of Geophysics, 48, https://doi.org/10.1029/2008RG000280, 2010a.

Martin, S. T., Andreae, M. O., Althausen, D., Artaxo, P., Baars, H., Borrmann, S., Chen, Q., Farmer, D. K., Guenther, A., Gunthe, S. S., Jimenez, J. L., Karl, T., Longo, K., Manzi, A., Müller, T., Pauliquevis, T., Petters, M. D., Prenni, A. J., Pöschl, U., Rizzo, L. V., Schneider, J., Smith, J. N., Swietlicki, E., Tota, J., Wang, J., Wiedensohler, A., and Zorn, S. R.: An overview of the Amazonian Aerosol Characterization Experiment 2008 (AMAZE-08), Atmos. Chem. Phys., 10, 11415-11438, 10.5194/acp-10-11415-2010, 2010b.

McFiggans, G., Mentel, T. F., Wildt, J., Pullinen, I., Kang, S., Kleist, E., Schmitt, S., Springer, M., Tillmann, R., Wu, C., Zhao, D., Hallquist, M., Faxon, C., Le Breton, M., Hallquist, Å. M., Simpson, D., Bergström, R., Jenkin, M. E., Ehn, M., Thornton, J. A., Alfarra, M. R., Bannan, T. J., Percival, C. J., Priestley, M., Topping, D., and Kiendler-Scharr, A.: Secondary organic aerosol reduced by mixture of atmospheric vapours, Nature, 565, 587-593, 10.1038/s41586-018-0871-y, 2019.

Merikanto, J., Spracklen, D. V., Mann, G. W., Pickering, S. J., and Carslaw, K. S.: Impact of nucleation on global CCN, Atmos. Chem. Phys., 9, 8601-8616, 10.5194/acp-9-8601-2009, 2009.

Mirme, A., Tamm, E., Mordas, G., Vana, M., Uin, J., Mirme, S., Bernotas, T., Laakso, L., Hirsikko, A., and Kulmala, M.: A wide-range multi-channel Air Ion Spectrometer, 2007.

Mirme, S. and Mirme, A.: The mathematical principles and design of the NAIS – a spectrometer for the measurement of cluster ion and nanometer aerosol size distributions, Atmos. Meas. Tech., 6, 1061-1071, 10.5194/amt-6-1061-2013, 2013.

Mönkkönen, P., Koponen, I. K., Lehtinen, K. E. J., Hämeri, K., Uma, R., and Kulmala, M.: Measurements in a highly polluted Asian mega city: observations of aerosol number size distribution, modal parameters and nucleation events, Atmos. Chem. Phys., 5, 57-66, 10.5194/acp-5-57-2005, 2005.

Myhre, G.: Consistency Between Satellite-Derived and Modeled Estimates of the Direct Aerosol Effect, Science, 325, 187-190, doi:10.1126/science.1174461, 2009.

Németh, Z., Rosati, B., Zíková, N., Salma, I., Bozó, L., Dameto de España, C., Schwarz, J., Ždímal, V., and Wonaschütz, A.: Comparison of atmospheric new particle formation events in three Central European cities, Atmospheric Environment, 178, 191-197, https://doi.org/10.1016/j.atmosenv.2018.01.035, 2018.

Ni, R., Su, H., Burnett, R. T., Guo, Y., and Cheng, Y.: Long-term exposure to PM_{2.5} has significant adverse effects on childhood and adult asthma: A global meta-analysis and health impact assessment, One Earth, 7, 1953-1969, 10.1016/j.oneear.2024.09.022, 2024.

Nieminen, T., Kerminen, V. M., Petäjä, T., Aalto, P. P., Arshinov, M., Asmi, E., Baltensperger, U., Beddows, D. C. S., Beukes, J. P., Collins, D., Ding, A., Harrison, R. M., Henzing, B., Hooda, R., Hu, M., Hõrrak, U., Kivekäs, N., Komsaare, K., Krejci, R., Kristensson, A., Laakso, L., Laaksonen, A., Leaitch, W. R., Lihavainen, H., Mihalopoulos, N., Németh, Z., Nie, W., O'Dowd, C., Salma, I., Sellegri, K., Svenningsson, B., Swietlicki, E., Tunved, P., Ulevicius, V., Vakkari, V., Vana, M., Wiedensohler, A., Wu, Z., Virtanen, A., and Kulmala, M.: Global analysis of continental boundary layer new particle formation based on long-term measurements, Atmos. Chem. Phys., 18, 14737-14756, 10.5194/acp-18-14737-2018, 2018.

Okuyama, K., Kousaka, Y., and Motouchi, T.: Condensational Growth of Ultrafine Aerosol Particles in a New Particle Size Magnifier, Aerosol Science and Technology, 3, 353-366, 10.1080/02786828408959024, 1984.

Olin, M., Okuljar, M., Rissanen, M. P., Kalliokoski, J., Shen, J., Dada, L., Lampimäki, M., Wu, Y., Lohila, A., Duplissy, J., Sipilä, M., Petäjä, T., Kulmala, M., and Dal Maso, M.: Measurement report: Atmospheric new particle formation in a coastal agricultural site explained with binPMF analysis of nitrate CI-APi-TOF spectra, Atmos. Chem. Phys., 22, 8097-8115, 10.5194/acp-22-8097-2022, 2022.

Pikridas, M., Sciare, J., Freutel, F., Crumeyrolle, S., von der Weiden-Reinmüller, S. L., Borbon, A., Schwarzenboeck, A., Merkel, M., Crippa, M., Kostenidou, E., Psichoudaki, M., Hildebrandt, L., Engelhart, G. J., Petäjä, T., Prévôt, A. S. H., Drewnick, F., Baltensperger, U., Wiedensohler, A., Kulmala, M., Beekmann, M., and Pandis, S. N.: In situ formation and spatial variability of particle number concentration in a European megacity, Atmos. Chem. Phys., 15, 10219-10237, 10.5194/acp-15-10219-2015, 2015.

Pöhlker, C., Wiedemann, K. T., Sinha, B., Shiraiwa, M., Gunthe, S. S., Smith, M., Su, H., Artaxo, P., Chen, Q., Cheng, Y., Elbert, W., Gilles, M. K., Kilcoyne, A. L. D., Moffet, R. C., Weigand, M., Martin, S. T., Pöschl, U., and Andreae, M. O.: Biogenic Potassium Salt Particles as Seeds for Secondary Organic Aerosol in the Amazon, Science, 337, 1075-1078, doi:10.1126/science.1223264, 2012.

Pöhlker, C., Walter, D., Paulsen, H., Könemann, T., Rodríguez-Caballero, E., Moran-Zuloaga, D., Brito, J., Carbone, S., Degrendele, C., Després, V. R., Ditas, F., Holanda, B. A., Kaiser, J. W., Lammel, G., Lavrič, J. V., Ming, J., Pickersgill, D., Pöhlker, M. L., Praß, M., Löbs, N., Saturno, J., Sörgel, M., Wang, Q., Weber, B., Wolff, S., Artaxo, P., Pöschl, U., and Andreae, M. O.: Land cover and its transformation in the backward trajectory footprint region of the Amazon Tall Tower Observatory, Atmos. Chem. Phys., 19, 8425-8470, 10.5194/acp-19-8425-2019, 2019.

Pöhlker, M. L., Pöhlker, C., Ditas, F., Klimach, T., Hrabe de Angelis, I., Araújo, A., Brito, J., Carbone, S., Cheng, Y., Chi, X., Ditz, R., Gunthe, S. S., Kesselmeier, J., Könemann, T., Lavrič, J. V., Martin, S. T., Mikhailov, E., Moran-Zuloaga, D., Rose, D., Saturno, J., Su, H., Thalman, R., Walter, D., Wang, J., Wolff, S., Barbosa, H. M. J., Artaxo, P., Andreae, M. O., and Pöschl, U.: Long-term observations of cloud condensation nuclei in the Amazon rain forest – Part 1: Aerosol size distribution, hygroscopicity, and new model parametrizations for CCN prediction, Atmos. Chem. Phys., 16, 15709-15740, 10.5194/acp-16-15709-2016, 2016.

Pöhlker, M. L., Ditas, F., Saturno, J., Klimach, T., Hrabě de Angelis, I., Araùjo, A. C., Brito, J., Carbone, S., Cheng, Y., Chi, X., Ditz, R., Gunthe, S. S., Holanda, B. A., Kandler, K., Kesselmeier, J., Könemann, T., Krüger, O. O., Lavrič, J. V., Martin, S. T., Mikhailov, E., Moran-Zuloaga, D., Rizzo, L. V., Rose, D., Su, H., Thalman, R., Walter, D., Wang, J., Wolff, S., Barbosa, H. M. J., Artaxo, P., Andreae, M. O., Pöschl, U., and Pöhlker, C.: Long-term observations of cloud condensation nuclei over the Amazon rain forest – Part 2: Variability and characteristics of biomass burning, long-range transport, and pristine rain forest aerosols, Atmos. Chem. Phys., 18, 10289-10331, 10.5194/acp-18-10289-2018, 2018.

Pöschl, U.: Atmospheric Aerosols: Composition, Transformation, Climate and Health Effects, Angewandte Chemie International Edition, 44, 7520-7540, https://doi.org/10.1002/anie.200501122, 2005.

Pöschl, U. and Shiraiwa, M.: Multiphase Chemistry at the Atmosphere–Biosphere Interface Influencing Climate and Public Health in the Anthropocene, Chemical Reviews, 115, 4440-4475, 10.1021/cr500487s, 2015.

Qi, X. M., Ding, A. J., Nie, W., Petäjä, T., Kerminen, V. M., Herrmann, E., Xie, Y. N., Zheng, L. F., Manninen, H., Aalto, P., Sun, J. N., Xu, Z. N., Chi, X. G., Huang, X., Boy, M., Virkkula, A., Yang, X. Q., Fu, C. B., and Kulmala, M.: Aerosol size distribution and new particle formation in the western Yangtze River Delta of China: 2 years of measurements at the SORPES station, Atmos. Chem. Phys., 15, 12445-12464, 10.5194/acp-15-12445-2015, 2015.

Ravishankara, A. R.: Heterogeneous and Multiphase Chemistry in the Troposphere, Science, 276, 1058-1065, 10.1126/science.276.5315.1058, 1997.

Reche, C., Querol, X., Alastuey, A., Viana, M., Pey, J., Moreno, T., Rodríguez, S., González, Y., Fernández-Camacho, R., de la Rosa, J., Dall'Osto, M., Prévôt, A. S. H., Hueglin, C., Harrison, R. M., and Quincey, P.: New considerations for PM, Black Carbon and particle number concentration for air quality monitoring across different European cities, Atmos. Chem. Phys., 11, 6207-6227, 10.5194/acp-11-6207-2011, 2011.

Reutter, P., Su, H., Trentmann, J., Simmel, M., Rose, D., Gunthe, S. S., Wernli, H., Andreae, M. O., and Pöschl, U.: Aerosol- and updraft-limited regimes of cloud droplet formation: influence of particle number, size and hygroscopicity on the activation of cloud condensation nuclei (CCN), Atmos. Chem. Phys., 9, 7067-7080, 10.5194/acp-9-7067-2009, 2009.

Ridolfo, S., Amato, F., and Querol, X.: Particle number size distributions and concentrations in transportation environments: a review, Environment International, 187, 108696, https://doi.org/10.1016/j.envint.2024.108696, 2024.

Riemer, N., Ault, A. P., West, M., Craig, R. L., and Curtis, J. H.: Aerosol Mixing State: Measurements, Modeling, and Impacts, Reviews of Geophysics, 57, 187-249, 10.1029/2018rg000615, 2019.

Rissler, J., Swietlicki, E., Zhou, J., Roberts, G., Andreae, M. O., Gatti, L. V., and Artaxo, P.: Physical properties of the sub-micrometer aerosol over the Amazon rain forest during the wet-to-dry season transition - comparison of modeled and measured CCN concentrations, Atmos. Chem. Phys., 4, 2119-2143, 10.5194/acp-4-2119-2004, 2004.

Rissler, J., Vestin, A., Swietlicki, E., Fisch, G., Zhou, J., Artaxo, P., and Andreae, M. O.: Size distribution and hygroscopic properties of aerosol particles from dry-season biomass burning in Amazonia, Atmospheric Chemistry and Physics, 6, 471-491, 10.5194/acp-6-471-2006, 2006a.

Rissler, J., Vestin, A., Swietlicki, E., Fisch, G., Zhou, J., Artaxo, P., and Andreae, M. O.: Size distribution and hygroscopic properties of aerosol particles from dry-season biomass burning in Amazonia, Atmos. Chem. Phys., 6, 471-491, 10.5194/acp-6-471-2006, 2006b.

Rizzo, L. V., Roldin, P., Brito, J., Backman, J., Swietlicki, E., Krejci, R., Tunved, P., Petäjä, T., Kulmala, M., and Artaxo, P.: Multi-year statistical and modeling analysis of submicrometer aerosol number size distributions at a rain forest site in Amazonia, Atmos. Chem. Phys., 18, 10255-10274, 10.5194/acp-18-10255-2018, 2018.

Rose, C., Sellegri, K., Asmi, E., Hervo, M., Freney, E., Colomb, A., Junninen, H., Duplissy, J., Sipilä, M., Kontkanen, J., Lehtipalo, K., and Kulmala, M.: Major contribution of neutral clusters to new particle formation at the interface between the boundary layer and the free troposphere, Atmos. Chem. Phys., 15, 3413-3428, 10.5194/acp-15-3413-2015, 2015.

Rose, C., Zha, Q., Dada, L., Yan, C., Lehtipalo, K., Junninen, H., Mazon, S. B., Jokinen, T., Sarnela, N., Sipilä, M., Petäjä, T., Kerminen, V.-M., Bianchi, F., and Kulmala, M.: Observations of biogenic ion-induced cluster formation in the atmosphere, Science Advances, 4, eaar5218, doi:10.1126/sciadv.aar5218, 2018.

Rosenfeld, D., Lohmann, U., Raga, G. B., O'Dowd, C. D., Kulmala, M., Fuzzi, S., Reissell, A., and Andreae, M. O.: Flood or Drought: How Do Aerosols Affect Precipitation?, Science, 321, 1309-1313, 10.1126/science.1160606, 2008.

Rowell, A., Brean, J., Beddows, D. C. S., Shi, Z., Kumar, A., Rissanen, M., Dal Maso, M., Mettke, P., Weinhold, K., Merkel, M., and Harrison, R. M.: The behaviour of charged particles (ions) during new particle formation events in urban Leipzig, Germany, Atmos. Chem. Phys., 24, 10349-10361, 10.5194/acp-24-10349-2024, 2024.

Schraufnagel, D. E.: The health effects of ultrafine particles, Experimental & Molecular Medicine, 52, 311-317, 10.1038/s12276-020-0403-3, 2020.

Seinfeld, J. H. and Pandis, S. N.: Atmospheric Chemistry and Physics: From Air Pollution to Climate Change, 3rd Edition, 2016.

Shang, D., Peng, J., Guo, S., Wu, Z., and Hu, M.: Secondary aerosol formation in winter haze over the Beijing-Tianjin-Hebei Region, China, Frontiers of Environmental Science & Engineering, 15, 34, 10.1007/s11783-020-1326-x, 2020.

Sinclair, D. and Hoopes, G. S.: A continuous flow condensation nucleus counter, Journal of Aerosol Science, 6, 1-7, https://doi.org/10.1016/0021-8502(75)90036-1, 1975.

Sipilä, M., Berndt, T., Petäjä, T., Brus, D., Vanhanen, J., Stratmann, F., Patokoski, J., Mauldin, R. L., Hyvärinen, A.-P., Lihavainen, H., and Kulmala, M.: The Role of Sulfuric Acid in Atmospheric Nucleation, Science, 327, 1243-1246, 10.1126/science.1180315, 2010.

Smith, J. N., Draper, D. C., Chee, S., Dam, M., Glicker, H., Myers, D., Thomas, A. E., Lawler, M. J., and Myllys, N.: Atmospheric clusters to nanoparticles: Recent progress and challenges in closing the gap in chemical composition, Journal of Aerosol Science, 153, 105733, https://doi.org/10.1016/j.jaerosci.2020.105733, 2021.

Stolzenburg, D., Cai, R., Blichner, S. M., Kontkanen, J., Zhou, P., Makkonen, R., Kerminen, V.-M., Kulmala, M., Riipinen, I., and Kangasluoma, J.: Atmospheric nanoparticle growth, Reviews of Modern Physics, 95, 045002, 10.1103/RevModPhys.95.045002, 2023.

Stolzenburg, M. R. and McMurry, P. H.: An Ultrafine Aerosol Condensation Nucleus Counter, Aerosol Science and Technology, 14, 48-65, 10.1080/02786829108959470, 1991.

Su, H., Cheng, Y., and Pöschl, U.: New Multiphase Chemical Processes Influencing Atmospheric Aerosols, Air Quality, and Climate in the Anthropocene, Accounts of Chemical Research, 10.1021/acs.accounts.0c00246, 2020.

Sulo, J., Enroth, J., Pajunoja, A., Vanhanen, J., Lehtipalo, K., Petäjä, T., and Kulmala, M.: Pushing nano-aerosol measurements towards a new decade – technical note on the Airmodus particle size magnifier 2.0, Aerosol Research, 2, 13-20, 10.5194/ar-2-13-2024, 2024.

Sulo, J., Sarnela, N., Kontkanen, J., Ahonen, L., Paasonen, P., Laurila, T., Jokinen, T., Kangasluoma, J., Junninen, H., Sipilä, M., Petäjä, T., Kulmala, M., and Lehtipalo, K.: Long-term measurement of sub-3 nm particles and their precursor gases in the boreal forest, Atmos. Chem. Phys., 21, 695-715, 10.5194/acp-21-695-2021, 2021.

Sun, J., Hermann, M., Weinhold, K., Merkel, M., Birmili, W., Yang, Y., Tuch, T., Flentje, H., Briel, B., Ries, L., Couret, C., Elsasser, M., Sohmer, R., Wirtz, K., Meinhardt, F., Schütze, M., Bath, O., Hellack, B., Kerminen, V. M., Kulmala, M., Ma, N., and Wiedensohler, A.: Measurement report: Contribution of atmospheric new particle formation to ultrafine particle concentration, cloud condensation nuclei, and radiative forcing – results from 5-year observations in central Europe, Atmos. Chem. Phys., 24, 10667-10687, 10.5194/acp-24-10667-2024, 2024.

Sun, Y., Lei, L., Zhou, W., Chen, C., He, Y., Sun, J., Li, Z., Xu, W., Wang, Q., Ji, D., Fu, P., Wang, Z., and Worsnop, D. R.: A chemical cocktail during the COVID-19 outbreak in Beijing, China: Insights from six-year aerosol particle composition measurements

during the Chinese New Year holiday, Science of The Total Environment, 742, 140739, https://doi.org/10.1016/j.scitotenv.2020.140739, 2020a.

Sun, Y., He, Y., Kuang, Y., Xu, W., Song, S., Ma, N., Tao, J., Cheng, P., Wu, C., Su, H., Cheng, Y., Xie, C., Chen, C., Lei, L., Qiu, Y., Fu, P., Croteau, P., and Worsnop, D. R.: Chemical Differences Between PM1 and PM2.5 in Highly Polluted Environment and Implications in Air Pollution Studies, Geophysical Research Letters, 47, e2019GL086288, https://doi.org/10.1029/2019GL086288, 2020b.

Tammet, H., Hõrrak, U., and Kulmala, M.: Negatively charged nanoparticles produced by splashing of water, Atmos. Chem. Phys., 9, 357-367, 10.5194/acp-9-357-2009, 2009.

Tang, I. N., Munkelwitz, H. R., and Davis, J. G.: Aerosol growth studies—II. Preparation and growth measurements of monodisperse salt aerosols, Journal of Aerosol Science, 8, 149-159, https://doi.org/10.1016/0021-8502(77)90002-7, 1977.

Tang, L., Shang, D., Fang, X., Wu, Z., Qiu, Y., Chen, S., Li, X., Zeng, L., Guo, S., and Hu, M.: More Significant Impacts From New Particle Formation on Haze Formation During COVID-19 Lockdown, Geophysical Research Letters, 48, e2020GL091591, https://doi.org/10.1029/2020GL091591, 2021.

Trebs, I., Meixner, F. X., Slanina, J., Otjes, R., Jongejan, P., and Andreae, M. O.: Real-time measurements of ammonia, acidic trace gases and water-soluble inorganic aerosol species at a rural site in the Amazon Basin, Atmos. Chem. Phys., 4, 967-987, 10.5194/acp-4-967-2004, 2004.

Tröstl, J., Chuang, W. K., Gordon, H., Heinritzi, M., Yan, C., Molteni, U., Ahlm, L., Frege, C., Bianchi, F., Wagner, R., Simon, M., Lehtipalo, K., Williamson, C., Craven, J. S., Duplissy, J., Adamov, A., Almeida, J., Bernhammer, A.-K., Breitenlechner, M., Brilke, S., Dias, A., Ehrhart, S., Flagan, R. C., Franchin, A., Fuchs, C., Guida, R., Gysel, M., Hansel, A., Hoyle, C. R., Jokinen, T., Junninen, H., Kangasluoma, J., Keskinen, H., Kim, J., Krapf, M., Kürten, A., Laaksonen, A., Lawler, M., Leiminger, M., Mathot, S., Möhler, O., Nieminen, T., Onnela, A., Petäjä, T., Piel, F. M., Miettinen, P., Rissanen, M. P., Rondo, L., Sarnela, N., Schobesberger, S., Sengupta, K., Sipilä, M., Smith, J. N., Steiner, G., Tomè, A., Virtanen, A., Wagner, A. C., Weingartner, E., Wimmer, D., Winkler, P. M., Ye, P., Carslaw, K. S., Curtius, J., Dommen, J., Kirkby, J., Kulmala, M., Riipinen, I., Worsnop, D. R., Donahue, N. M., and Baltensperger, U.: The role of low-volatility organic compounds in initial particle growth in the atmosphere, Nature, 533, 527-531, 10.1038/nature18271, 2016.

Tuch, T. M., Wehner, B., Pitz, M., Cyrys, J., Heinrich, J., Kreyling, W. G., Wichmann, H. E., and Wiedensohler, A.: Long-term measurements of size-segregated ambient aerosol in two German cities located 100km apart, Atmospheric Environment, 37, 4687-4700, https://doi.org/10.1016/j.atmosenv.2003.07.010, 2003.

Vanhanen, J., Mikkilä, J., Lehtipalo, K., Sipilä, M., Manninen, H. E., Siivola, E., Petäjä, T., and Kulmala, M.: Particle Size Magnifier for Nano-CN Detection, Aerosol Science and Technology, 45, 533-542, 10.1080/02786826.2010.547889, 2011.

Voigtländer, J., Tuch, T., Birmili, W., and Wiedensohler, A.: Correlation between traffic density and particle size distribution in a street canyon and the dependence on wind direction, Atmos. Chem. Phys., 6, 4275-4286, 10.5194/acp-6-4275-2006, 2006.

von Bismarck-Osten, C., Birmili, W., Ketzel, M., Massling, A., Petäjä, T., and Weber, S.: Characterization of parameters influencing the spatio-temporal variability of urban particle number size distributions in four European cities, Atmospheric Environment, 77, 415-429, https://doi.org/10.1016/j.atmosenv.2013.05.029, 2013.

von der Weiden, S. L., Drewnick, F., and Borrmann, S.: Particle Loss Calculator – a new software tool for the assessment of the performance of aerosol inlet systems, Atmos. Meas. Tech., 2, 479-494, 10.5194/amt-2-479-2009, 2009.

Vu, T. V., Delgado-Saborit, J. M., and Harrison, R. M.: Review: Particle number size distributions from seven major sources and implications for source apportionment studies, Atmospheric Environment, 122, 114-132, https://doi.org/10.1016/j.atmosenv.2015.09.027, 2015.

Wang, J., Li, M., Li, L., Zheng, R., Fan, X., Hong, Y., Xu, L., Chen, J., and Hu, B.: Particle number size distribution and new particle formation in Xiamen, the coastal city of Southeast China in wintertime, Science of The Total Environment, 826, 154208, https://doi.org/10.1016/j.scitotenv.2022.154208, 2022.

Wang, J., Krejci, R., Giangrande, S., Kuang, C., Barbosa, H. M. J., Brito, J., Carbone, S., Chi, X., Comstock, J., Ditas, F., Lavric, J., Manninen, H. E., Mei, F., Moran-Zuloaga, D., Pöhlker, C., Pöhlker, M. L., Saturno, J., Schmid, B., Souza, R. A. F., Springston, S. R., Tomlinson, J. M., Toto, T., Walter, D., Wimmer, D., Smith, J. N., Kulmala, M., Machado, L. A. T., Artaxo, P., Andreae, M. O., Petäjä, T., and Martin, S. T.: Amazon boundary layer aerosol concentration sustained by vertical transport during rainfall, Nature, 539, 416-419, 10.1038/nature19819, 2016.

Wang, K., Ma, X., Tian, R., and Yu, F.: Analysis of new particle formation events and comparisons to simulations of particle number concentrations based on GEOS-Chem–advanced particle microphysics in Beijing, China, Atmos. Chem. Phys., 23, 4091-4104, 10.5194/acp-23-4091-2023, 2023.

Wang, M., Kong, W., Marten, R., He, X.-C., Chen, D., Pfeifer, J., Heitto, A., Kontkanen, J., Dada, L., Kürten, A., Yli-Juuti, T., Manninen, H. E., Amanatidis, S., Amorim, A., Baalbaki, R., Baccarini, A., Bell, D. M., Bertozzi, B., Bräkling, S., Brilke, S., Murillo, L. C., Chiu, R., Chu, B., De Menezes, L.-P., Duplissy, J., Finkenzeller, H., Carracedo, L. G., Granzin, M., Guida, R., Hansel, A., Hofbauer, V., Krechmer, J., Lehtipalo, K., Lamkaddam, H., Lampimäki, M., Lee, C. P., Makhmutov, V., Marie, G., Mathot, S., Mauldin, R. L., Mentler, B., Müller, T., Onnela, A., Partoll, E., Petäjä, T., Philippov, M., Pospisilova, V., Ranjithkumar, A., Rissanen, M., Rörup, B., Scholz, W., Shen, J., Simon, M., Sipilä, M., Steiner, G., Stolzenburg, D., Tham, Y. J., Tomé, A., Wagner, A. C., Wang, D. S., Wang, Y., Weber, S. K., Winkler, P. M., Wlasits, P. J., Wu, Y., Xiao, M., Ye, Q., Zauner-Wieczorek, M., Zhou, X., Volkamer, R., Riipinen, I., Dommen, J., Curtius, J., Baltensperger, U., Kulmala, M., Worsnop, D. R., Kirkby, J., Seinfeld, J. H., El-Haddad, I., Flagan, R. C., and Donahue, N. M.: Rapid growth of new atmospheric particles by nitric acid and ammonia condensation, Nature, 581, 184-189, 10.1038/s41586-020-2270-4, 2020.

Wang, S. C. and Flagan, R. C.: Scanning Electrical Mobility Spectrometer, Aerosol Science and Technology, 13, 230-240, 10.1080/02786829008959441, 1990.

Wang, Z., Wu, Z., Yue, D., Shang, D., Guo, S., Sun, J., Ding, A., Wang, L., Jiang, J., Guo, H., Gao, J., Cheung, H. C., Morawska, L., Keywood, M., and Hu, M.: New particle formation in China: Current knowledge and further directions, Science of The Total Environment, 577, 258-266, https://doi.org/10.1016/j.scitotenv.2016.10.177, 2017.

Wang, Z. B., Hu, M., Wu, Z. J., Yue, D. L., He, L. Y., Huang, X. F., Liu, X. G., and Wiedensohler, A.: Long-term measurements of particle number size distributions and the relationships with air mass history and source apportionment in the summer of Beijing, Atmos. Chem. Phys., 13, 10159-10170, 10.5194/acp-13-10159-2013, 2013.

Wehner, B. and Wiedensohler, A.: Long term measurements of submicrometer urban aerosols: statistical analysis for correlations with meteorological conditions and trace gases, Atmos. Chem. Phys., 3, 867-879, 10.5194/acp-3-867-2003, 2003.

Wendisch, M., Pöschl, U., Andreae, M. O., Machado, L. A. T., Albrecht, R., Schlager, H., Rosenfeld, D., Martin, S. T., Abdelmonem, A., Afchine, A., Araùjo, A. C., Artaxo, P., Aufmhoff, H., Barbosa, H. M. J., Borrmann, S., Braga, R., Buchholz, B., Cecchini, M.

A., Costa, A., Curtius, J., Dollner, M., Dorf, M., Dreiling, V., Ebert, V., Ehrlich, A., Ewald, F., Fisch, G., Fix, A., Frank, F., Fütterer, D., Heckl, C., Heidelberg, F., Hüneke, T., Jäkel, E., Järvinen, E., Jurkat, T., Kanter, S., Kästner, U., Kenntner, M., Kesselmeier, J., Klimach, T., Knecht, M., Kohl, R., Kölling, T., Krämer, M., Krüger, M., Krisna, T. C., Lavric, J. V., Longo, K., Mahnke, C., Manzi, A. O., Mayer, B., Mertes, S., Minikin, A., Molleker, S., Münch, S., Nillius, B., Pfeilsticker, K., Pöhlker, C., Roiger, A., Rose, D., Rosenow, D., Sauer, D., Schnaiter, M., Schneider, J., Schulz, C., de Souza, R. A. F., Spanu, A., Stock, P., Vila, D., Voigt, C., Walser, A., Walter, D., Weigel, R., Weinzierl, B., Werner, F., Yamasoe, M. A., Ziereis, H., Zinner, T., and Zöger, M.: ACRIDICON–CHUVA Campaign: Studying Tropical Deep Convective Clouds and Precipitation over Amazonia Using the New German Research Aircraft HALO, Bulletin of the American Meteorological Society, 97, 1885-1908, https://doi.org/10.1175/BAMS-D-14-00255.1, 2016.

Whitby, K. T.: The physical characteristics of sulfur aerosols, Atmospheric Environment (1967), 12, 135-159, https://doi.org/10.1016/0004-6981(78)90196-8, 1978.

Wiedensohler, A., Lütkemeier, E., Feldpausch, M., and Helsper, C.: Investigation of the bipolar charge distribution at various gas conditions, Journal of Aerosol Science, 17, 413-416, https://doi.org/10.1016/0021-8502(86)90118-7, 1986.

Williamson, C. J., Kupc, A., Axisa, D., Bilsback, K. R., Bui, T., Campuzano-Jost, P., Dollner, M., Froyd, K. D., Hodshire, A. L., Jimenez, J. L., Kodros, J. K., Luo, G., Murphy, D. M., Nault, B. A., Ray, E. A., Weinzierl, B., Wilson, J. C., Yu, F., Yu, P., Pierce, J. R., and Brock, C. A.: A large source of cloud condensation nuclei from new particle formation in the tropics, Nature, 574, 399-403, 10.1038/s41586-019-1638-9, 2019.

Wimmer, D., Buenrostro Mazon, S., Manninen, H. E., Kangasluoma, J., Franchin, A., Nieminen, T., Backman, J., Wang, J., Kuang, C., Krejci, R., Brito, J., Goncalves Morais, F., Martin, S. T., Artaxo, P., Kulmala, M., Kerminen, V.-M., and Petäjä, T.: Ground-based observation of clusters and nucleation-mode particles in the Amazon, Atmospheric Chemistry and Physics, 18, 13245-13264, 10.5194/acp-18-13245-2018, 2018.

Wu, S., Tao, J., Ma, N., Kuang, Y., Zhang, Y., He, Y., Sun, Y., Xu, W., Hong, J., Xie, L., Wang, Q., Su, H., and Cheng, Y.: Particle number size distribution of PM1 and PM10 in fogs and implications on fog droplet evolutions, Atmospheric Environment, 277, 119086, https://doi.org/10.1016/j.atmosenv.2022.119086, 2022.

Wu, T. and Boor, B. E.: Urban aerosol size distributions: a global perspective, Atmos. Chem. Phys., 21, 8883-8914, 10.5194/acp-21-8883-2021, 2021.

Wu, Z., Hu, M., Liu, S., Wehner, B., Bauer, S., Ma ßling, A., Wiedensohler, A., Petäjä, T., Dal Maso, M., and Kulmala, M.: New particle formation in Beijing, China: Statistical analysis of a 1-year data set, Journal of Geophysical Research: Atmospheres, 112, https://doi.org/10.1029/2006JD007406, 2007.

Xiao, M., Hoyle, C. R., Dada, L., Stolzenburg, D., Kürten, A., Wang, M., Lamkaddam, H., Garmash, O., Mentler, B., Molteni, U., Baccarini, A., Simon, M., He, X. C., Lehtipalo, K., Ahonen, L. R., Baalbaki, R., Bauer, P. S., Beck, L., Bell, D., Bianchi, F., Brilke, S., Chen, D., Chiu, R., Dias, A., Duplissy, J., Finkenzeller, H., Gordon, H., Hofbauer, V., Kim, C., Koenig, T. K., Lampilahti, J., Lee, C. P., Li, Z., Mai, H., Makhmutov, V., Manninen, H. E., Marten, R., Mathot, S., Mauldin, R. L., Nie, W., Onnela, A., Partoll, E., Petäjä, T., Pfeifer, J., Pospisilova, V., Quéléver, L. L. J., Rissanen, M., Schobesberger, S., Schuchmann, S., Stozhkov, Y., Tauber, C., Tham, Y. J., Tomé, A., Vazquez-Pufleau, M., Wagner, A. C., Wagner, R., Wang, Y., Weitz, L., Wimmer, D., Wu, Y., Yan, C., Ye, P., Ye, Q., Zha, Q., Zhou, X., Amorim, A., Carslaw, K., Curtius, J., Hansel, A., Volkamer, R., Winkler, P. M., Flagan, R. C., Kulmala, M., Worsnop, D.

R., Kirkby, J., Donahue, N. M., Baltensperger, U., El Haddad, I., and Dommen, J.: The driving factors of new particle formation and growth in the polluted boundary layer, Atmos. Chem. Phys., 21, 14275-14291, 10.5194/acp-21-14275-2021, 2021.

Xiao, S., Wang, M. Y., Yao, L., Kulmala, M., Zhou, B., Yang, X., Chen, J. M., Wang, D. F., Fu, Q. Y., Worsnop, D. R., and Wang, L.: Strong atmospheric new particle formation in winter in urban Shanghai, China, Atmos. Chem. Phys., 15, 1769-1781, 10.5194/acp-15-1769-2015, 2015.

Yan, C., Yin, R., Lu, Y., Dada, L., Yang, D., Fu, Y., Kontkanen, J., Deng, C., Garmash, O., Ruan, J., Baalbaki, R., Schervish, M., Cai, R., Bloss, M., Chan, T., Chen, T., Chen, Q., Chen, X., Chen, Y., Chu, B., Dällenbach, K., Foreback, B., He, X., Heikkinen, L., Jokinen, T., Junninen, H., Kangasluoma, J., Kokkonen, T., Kurppa, M., Lehtipalo, K., Li, H., Li, H., Li, X., Liu, Y., Ma, Q., Paasonen, P., Rantala, P., Pileci, R. E., Rusanen, A., Sarnela, N., Simonen, P., Wang, S., Wang, W., Wang, Y., Xue, M., Yang, G., Yao, L., Zhou, Y., Kujansuu, J., Petäjä, T., Nie, W., Ma, Y., Ge, M., He, H., Donahue, N. M., Worsnop, D. R., Kerminen, V.-M., Wang, L., Liu, Y., Zheng, J., Kulmala, M., Jiang, J., and Bianchi, F.: The Synergistic Role of Sulfuric Acid, Bases, and Oxidized Organics Governing New-Particle Formation in Beijing, Geophysical Research Letters, 48, e2020GL091944, https://doi.org/10.1029/2020GL091944, 2021.

Yao, L., Garmash, O., Bianchi, F., Zheng, J., Yan, C., Kontkanen, J., Junninen, H., Mazon, S. B., Ehn, M., Paasonen, P., Sipilä, M., Wang, M., Wang, X., Xiao, S., Chen, H., Lu, Y., Zhang, B., Wang, D., Fu, Q., Geng, F., Li, L., Wang, H., Qiao, L., Yang, X., Chen, J., Kerminen, V.-M., Petäjä, T., Worsnop, D. R., Kulmala, M., and Wang, L.: Atmospheric new particle formation from sulfuric acid and amines in a Chinese megacity, Science, 361, 278-281, 10.1126/science.aao4839, 2018.

Yu, H., Zhou, L., Dai, L., Shen, W., Dai, W., Zheng, J., Ma, Y., and Chen, M.: Nucleation and growth of sub-3 nm particles in the polluted urban atmosphere of a megacity in China, Atmos. Chem. Phys., 16, 2641-2657, 10.5194/acp-16-2641-2016, 2016.

Yu, H., Gannet Hallar, A., You, Y., Sedlacek, A., Springston, S., Kanawade, V. P., Lee, Y.-N., Wang, J., Kuang, C., McGraw, R. L., McCubbin, I., Mikkila, J., and Lee, S.-H.: Sub-3 nm particles observed at the coastal and continental sites in the United States, Journal of Geophysical Research: Atmospheres, 119, 860-879, https://doi.org/10.1002/2013JD020841, 2014.

Zhang, Q., Jimenez, J. L., Canagaratna, M. R., Ulbrich, I. M., Ng, N. L., Worsnop, D. R., and Sun, Y.: Understanding atmospheric organic aerosols via factor analysis of aerosol mass spectrometry: a review, Analytical and Bioanalytical Chemistry, 401, 3045-3067, 10.1007/s00216-011-5355-y, 2011.

Zhang, R., Khalizov, A., Wang, L., Hu, M., and Xu, W.: Nucleation and Growth of Nanoparticles in the Atmosphere, Chemical Reviews, 112, 1957-2011, 10.1021/cr2001756, 2012.

Zhang, R., Suh, I., Zhao, J., Zhang, D., Fortner, E. C., Tie, X., Molina, L. T., and Molina, M. J.: Atmospheric New Particle Formation Enhanced by Organic Acids, Science, 304, 1487-1490, 10.1126/science.1095139, 2004.

Zhao, B., Donahue, N. M., Zhang, K., Mao, L., Shrivastava, M., Ma, P.-L., Shen, J., Wang, S., Sun, J., Gordon, H., Tang, S., Fast, J., Wang, M., Gao, Y., Yan, C., Singh, B., Li, Z., Huang, L., Lou, S., Lin, G., Wang, H., Jiang, J., Ding, A., Nie, W., Qi, X., Chi, X., and Wang, L.: Global variability in atmospheric new particle formation mechanisms, Nature, 631, 98-105, 10.1038/s41586-024-07547-1, 2024.

Zheng, G., Su, H., Wang, S., Andreae, M. O., Pöschl, U., and Cheng, Y.: Multiphase buffer theory explains contrasts in atmospheric aerosol acidity, Science, 369, 1374-1377, doi:10.1126/science.aba3719, 2020.

Zheng, G. J., Duan, F. K., Su, H., Ma, Y. L., Cheng, Y., Zheng, B., Zhang, Q., Huang, T., Kimoto, T., Chang, D., Pöschl, U., Cheng, Y. F., and He, K. B.: Exploring the severe winter haze in Beijing: the impact of synoptic weather, regional transport and heterogeneous reactions, Atmos. Chem. Phys., 15, 2969-2983, 10.5194/acp-15-2969-2015, 2015.

Zhou, J., Swietlicki, E., Hansson, H. C., and Artaxo, P.: Submicrometer aerosol particle size distribution and hygroscopic growth measured in the Amazon rain forest during the wet season, Journal of Geophysical Research, 107, 10.1029/2000jd000203, 2002.

Zhou, Y., Hakala, S., Yan, C., Gao, Y., Yao, X., Chu, B., Chan, T., Kangasluoma, J., Gani, S., Kontkanen, J., Paasonen, P., Liu, Y., Petäjä, T., Kulmala, M., and Dada, L.: Measurement report: New particle formation characteristics at an urban and a mountain station in northern China, Atmos. Chem. Phys., 21, 17885-17906, 10.5194/acp-21-17885-2021, 2021.

Zhou, Y., Ma, N., Wang, Q., Wang, Z., Chen, C., Tao, J., Hong, J., Peng, L., He, Y., Xie, L., Zhu, S., Zhang, Y., Li, G., Xu, W., Cheng, P., Kuhn, U., Zhou, G., Fu, P., Zhang, Q., Su, H., and Cheng, Y.: Bimodal distribution of size-resolved particle effective density: results from a short campaign in a rural environment over the North China Plain, Atmos. Chem. Phys., 22, 2029-2047, 10.5194/acp-22-2029-2022, 2022.

A. List of Publication

Peer-Reviewed publications

B. Acknowledgements

C. Curriculum Vitae